Technical Report

TR-09-31

Long term test of buffer material at the Äspö HRL, LOT project

Final report on the A0 test parcel

Ola Karnland, Siv Olsson, Torbjörn Sandén, Billy Fälth
Clay Technology AB

Mats Jansson, Trygve E Eriksen, Kjell Svärdström
KTH

Bo Rosborg, Studsvik AB/Rosborg consulting

Arto Muurinen, VTT

February 2011

Svensk Kärnbränslehantering AB
Swedish Nuclear Fuel
and Waste Management Co

Box 250, SE-101 24 Stockholm
Phone +46 8 459 84 00

ISSN 1404-0344
SKB TR-09-31

Long term test of buffer material at the Äspö HRL, LOT project

Final report on the A0 test parcel

Ola Karnland, Siv Olsson, Torbjörn Sandén, Billy Fälth
Clay Technology AB

Mats Jansson, Trygve E Eriksen, Kjell Svärdström
KTH

Bo Rosborg, Studsvik AB/Rosborg consulting

Arto Muurinen, VTT

February 2011

Keywords: Bentonite, Buffer, Clay, Copper corrosion, Diffusion, Field experiment, LOT, Mineralogy, Montmorillonite, Physical properties, Radioactive waste, Repository, SKBdoc Id 1254772, Äspö.

Preface

Main Report

Ola Karnland, Siv Olsson, Torbjörn Sandén, Billy Fälth
Clay Technology AB, Lund

Appendices

1 Tracer diffusion test: Mats Jansson, Trygve E Eriksen and Kjell Svärdström, KTH

2 Copper coupon test: Bo Rosborg, Studsvik AB/ Rosborg consulting

3 Bentonite block and sensor configuration

Posiva financed work

4 Water analyses: Arto Muurinen, VTT

Abstract

In the Swedish repository concept for nuclear waste (KBS-3 concept), the spent nuclear fuel will be stored in copper canisters surrounded by compacted bentonite. The decaying power of the fuel will increase the temperature in the repository which, in combination with the uptake of ground-water, could be expected to produce minor mineralogical changes in the bentonite. The ongoing LOT test series at the Äspö Hard Rock Laboratory are focused on identifying and quantifying any mineralogical alterations in the bentonite exposed to typical repository-like conditions. Further, buffer-related processes concerning copper corrosion, cation transport, and bacterial survival/activity are studied. In total, the LOT project includes seven test parcels, which contain a central Cu-tube surrounded by cylindrical bentonite blocks to a total diameter of 30 cm as well as temperature, total pressure, water pressure and humidity sensors. In each test parcel, an electrical heater placed inside the copper tube is used to simulate the heat generation from the decaying spent fuel. Three test parcels (S1 to S3) have been exposed to standard KBS-3 conditions (maximum temperature below 100°C) and three parcels (A1 to A3) to adverse conditions (maximum temperature below ~140°C). Both the standard and the adverse test series include short term tests (1 to 2 years), medium term tests (> 5 years) and long term tests (> 10 years).

The present report concerns an additional short term test, thereby the designation A0, which was exposed to adverse conditions for approximately 1.5 years. Cu-coupons, ^{134}Cs and ^{57}Co tracers and specific chemical agents were placed in the bentonite at defined positions. After field exposure, the entire test parcel was released from the rock by overlapping percussion drilling and wire sawing. The parcel was lifted and divided at the test site and the bentonite material was sampled for specified analyses. The main aspects of the various tests and analyses may be summarized in the following items:

- physical properties (water content, density, swelling pressure and hydraulic conductivity),
- mineralogical alteration of the bentonite,
- water chemistry,
- distribution of added agents (e.g $CaSO_4$ of ^{134}Cs and ^{57}Co) and
- copper corrosion.

Reference material and exposed test material were examined by a combination of mineralogical analysis methods such as X-ray diffraction, cation exchange capacity analyses, element analyses according to a predefined test program. The most important results from all performed analyses may be summarized in the following items:

- redistribution of easily dissolved accessory minerals in the bentonite, in particular $CaSO_4$,
- no formation of illite or any other typical montmorillonite alteration minerals,
- diffusive transport of trace elements was in accordance with previous studies,
- corrosion rate of metallic copper was in agreement with model predictions and previous tests.

An overarching conclusion is that the observed mineralogical alteration, as a consequence of the water saturation process and the exposure to high temperature, are small and that, in any case, this alteration did not change the physical properties to such an extent that the buffer function is jeopardized.

Sammanfattning

I det svenska KBS-3 konceptet för slutförvar av utbränt kärnbränsle förvaras bränslet i kopparkapslar vilka omges av kompakterad bentonit. Bränslets radioaktiva sönderfall kommer att höja temperaturen i förvaret vilket tillsammans med upptag av grundvatten förväntas orsaka mindre mineralogiska förändringar i bentoniten.

Det nu pågående LOT projektet vid Äspö berglaboratorium syftar till att identifiera och kvantifiera sådana mineralogiska förändringar i bentoniten som följd av exponering för en förvarsliknande miljö. Dessutom undersöks relaterade processer i bentoniten som rör kopparkorrosion, diffusion av katjoner, samt överlevnad och aktivitet hos bakterier. Totalt används sju försökspaket, vilka innehåller ett centralt cirka 4 m långt kopparrör omgivet av cylinderringar av kompakterad bentonit. En elektrisk värmare inne i kopparröret används för att simulera resteffekten från det utbrända bränslet. Temperatur, totaltryck, vattentryck och fuktighet mäts via givare som placerats i bentoniten. Projektet innefattade ursprungligen tre försökspaket (S1 till S3) som är utsatta för typiska KBS-3 förhållanden med en maximal temperatur som understiger 100°C, och tre försökspaket (A1 till A3) som är utsatta för speciellt ogynnsamma förhållanden, framförallt förhöjd temperatur till maximalt cirka 140°C. Båda försökstyperna genomförs som korttids- (1 till 2 år), medellånga (> 5 år) och långtidsförsök (> 10 år).

Den nu aktuella rapporten avser ett extra korttidsförsök, därav beteckningen A0, i vilket bentoniten utsatts för en maximal temperatur på cirka 140°C. Kopparkuponger, ^{134}Cs and ^{57}Co spårämnen, och utvalda mineral fanns placerade på bestämda positioner i bentoniten. Efter cirka 1.5 års exponering i fält friborrades A0-paketet varefter det lyftes, delades och provtogs för specificerade tester och analyser med avseende på:

- bentonitens fysikaliska egenskaper (vatteninnehåll, densitet, svälltryck och hydraulisk konduktivitet),
- mineralogiska förändringar i bentoniten,
- vattenkemi,
- fördelning i bentoniten av tillförda substanser (t.ex. gips, ^{134}Cs och ^{57}Co),
- korrosion av kopparkuponger.

Merparten av analyserna avsåg bentonitens mineralogi. Referensmaterial och exponerat försöksmaterial har undersökts med en bred uppsättning mineralogiska analysmetoder såsom röntgendiffraktometri, katjonbytesanalys, och elementanalys enligt ett i huvudsak förutbestämt testprogram. De mest betydelsefulla resultaten från alla genomförda analyser och tester kan sammanfattas i följande punkter:

- omfördelning av lättlösliga mineral i bentoniten, speciellt gäller detta kalciumsulfat (gips),
- ingen nybildning av illit eller andra typiska omvandlingsmineral från montmorillonit,
- diffusionsegenskaperna för ^{134}Cs och ^{57}Co överensstämmer med tidigare undersökningar,
- uppmätt korrosionshastigheten av metallisk koppar överensstämmer med resultat från tidigare försök samt med modellberäkningar.

En övergripande slutsats är att endast små mineralogiska förändringar har skett i bentoniten som följd av vattenmättnaden och exponeringen för höga temperaturer, och att dessa förändringar inte har lett till påtagligt försämrade fysikaliska egenskaper.

Contents

1 Background

1.1 General

Bentonite clay has been proposed as buffer material in several concepts for nuclear high level waste (HLW) repositories. In the Swedish KBS-3 concept the demands on the bentonite buffer are to serve as mechanical support for the canister, reduce the effects on the canister of possible rock displacement, and minimize water flow over the deposition holes. The transport through the buffer is expected to be controlled principally by diffusion, both with respect to corrosive components in the groundwater and to corrosion products and escaping radionuclides in case of a canister failure.

Comprehensive research and development work has been carried out during the last thirty years in order to determine the basic behavior of unaltered bentonite material. The results have been reported in numerous technical reports, and provisional computer codes concerning both unsaturated and saturated buffer conditions are available (e.g. Börgesson et al. 1995). The models are believed to describe well the behavior of unaltered MX-80 bentonite buffer after water saturation with respect to physical properties, e.g. swelling pressure, hydraulic conductivity and rheological behavior. Further, techniques for bentonite block production and application have been developed in order to fulfill the requirements concerning density, homogeneity, handling etc. (Johannesson et al. 1995).

The decaying spent fuel in the HLW canisters will increase the temperature of the bentonite buffer. Initially there will also be a thermal gradient over the buffer by which original water will be redistributed parallel to an uptake of water from the surrounding rock. A number of laboratory test series, made by different research groups, have resulted in various buffer alteration models which are discussed in (Karnland and Birgersson 2006). According to these models no significant alteration of the buffer is expected to take place at the prevailing physico-chemical conditions in a KBS-3 repository neither during, nor after water saturation. The models may to a certain degree be validated in long term field tests. Former large scale field tests in Sweden, Canada, Switzerland and Japan have in different respects deviated from possible KBS-3 repository conditions and the testing periods have generally been dominated by initial processes, i.e. water uptake and temperature increase.

The present LOT test series is consequently focused on the long term performance of the bentonite buffer, i.e. the conditions after full water saturation, and on buffer related processes in a water-saturated bentonite buffer concerning microbiology, cation transport, and copper corrosion. The LOT test series originally included six test parcels with two short term tests (~1 year), two medium term tests (~5 years), and two long term tests (~10 years). Due to the retrieval problems with one of the short term test parcels (A1) (Karnland et al. 2000) an additional short term test parcel was installed in order to confirm and complement the results from the A1 analyses. This report concerns the additional parcel, termed A0, with respect to:

- Background.
- Construction.
- Field results.
- Results from laboratory analyses of field exposed material concerning
  - physical properties,
  - mineralogy,
  - cesium and cobalt diffusion,
  - copper corrosion.

The underlying chemical and mineralogical processes are not discussed in this report, but are generally addressed by geochemical modeling of the LOT project results.

The LOT project was initiated and is financed by SKB (Sweden). Posiva have contributed from project start by financing clay water analyses performed by VTT, Finland.

2 Objectives

2.1 General

The bentonite buffer material in the KBS-3 concept is a natural mixture of montmorillonite and several common accessory minerals, e.g. quartz, feldspar, calcite, siderite and pyrite. The bentonite material is chosen because of the specific physico-chemical properties, which primarily are due to interaction between the montmorillonite component and water. These properties are of fundamental importance for the repository function during the entire lifetime of the repository. The stability of the montmorillonite mineral is therefore of vital importance for the buffer performance and is one of the main issues in the LOT project. Also possible changes of the accessory minerals may be important as they may dissolve and precipitate and thereby may alter, in particular, the rheological properties of the buffer material.

The main aspects of the LOT one year tests were to check that compaction, placement and water saturation did not significantly change the physical properties of the buffer. In the following parts of the project, i.e. medium and long term exposure to repository similar conditions, the main aspects are to check that the repository temperature and geochemical conditions after water saturation do not significantly change the physical properties of the buffer.

The test layout also makes it possible to study other important processes in the canister-buffer-rock system. The general objectives in the LOT test series may be summarized in the following items, and the specific issues of interest are described in the following sections:

- Collect data for validation of models concerning buffer performance under quasi-steady state conditions after water saturation, e.g. swelling pressure, hydraulic conductivity and rheological properties.
- Check existing models concerning buffer degrading processes, e.g. mineral redistribution and montmorillonite alteration.
- Produce data concerning “critical gas penetration pressure” and gas transport capacity. This item has not been studied in the present A0 test parcel.
- Check existing models concerning cation diffusion in bentonite.
- Collect information concerning survival, activity and migration of bacteria in bentonite under repository-like conditions. This item has not been studied in the present A0 test parcel.
- Check calculated data concerning copper corrosion, and collect information regarding the character of possible corrosion products.
- Collect information, which may facilitate the realization of the full-scale test series (e.g. the Prototype project) with respect to preparation, instrumentation, retrieval, subsequent analyses, evaluation and data handling. This item was of special importance with respect to the retrieval of the present A0 test parcel since there were serious problems during the uptake of the previous LOT A1 test parcel.

2.2 Physical buffer properties

The clay/water system in a KBS-3 repository is expected to have well known physical properties, of which swelling pressure, hydraulic conductivity and plasticity are the most important. A large number of data from laboratory tests are available in reports produced by SKB and corresponding organizations in other countries (e.g. AECL, Andra, Enresa, Nagra, PNC and Posiva).

A main hypothesis in this project is that the initial swelling pressure, hydraulic conductivity and plasticity of the water saturated bentonite material are well described and possible to predict for a KBS-3 construction by the present laboratory results and models.

2.3 Buffer stability

2.3.1 General

One reason for choosing bentonite as buffer material is its long term stability in nature. It is frequently found in very old geological formations also in relation to the lifetime of a HLW repository. As an example, the Wyoming formation from which the commercial MX-80 bentonite is produced is from the Cretaceous period (~65 million years ago) (Slaughter and Early 1965). In a future repository, however, the bentonite will be exposed to a new environment with respect mainly to temperature and ground-water chemistry (Figure 2-1). Consequently, different alteration processes have been studied with respect to repository conditions, and to a larger extent, much work has been made mainly in relation to oil exploration. A large number of articles concerning measured natural alteration and alteration models have been published over the last 50 years in scientific clay literature, e.g. Clay Minerals, Clays and Clay Minerals, and Applied Clay Science, and several books have been written on this subject (Karnland and Birgersson 2006).

The design criteria for the KBS-3 repository stipulate that the temperature in the buffer should not exceed 100°C, including a safety margin of 10°C, in any position at any time. The expected temperature evolution has been calculated for the present repository layout to lead to a maximum temperature below 90°C, and a maximum temperature gradient below 24°C over the 0.35 m thick buffer material (Figure 2-1) (Hökmark and Fälth 2003).

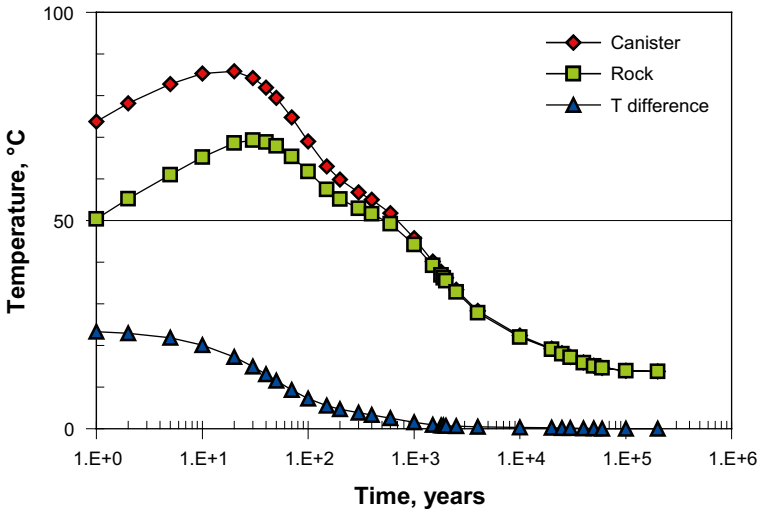

Figure 2-1. *Calculated temperature evolution in a typical KBS-3 deposition hole showing the buffer temperatures at the interfaces to the canister and the rock, and the temperature gradient over the buffer, respectively. Calculated from data in (Hökmark and Fälth 2003).*

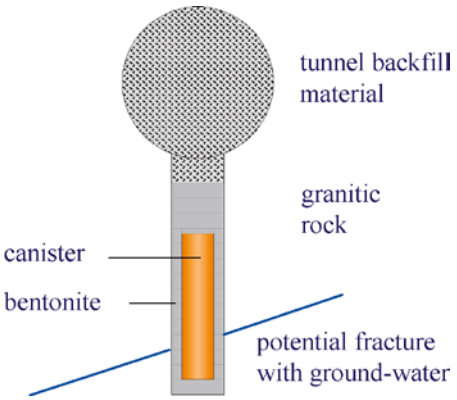

Figure 2-2. *Schematic view of a cross section through a deposition tunnel and deposition hole in a KBS-3 repository.*

Chemical/mineralogical changes of possible importance in a KBS-3 repository may be listed as follows:

- Enrichment of substances emanating from the groundwater.
- Dissolution and precipitation of accessory minerals.
- Montmorillonite surface reactions
  - ion exchange, e.g. from sodium to calcium,
  - sorption of ions,
  - pH buffering of the montmorillonite.
- Montmorillonite structural alteration
  - in situ alteration e.g. into illite,
  - incongruent dissolution, e.g. release of silica,
  - congruent dissolution.

Depending on the overall conditions all these types of processes may result in significant changes of the physical properties of the buffer.

2.3.2 Dissolution and precipitation

Different enrichment processes of dissolved substances may take place due to the temperature gradient which prevails over the KBS-3 buffer during the elevated temperature phase, i.e. ~10,000 years. Precipitations may cement the buffer and change mainly the rheological properties of the buffer functions (Pusch et al. 1993). One such possible process is ion transport parallel to water uptake from the outer cooler parts of the bentonite, or from the surrounding groundwater, to the wetting front in the originally unsaturated bentonite. The transport is assumed to take place by an evaporation/condensation process in which water is sucked in from cooler parts and evaporates at the wetting front. Dissolved salts will thereby be deposited at the wetting front.

A second possible process is precipitation of minerals, which have lower solubility at higher temperature, e.g. calcium sulfate (gypsum/anhydrite) and calcium carbonate (calcite). This process may take place also in a fully water saturated bentonite and the potential problem is consequently larger. The process will come to a standstill after limited enrichment if the buffer material alone is the source of the original pore water concentration. The total maximum effect will then be possible to calculate. On the other hand, if the surrounding groundwater is the source of substances then the enrichment process may continue until the precipitation stops due to spatial limitations.

According to preparatory laboratory experiments the following conditions reduces enrichment of easily dissolved minerals in a bentonite buffer:

- High buffer density.
- Low content of accessory minerals in the buffer.
- Low electrolyte content in the surrounding water.
- High water pressure.

The use of pre-saturated bentonite blocks, supply of water with low electrolyte concentration in open slots, and a fast restoration of the hydrostatic pressure may consequently reduce mineral redistribution and enrichment in a KBS-3 repository. No such preventive techniques were used in the present test. Instead, the initial water-to-solid mass ratio was low and the slots were filled with groundwater in order to maximize the precipitation effects. Further, the processes were enhanced in the current A0 parcel by elevated temperature, and higher temperature gradient compared to KBS-3 conditions, and by placing reactive substances at specified positions in the parcel.

The hypothesis was that the precipitation should be limited and that no major cementation of the buffer should take place.

2.3.3 Smectite-to-illite conversion

Depending on the conditions, alteration of minerals in the smectite group, to which montmorillonite belongs, may take place and form a number of related minerals, e.g. illite, chlorite or zeolites. In nature the most common smectite alteration at elevated temperature is transformation into illite. This type of conversion has also been considered as the most probable, or rather least improbable, under repository conditions. Fortunately, the smectite-to-illite reaction has been extensively studied for several decades mainly because of its relevance to oil prospecting. Different parameters have been proposed as kinetic controlling factors, but there is no general consensus on the reactions involved in the conversion. Based on geological analogues and laboratory experiments the following main factors have been proposed as kinetic controlling variables (no ranking):

- Overburden pressure (Weaver 1959).
- Temperature (Perry and Hower 1970).
- Potassium activity (Hower et al. 1976).
- Aluminum activity (Boles and Frank 1979).
- pH (Eberl et al. 1993).
- Dehydration (Couture 1985).
- Silica activity (Abercrombie et al. 1994).

According to the kinetic model proposed by (Huang et al. 1993), the overall kinetics of the smectite-to-illite reaction can be described by the equation:

$$\frac{dS}{dt} = A \cdot \left[K^+\right] \cdot S^2 \cdot \exp\left(\frac{-E_a}{R \cdot T}\right) \qquad \text{Equation 2-1}$$

where S is the smectite fraction in the illite/smectite material, t is time, A is the frequency factor, E_a is the activation energy and R is the universal gas constant, and T is temperature. After integration of Equation 2-1, the smectite content at a certain time can be calculated according to:

$$S = \frac{S_0}{1 + S_0 \cdot \left[K^+\right] \cdot A \cdot \exp\left(\frac{-E_a}{R \cdot T}\right) \cdot t} \qquad \text{Equation 2-2}$$

Where S_0 is the smectite fraction at $t = 0$. The potassium concentration in the Äspö groundwater are measured to be in the range of a few ppm up to 45 ppm (Laaksoharju et al. 1995). Arguments for using the Huang et al. model and aspects on uncertainties are discussed in (Karnland and Birgersson 2006). According to the model, practically no clay conversion will take place in a KBS-3 repository at these conditions as shown in Figure 2-3. However, the rate law and Arrhenius parameters are determined from relatively short-term laboratory experiments at temperatures (250–325°C) significantly higher than repository conditions, and from geological analogues, which differ from repository conditions in several aspects. The uncertainty in calculated conversion increases with the difference in temperature between test condition and calculated condition. Therefore, the LOT test series aims at checking the model results and determining whether the reaction rate is substantially faster than predicted by the model. The LOT experiments are performed at ”as repository like conditions” as possible in standard (S) type experiments, and at “adverse conditions” in (A) type experiments, which include moderately increased temperature (maximum 140°C) and potassium feldspar. The latter tests are further conservative in the sense that the transport of potassium, which is considered as one of the major hindrances for illitization (Hower et al. 1976, Huang et al. 1993) in a repository is overcome by the added internal potassium source.

2.3.4 Effects of cementitious pore water

Possible effects on the bentonite of exposure to cementitious pore water are believed to result from the following reactions (Eberl et al. 1993, Karnland and Birgersson 2006, Karnland et al. 2007):

- Replacement of the original charge balancing cations, e.g. sodium against calcium.
- Cementation of the bentonite due to precipitation of cementitious compounds (e.g. calcium-silica-hydrates and calcite) in clay pore space.
- Attack on the accessory minerals (e.g. cristobalite) in the bentonite.
- Alteration of clay mineral due to the induced high pH.

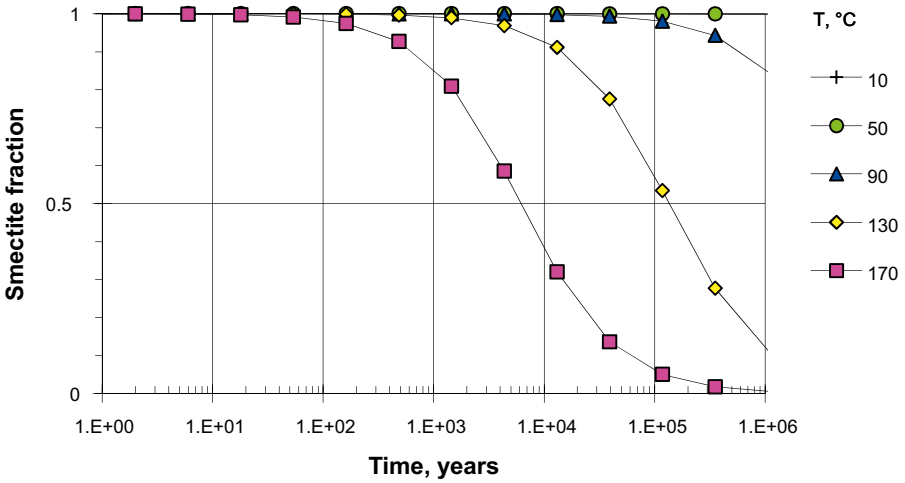

Figure 2-3. *Remaining smectite fraction for different temperatures in a hydrothermal system with [K^+] = 0.002 mole/liter (80 ppm) according to the (Huang et al. 1993) kinetic model and laboratory determined constants (Ea = 27.4 kcal/mole and A = 8.5E4).*

The hypothesis is that bentonite under repository conditions resists short-term attack from cementitious pore water without major alteration. The main aspects of this part of the project are to confirm/reject results from laboratory experiments, which showed ion exchange, minor mineral dissolution/neo-formation and no or minor montmorillonite alteration.

2.4 Microbiology

No microbiological analyses were included in the A0 parcel program, mainly because of the high temperature and the relatively low degree of water saturation.

2.5 Cation migration

The diffusion of radionuclides in compacted bentonite has been studied rather extensively in laboratory experiments with synthetic groundwater. The pore water diffusion model, generally used to interpret the experimental data, is based on the assumption that diffusion takes place in pore water and is retarded by sorption of the diffusing species on the solid phase. This model may be adequate for cations sorbed on the solid phase by surface complexation mechanisms, e.g. Co^{2+}. For cationic species present in the clay due to ion exchange, e.g. Cs^+ and Sr^{2+}, experimental data indicate an additional diffusion mechanism in which migration takes place within the nano-sized interlayer space between the montmorillonite surfaces. The diffusivities of Cs^+ and Co^{2+} in compacted bentonite saturated with groundwater of different ionic strength (salinity) are rather well documented at room temperature and, in principle, it should be possible to model the diffusive transport of these cations in the actual bentonite system.

A common theory is that cation transport may take place by two different transport mechanisms, i.e. by diffusion in pore water which is not affected by the montmorillonite and by an additional migration between individual montmorillonite mineral layers next to the mineral surface. Recently, it has been shown that the interlayer volumes play an important role in compacted bentonite in general, and that laboratory diffusion data may principally be explained by two interlayer ion equilibrium processes; Donnan equilibrium and ion exchange (Birgersson and Karnland 2009).

A difference in diffusive transport is expected between cations sorbed by surface complexation mechanisms, e.g. Co^{2+}, and cationic species present as exchangeable ions, e.g. Cs^+ and Sr^{2+}. A faster transport is therefore expected to take place for the latter cations. In the present A0 parcel the diffusive behavior of $^{134}Cs^+$ and $^{57}Co^{2+}$ was studied.

2.6 Copper corrosion

The corrosion rate of the canister is in principle determined by the chemical reactivity at the canister surface and the mass transfer to and from this surface. For a specific canister, the corrosion rate depends on the geochemical conditions in the close vicinity of the copper surface, i.e. the type, content and mobility of dissolved constituents in the surrounding bentonite buffer. Thermodynamic calculations show that alteration products of copper are stable and that the corrosion process is expected to be affected by the redox conditions of the clay medium (Wersin et al. 1993).

In general there are different types of uncertainties associated with estimation of the corrosion rate of copper in bentonite:

- Model validity.
- Time scale of oxic/anoxic transition.
- Pitting factor.
- Transport properties of the clay.

Modeling that takes into account diffusive transport in addition to flow, equilibrium reactions and kinetic processes at the bentonite-canister interface has been made (Wersin et al. 1994). The results indicate conservative corrosion rates of $2 \cdot 10^{-8}$ and $7 \cdot 10^{-6}$ m/y for anoxic and oxic conditions, respectively. A sensitivity analysis indicates that the main uncertainties arise from the diffusion properties of the clay.

The present test aims at determining the mean corrosion rate, and identifying possible pitting and corrosion products. The main hypothesis is that the mean corrosion rate under the initial oxic conditions will be at most $7 \cdot 10^{-6}$ m/y.

2.7 Gas transport

No gas pressure test was included in the A0 parcel program, mainly because this issue is the subject of the ongoing full scale Lasgit project at the Äspö HRL.

3 Experimental concept

3.1 General

3.1.1 Principles

The LOT test series may be described as a multi-task experiment in which relatively small test parcels are exposed to field conditions at Äspö HRL. The series include three parcels which are exposed to conditions similar to those expected in a KBS-3 repository and four parcels which are exposed to conditions which should accelerate alteration processes. The test parcels are comprised of prefabricated bentonite blocks placed around a copper tube in vertical boreholes drilled into granitic rock. After exposure to field conditions for a defined period of time, each parcel is extracted by overlapping core drilling outside the original borehole, and the whole test parcel is lifted and partitioned. Material from defined positions in the parcel and reference material are thereafter examined by well-defined tests and analyses in order to provide data to test the different hypotheses.

The dimensions of the parcels are considerably smaller, especially with regard to diameter, than an actual KBS-3 deposition package in order to:

- Shorten the water saturation period and thereby have saturated conditions during a substantial part of the test period.
- Get a higher temperature gradient over the buffer material.
- Facilitate sampling, i.e. release and up-lift of the exposed test parcel in one piece.

3.1.2 Adverse conditions

Mineralogical stability of the bentonite clay is one of the grounds for the choice of bentonite as buffer material. Nevertheless, alteration processes will take place in the buffer but are predicted to be very slow under KBS-3 repository conditions. The following accelerating conditions compared to KBS-3 conditions were therefore used in order to make it possible to study slow alteration processes in the relatively short duration time of the experiments:

- Higher temperature.
- Higher temperature gradient.
- Higher content of accessory minerals (calcite, gypsum, K-feldspar).
- Introduction of new substances (Portland cement).

The expected effect of these accelerating conditions (buffer adverse conditions) may be summarized in the following discussion.

The initial rate of a bimolecular reaction

$$aA + bB \rightarrow \text{products} \qquad \text{Equation 3-1}$$

can be described by the standard rate law

$$\text{Rate} = k\,[A]^n\,[B]^m \qquad \text{Equation 3-2}$$

where n and m are constants, and k is a rate constant which can be expressed by the Arrhenius relationship

$$k = zp \cdot \exp(-E_a / RT)\,, \qquad \text{Equation 3-3}$$

where z is the collision frequency factor, p is the steric factor, E_a is the activation energy, R is the gas constant and T is the temperature.

This reaction rate theory consequently implies:

- The reaction rate increases with increasing concentration of a reactant.
- The reaction rate increases with increasing temperature.
- The temperature effect increases with increasing activation energy.
- The temperature increase effect is reduced with increasing temperature.

For the case of illitization with the high activation energy (114,700 J/mole), measured by (Huang et al. 1993), a temperature increase of 10 K results in an almost tripled reaction rate. Consequently, the increase from 90°C, which is the upper temperature limit in the KBS-3 buffer, to the maximum temperature in the adverse conditions parcels (130°C) leads to an increased illitization rate of around 40 times according to the Huang et al. model. The calculated maximum temperature one hundred years after fuel deposition is around 70°C and the corresponding temperature after 1,000 years is 50°C (Figure 2-1). The temperature in the outermost part of the bentonite will initially be around 20°C lower than the innermost part. A comparison between the 130°C temperature in the adverse condition parcel and the maximum bentonite temperature after 100 years (70°C) gives an increase in the reaction rate by a factor of almost 400. A 1-year test at 130°C consequently represents a significant part of the thermal load in a KBS-3 repository with respect to kinetically controlled slow processes.

However, the LOT A0 test is expected to show mineralogical effects of processes governed by the water saturation and only limited effects of the heating alone.

3.2 Experimental configuration

3.2.1 Test program

In total, the LOT test series includes seven test parcels (Table 3-1) of which three parcels are exposed to standard KBS-3 conditions, and four parcels are exposed to adverse conditions. The present report concerns the A0 parcel.

3.3 Test site

3.3.1 General

The LOT main test series is run in the G-tunnel, which is situated in the western part of the present Äspö hard rock laboratory (Figure 3-1). The depth from surface is around 450 m and the rock consists mainly of Äspö diorite, which is crossed by some pegmatite dikes and bands of fine-grained granite. A few water-bearing fractures are visible, but the tunnel may be considered dry relative to the average Äspö rock volume.

Table 3-1. Test program for the ”Long Term Test of Buffer Material” series. A = adverse conditions, S = standard conditions, T = temperature, [K+] = potassium concentration, pH = high pH from cement, am = accessory minerals added.

Type	No.	max T, °C	Controlled parameter	Time, years	Remark
A	1	130	T, [K+], pH, am	1	pilot test
A	0	150	T, [K+], pH, am	1	A1 complement
A	2	120–150	T, [K+], pH, am	> 5	main test
A	3	120–150	T	>> 5	main test
S	1	90	T	1	pilot test
S	2	90	T	> 5	main test
S	3	90	T	>> 5	main test

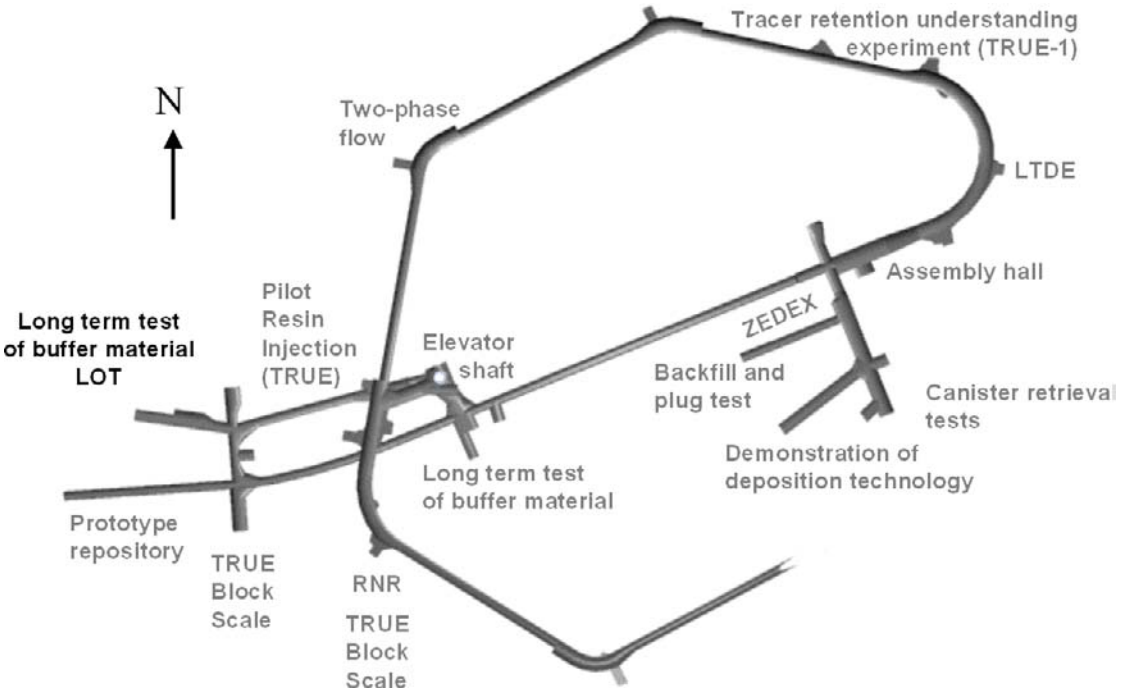

Figure 3-1. *The present LOT test site is located in the G-tunnel in the western part of the research area, and close to the lowest part of the Äspö tunnel.*

3.3.2 Pilot holes

Five 76 mm vertical pilot holes were drilled in line on the northern side of the G-tunnel between March 2nd and March 4th 1999. The holes were approximately 8 m deep and with a relative distance of 4.5 m. The holes were termed KG0033G01, KG0037G01, KG0042G01, KG0046G01 and KG0051G01, where K denotes core-drilled, G denotes the G-tunnel, the figure (e.g. 0033) denotes the length in meters from tunnel entrance and G denotes floor position. The KG0033G01 hole was used for the present A0 test.

No definite suitability criteria were defined for the test holes, but the water pressure in the holes has to be higher than the vapor pressure at the chosen test temperature. Further, water inflow had to be low enough to allow the placement of the test parcels and to exclude the risk of piping and erosion after closure.

Shortly after drilling, mechanical packers were installed. The boreholes were shut in and kept closed until the start of flow and pressure measurements were performed. The flow measurements were made by use of double packers with 1 m spacing in the upper 4 m and a single packer was used for the bottom part (4 m to 8 m). The results of the flow measurements are presented in Table 3-2.

Table 3-2. Flow rates (ml/min) measured in intervals of the five pilot boreholes for the LOT tests in the G-tunnel of ÄSPÖ HRL, April 1999. The pilot hole for the A0 test is marked by bold text.

Section	Borehole: KG0033G01	KG0037G01	KG0042G01	KG0046G01	KG0051G01
1.4–8.05	**0.025**	0.02	–0.12	1.3	0.025
1.00–2.00	**0.07**	0.09	± 0	0.1	0.07
2.00–3.00	**0.07**	0.07	0.04	0.14	0.01
3.00–4.00	**0.06**	0.14	0.05	0.08	0.07
4.00–8.05	**0.01**	0.06	0.01	0.60	0.01

The general conclusions from the pilot hole characterization program were that the water inflow was low, and that the water inlet points were few in all holes. The test time was therefore expected to be much longer than acceptable. Instead of abandoning the site, it was decided to add external ground-water into the test holes during the test period. A water supply hole (HG0038B01) was drilled into the northern wall where a water-bearing fracture was found a few meters into the rock. The water pressure was determined to be around 1.2 MPa and the flow was more than sufficient to support all test holes. The water supply hole was packed off and a system of titanium tubes was used to inject water into the test holes.

The ground-water composition was measured in bore-hole HG0038B01 within the Äspö HRL campaigns and typical composition of main elements is given in (Table 3-3)

Table 3-3. Main composition of the ground-water in water supply bore hole HG0038B01 in 2000 and 2001.

HG0038B01 Units	Na mM	K mM	Ca mM	Mg mM	HCO3 mM	Cl mM	SO4 mM	Br mM	F mM	Si mM	HS mM	pH	E.C. mS/m
2000-04-14	98.7	0.236	43.4	2.21	0.852	185	4.84	0.504		0.178		7.4	1,750
2001-09-26	104	0.246	49.6	2.15	0.705	195	4.94	0.617	0.125	0.196	0.000604	7.4	1,930

3.3.3 Test holes

The five pilot holes were enlarged to a diameter of 300 mm to a depth of 4 m. The enlargement was made by percussion drilling because this technique was thought to best simulate the core TBM-type drilling with respect to surface damage and thereby to water conductivity. The test holes were named according to the standard Äspö database nomenclature; HG0033G01, HG0037G01, HG0042G01, HG0046G01 and HG0051G01. The test hole HG0033G01 was used for the present A0 parcel.

The diameter and the straightness of the test holes were checked and the diameter was measured to exceed 300 mm by up to 10 mm in some parts.

3.4 Test parcel construction

3.4.1 General

The basic demand for the test parcel construction was to keep a defined maximum temperature in the central part of the clay column during the test time span. An important part of the system was therefore the temperature measurement and power regulation system. A central heater inside an open tube was chosen, as this allows for heater change during the test period in case of a failure. The central tube was made of copper in order to simulate the KBS-3 copper canister, and thereby keep as realistic chemical conditions as possible. The A0 test parcel contained a heater, a central tube, bentonite blocks, measurement sensors and chemical additives, which are individually described in the following sections.

3.4.2 Heater

A specially designed electric heater from Backer Elektro-värme AB, Sösdala, Sweden was used. The total length was 4,650 mm, and the active bottom part had a length of 2,000 mm. Three individual stainless steel (SS2348) elements with a diameter of 14 mm were brazed into a stainless steel (SS2343) flange, which was designed in order to let the heater hang down from the top of the copper tube. The maximum power was decided to be 2 kW (230/400 V, AC), i.e. each element has a maximum power of 667 W (230 V) corresponding to 0.7 W/cm². The expected power need was based on the previously performed pilot tests A1 and S1, which were in agreement with scoping calculations made by MICROFIELD finite element computer code performed by Harald Hökmark, Clay Technology AB.

3.4.3 Central tubes

The copper tube (SS 5015-04), simulating the canister, had a length of 4,700 mm, an inner diameter of 100 mm and a wall thickness of 4 mm. At the bottom end a copper plate and 4 copper reinforcement parts were brazed by use of soldering silver. A detachable lifting device was placed at the top of the tube during the placement. The maximum possible external pressure acting on the outside of the central tube was expected to be less than 10 MPa (bentonite swelling pressure plus hydrostatic water pressure), which corresponds to a maximum compression stress of 140 MPa acting at the inner radius. The quality of the hard-drawn copper used to manufacture the central tube provides a yield point exceeding 200 MPa, which is sufficient to withstand the estimated compression stress.

No water/steam leakage into the tube could be accepted regarding both the heater function and the mass transport conditions. The impenetrability was therefore tested after the soldering by use of a helium source inside the copper tube and an external detector.

3.4.4 Blocks

Wyoming bentonite with the commercial name MX-80 was the source material for all bentonite components in the system. It was delivered by Askania AB and manufactured by Volclay LTD, Mersyside, UK. The material was delivered in 25 kg sacks in one consignment.

The material is dominated by natural mainly sodium montmorillonite clay (~ 80% by weight). Accessory minerals are quartz (~4%), tridymite (~4%), cristobalite (~3%), feldspars (~4%), muscovite/illite (~4%) sulfides (~0.2%), and small amounts of several other minerals and organic carbon (~0.4%). Dispersed in distilled water the clay fraction (grain size < 2 μm) makes up around 80%. The mean mineralogical composition of the montmorillonite is given by:

$$(Si_{7.92}\ Al_{0.08})\ (Al_{3.10}\ Fe^{3+}_{0.4} Fe^{2+}_{0.02}\ Mg_{0.48})\ O_{20}(OH)_4 \qquad Na_{0.48}\ Ca_{0.04}\ Mg_{0.02}$$

The cation exchange capacity is around 0.75 eq/kg bulk material and around 0.85 eq/kg clay in the <2 μm fraction. The natural exchangeable cations are sodium (~70%), calcium (~20%), magnesium (~6%) and small amounts of potassium (~2%). The specific surface area is around $5.5 \cdot 10^5$ m^2/kg material and the grain density is around 2,750 kg/m^3 (Karnland et al. 2006).

The various blocks and plugs produced for the A0 parcel may be divided in the following groups:

- Standard blocks with a slightly conical form and a maximum outer diameter of 281 mm and a height of 100 mm.
- Special blocks, which were prepared from standard blocks, with excavations for reinforcements, instruments, copper plates or 20 mm test plugs.
- 20 mm diameter bentonite plugs with or without different additives, used in the tracer tests and accessory mineral enrichment tests.

The choice of block compaction technique was based on experiences from previous SKB projects concerning block production (Johannesson et al. 1995). A uniaxial compaction device was constructed in order to produce blocks with the accurate dimensions, density and composition. A slight axial conic form and chamfered edges between mantle and end sides were used in order to facilitate the expulsion after compaction and to avoid subsequent stress induced cracks. A small amount of molybdenum sulfide grease was used to smear the mantel surfaces in order to reduce friction.

The bentonite material was compacted without pre-treatment. Water-to-solid mass ratio was measured in each 25 kg sack in order to determine the amount of solid bentonite in each block batch. The governing figure for the production was a final density of 2,000 kg/m^3 in the test hole after expansion by water uptake, since this is the reference KBS-3 bentonite bulk density. Mass calculations were made by use of a bentonite solid density of 2,750 kg/m^3, a mean block radius of 139.3 mm and an inner radius of 56 mm, a borehole radius of 150 mm, copper tube radius of 54 mm, and the measured water-to-solid mass ratio in the bentonite, which was 0.102 (± 0.01). Extra blocks were made in the production series in order to analyze their homogeneity. For each produced block, approximately 250 g of the same material, i.e. from the same 25 kg sack, was marked and stored as reference material for background analyses.

The blocks predestined for gauges or plugs were made from standard blocks by drilling and carving out the necessary volume. The bentonite material is well suited for this technique and the produced unintentional gaps between the gauges and the bentonite are small and insignificant with respect to the final buffer density.

The special blocks produced for the A0 parcel had the following modifications:

block no.	modifications/excavations for
01	copper bottom-plate reinforcements
02	3 thermocouples
05	20 mm cylindrical holes for tracer tests, 3 water inlet filters
08	5 thermocouples, 1 total pressure gauge, 1 water pressure gauge, 1 relative humidity gauge
10	4 plugs of 10% $CaCO_3$ and 1 water sampling cup
12	4 plugs of 10% $CaSO_4$ and 1 water sampling cup
14	6 thermocouples, 1 total pressure gauge, 1 water pressure gauge, 2 relative humidity gauges
16	12 plugs of 50% K-feldspar and 1 water sampling cup
18	6 water sampling cups and 3 water inlet filters
20	5 thermocouples, 1 total pressure gauge, 1 relative humidity gauge
22	2 copper plates (A and B)
24	6 cement plugs, 1 water sampling cup
26	3 thermocouples
30	2 copper plates (C and D)
32	1 thermocouple, 3 water sampling cups, 3 water inlet filters
34	6 cement plugs, 2 water sampling cups
38	1 thermocouple

All of the blocks were designed for defined positions in the test parcels and given a specific denomination. The instrumentation and sampling scheme was based on a virtual partitioning of the blocks into 9 radial sections and 3 axial sections. The first section ranging from the inner mantel surface and 2 cm outwards was termed Section 1, and the following volume, i.e. between 2 and 4 cm from the inner mantel surface, was termed Section 3, etc. The last section was consequently 9, and this section only had an initial extension outwards of ~1 cm. After swelling, due to water uptake, Section 9 represented the volume between 8 and ~10 cm (rock wall). Furthermore, the point of the compass was used to describe the horizontal orientation. The denomination of a specific point (center of a volume) is according to the example 08ASE3 where

08	block number (counted from the bottom of the parcel),
A	vertical level in the block,
SE	direction of compass in the test hole,
3	radial distance in centimeters from the inner mantel surface to the center of the specimen.

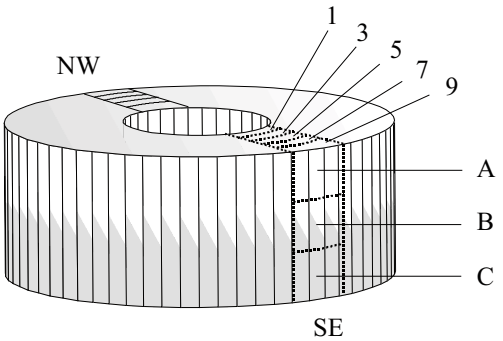

Figure 3-2. *Schematic block partition. SE and NW denote the directions of compass in the test-hole, figures denote the center of the specimens expressed in centimeters measured from the block inner mantel surface, and A, B and C denotes the three analyzed vertical positions in the blocks.*

Reference material from a specific block was termed according to the example A009R where

R reference material,

A0 parcel type and number,

09 block number (counted from the bottom of the parcel).

The layout of all special blocks is schematically shown in Appendix 3.

3.4.5 Test plugs

All bentonite-containing plugs had a cylindrical form with a length and diameter of 20 mm. They were compacted in a laboratory compaction device working by the same principle as the block compaction device, but no grease was used. The plugs were compacted to a bulk density of ~2,070 kg/m^3 regardless of the additives. The compaction was accordingly controlled by the final sample volume and not by the maximum compaction pressure.

The plugs were placed in cylindrical holes, which were drilled from the mantle surface into the specified blocks halfway between, and parallel to, the top and bottom surfaces. The hole diameter was constantly 21 mm, while the depth depended on the purpose of the test. The outer plugs were sprayed with a small amount of deionized water before they were inserted in order to let the bentonite swell slightly and thereby seal the slots. The positions of the plugs were marked by millimeter thick titanium wires inserted into drilled holes placed 10 mm above the center of the plugs. Two wires marked the northern position, and one wire marked the other three main directions of compass. The positions of all test plugs are shown schematically in Figure 3-3 and Appendix C.

The calcite plugs contained 10 wt% calcite. The calcite material was a finely ground pure quality which was thoroughly mixed with the bentonite and compacted to cylindrical plugs with a diameter of 20 mm and a height of 20 mm. Four holes were drilled at mid height from the cardinal points of the outer surface into block A010 to a depth of ~30 mm. A test plug was placed at the bottom of each hole, and the outermost part of the holes was sealed by a slightly wetted bentonite plug without additives just before the placement of the parcel.

The gypsum plugs contained 10 wt% gypsum. The used $CaSO_4$ 2 H_2O material was a finely ground pure quality which was thoroughly mixed with the bentonite and compacted to cylindrical plugs with a diameter of 20 mm and a height of 20 mm. Four holes were drilled at mid height from the cardinal points of the outer surface into block A012 to a depth of ~30 mm. A test plug was placed at the bottom of each hole, and the outermost part of the holes was sealed by a slightly wetted bentonite plug without additives just before the placement of the parcel.

The feldspar plugs contained 50 wt% K-feldspar. The material was finely ground and mixed with the bentonite and compacted to cylindrical plugs with a diameter of 20 mm and a height of 20 mm. Four holes were drilled at mid height from the cardinal points of the outer surface into block A016 to a depth of ~70 mm. Three test plugs were placed at the bottom of each hole, and the outermost part of the holes was sealed by a slightly wetted bentonite plug without additives just before the placement of the parcel.

The cement plugs were cast to a water-to-cement ratio (w/c) of 0.8 by use of an Aalborg white Portland cement and de-ionized water. The cement was allowed to harden in water for 14 days before the emplacement. Two cylindrical holes were drilled into block A024, and A034 from the north and from the south side to a depth of 80 mm. Four plugs were placed in each hole. No bentonite plugs were used for sealing.

The ^{134}Cs and ^{57}Co-tracer doped plugs contained a few cubic millimeters of bentonite, which were ion-exchanged to contain 1 MBq of ^{134}Cs and ^{57}Co, respectively. The prepared material was placed in the center of two bentonite plugs. Cylindrical holes were drilled from the north and south side into the outer surface in block A005. The diameter of the holes was 21 mm and the depth was 50 mm, meaning that the doped part was placed close to the center of the bentonite, halfway between the rock and the copper tube. The tracer-doped plugs were placed into the block as the parcel was lowered into the test hole.

The copper samples were placed in tiny slots drilled and sawed from the upper side of the blocks. The copper coupons were placed in the blocks during the pile up of the bentonite column. The samples were pre-characterized and marked with letters, for identification, and with smaller marks for localization during the post test investigation (see Appendix B).

3.5 Instrumentation

3.5.1 General

The basic aim for the field activity in the LOT tests is to expose the bentonite clay to conditions similar to those in a KBS-3 repository, and to expose the clay to adverse physico-chemical conditions, mainly by increasing the temperature. A fundamental demand was therefore to measure the temperature in order to regulate power, and to register the obtained temperature distribution in the whole A0 parcel. Relative humidity, pore-water pressure and swelling pressure reveal the state of saturation and were therefore also measured. An additional objective with the LOT series was to test equipment for the subsequent full scale buffer tests at Äspö. These demands in combination with the relatively limited volume in the clay and the potential risk for artifacts due to the instrumentation led to the following design considerations concerning instrumentation of the A0 parcel:

- 24 thermocouples.
- 3 total pressure gauges.
- 2 water pressure gauges.
- 3 tubes equipped with 3 filters each, i.e. 9 water inlet points, and 1 bottom filter.
- 4 relative humidity sensors.

The gauges and sensors were placed in the parcels as shown in Figure 3-3 and Appendix C.
The equipment was termed in accordance with the following example:

A0084P where

A0 parcel type and the number of the test,

08 block number counted from the bottom,

4 position in the block (according to Section 3.4.4),

P type of measuring equipment.

The following abbreviations of measuring equipment were used:

E temperature in the pressure gauges,

M relative humidity sensors,

P total pressure gauges,

T thermocouples,

W water pressure gauges.

3.5.2 Thermocouples

Temperature was generally measured by thermocouples with a hot junction type J according to IEC 584 standard. Additional temperature information was given by the pressure and humidity sensors, which had thermistors and Pt-100 sensors built-in, respectively. The thermocouples were delivered by BICC Thermoheat Limited, Hedgeley Road, Hebburn, Tyne & Wear NE31 1XR, England. The soldering spots were isolated by a cupro-nickel alloy, which also jacketed the wires up to the tunnel and into the measuring cabinet.

Thermocouples were concentrated in the clay volume around the heater in order to monitor the temperature gradient over the bentonite in detail. Thermocouples were placed in positions 1, 3, 5, 7, and 9 in blocks 08, 14, and 20. In block 14 there was an additional sensor on the copper surface. Three thermocouples were placed in positions 1, 5 and 9 in blocks 2 and 26. One thermocouple was placed in position 5 in blocks 32 and 38, respectively. All measuring soldering points were placed from the upper surface of the blocks, into pre-drilled holes, down to a depth of 35 mm.

Calibration is generally not needed for thermocouples, however, a function control was made by connecting all thermocouples to the actual data collecting system and a check was made that the thermocouples showed the prevailing temperature before installation.

3.5.3 Pressure gauges

Two different types of pressure gauges were used to make redundant pressure measurements: optical gauges in blocks 08 and 20 and vibrating wire gauges in block 14.

The optical gauges, model FOP, were manufactured and delivered by Roctest Ltd, 665 Pine Avenue, Saint-Lambert, Canada. The gauges were delivered with signed individual calibration data sheets and traceability numbers.

The vibrating wire gauges, model no. 4500TI-1500, were manufactured and delivered by Geokon Inc., 48 Spencer St. Lebanon, N.H. 03766, USA. The gauges were delivered with signed individual calibration data sheets and traceability numbers according to ANSI Z540-1.

The water pressure transferred by titanium tubes was measured by external gauges placed in the tunnel above the parcels. The gauges were produced by Druck Limited, Fir tree Lane, Groby, Leicester LE6 0FH, and delivered by AMTELE AB Box 66, SE-12722 Skärholmen, Sweden. Individual data sheets, including gauge serial no, were delivered with the sensors.

The factory calibrations and temperature compensations were used for all three types of pressure gauges in the following presentation of results.

3.5.4 Moisture gauges

The measuring principle for the humidity sensors is electrical capacity change, which principally gives a large measuring span and sufficient accuracy in order to follow the water uptake. The sensors were manufactured by Vaisala Oyj, Vanha Nurmijärventie 21, Fin-01670 Vantaa, Finland. The gauges were delivered with signed individual calibration data sheets. Traceability is guaranteed by the Vaisala Oyj.

The sensors were individually calibrated in order to check the delivery calibration data both with respect to relative humidity and to temperature dependence. The sensors were connected to the actual data collecting system, including all cables etc. The gauges were placed in specially designed plastic boxes, which were partly filled with saturated salt solutions of $(NH_4)_2SO_4$, KCl, $BaCl_2$ and KH_2PO_4. The temperature was kept at 22°C and the equilibrium relative humidity 81.2, 84.8, 90.4 and 94%, respectively, were used for the calibration.

The $BaCl_2$ solution was also used for the temperature compensation calibration, since the humidity equilibrium is relatively stable in the examined temperature range. Temperatures close to 40, 50 and 60°C were used and a linear function, describing apparent dRH as a function of T, was determined for each sensor. No significant differences between the factory calibration and the Clay Technology laboratory calibration were noticed with respect to relative humidity. The factory calibration and temperature compensation were therefore used in the following presentation of results.

3.5.5 Data collection and registration system

All measuring sensors and gauges were connected to DATASCAN units, which in turn were connected to a computer working under Windows NT placed in a cabin close to the test site. The software was named Orchestrator and was manufactured by Eurosoft Technology, UK. MSS AB, Åkersberga, delivered the software and DATASCAN units. The program has a range of output/input drivers and real time data acquisition which among others admitted the use of event-governed logging in addition to periodic logging and alarm functions. The standard logging interval was set to 1 hour during the entire test period. The alarm system was used in order to detect overheating, and the system was connected to the control room at the CLAB facility at the nearby nuclear power plant for 24 h supervision.

A standard interval of 1 hour was used for all collection of data since the course of events was expected to be relatively slow. In addition, an event governed data collection was programmed for each type of measuring equipment. A measurement was automatically triggered in the event that a particular signal exceeded or fell below a fixed value or fixed interval relative to that measured previously. The data acquisition unit was configured to simultaneously acquire data from all channels if an automatic trigger event occurred. Data recording and handling was carried out at three different levels of significance. The data used for regulating the system was considered to be the most important since a serious malfunction could lead to a complete failure of the test. At the second level of importance were the data needed for the evaluation of the test conditions. Thirdly, there were the general interest data which did not affect the success or failure of the test. As a consequence of this hierarchy, different alarm levels were used in the monitoring system.

Required measures were stipulated depending on the type of alarm, ranging from simple log notification to immediate actions from the safety guard at the nuclear power plant.

All recorded data was stored in the specific project computer and backup was regularly made at the Äspö HRL. The standard recorded data concerning temperature, pressure and humidity was copied approximately once a month from Clay Technology and stored in an SQL-database. The data was processed by means of MS EXCEL and thereafter stored in the SICADA database at Äspö.

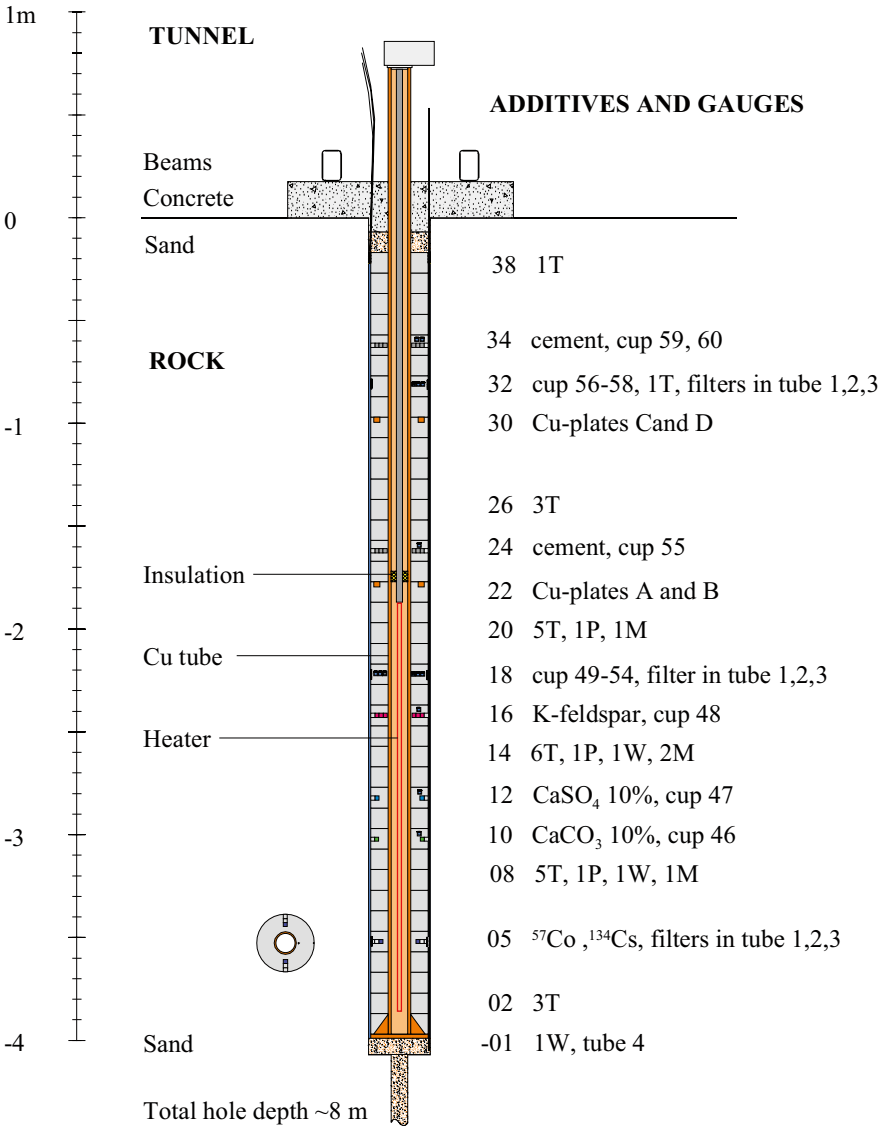

Figure 3-3. *Scaled schematic drawing of the A0 test parcel. Abbreviations are explained in Section 3.4.4 to Section 3.5.4.*

4 Field operation

4.1 Preparation

4.1.1 Parcel assembly

The entire parcel systems were prepared and checked in laboratories in Lund, dismantled and loaded on to a lorry for transport to Äspö HRL. At the test site, the water in the test hole was pumped out and the bottom part was filled with sand up to approximately 10 cm from the bottom of the enlarged hole. The central deep pilot hole with a diameter of 76 mm going down an additional 4 m was thereby also filled with sand. The test hole was covered with a building board and the copper tube was vertically fixed at a bottom support right on top of the test hole. The predestined blocks were thread onto the copper tube from above one by one from a scaffold **(**Figure 4-1).

The gauges and sensors were placed in the prepared cavities before successive blocks were added. The instruments were fixed in position only by overlying blocks. The cable containing tubes from each instrument were placed in slits excavated in the outer surface of the blocks above the instrument. The tubes were fixed during the construction of the parcels, but released during the parcel lowering in order to admit movements during the subsequent swelling of the bentonite. However, a few thin copper wires were used in order to keep the tubes somewhat fixed during the lowering operation (Figure 4-1 left). The various plugs were placed in position after all bentonite blocks were in place. The plugs were fixed and sealed by adding a small amount of water on the outer plug surface before they were pressed into position in the blocks. The tracer test plugs were the last to be placed in order to minimize the risk for contamination with ^{134}Cs and ^{57}Co. The entire mounting procedure of the A0 parcel at the test site was achieved within two days (although long days) since all blocks were prepared and the parcel was partly test built in the laboratory. The installation is described in AP TD F62-99-114.

Figure 4-1. *Example of activities during the lowering of the A0 parcel into the test hole. Left: Check of radiation from the radioactive tracer test plug in block no.5 during the initial lowering of the parcel. The wet spot is due to the small amount of water which was used to seal the test plug. Right: Only the 3 uppermost blocks (36 to 38) remain visible in the tunnel. Note the large number of cable containing tubes from the sensors on the outside of this upper part of the test parcel.*

4.1.2 Installation

The A0 parcel was installed into test hole HG0033G01 on December 16, 1999. The top of the copper tube was connected to the lift device mounted in the roof above the test hole. The parcel was slightly heaved and the bottom support and building board were removed. Water was again pumped out of the test hole, and the parcel was centered and slowly lowered into the test hole. The lowering was somewhat more complicated than for the previous parcels because the test hole was slightly bent. The total lowering operation took approximately 30 minutes. The upper slot between the bentonite and the rock was sealed with mineral insulation (Rockwool) in order to prevent sand falling down into the test hole. An approximately 10 cm thick sand layer was placed over the clay column and the cable containing tubes from all gauges and filters were brought together above the bentonite and fixed. The uppermost 10 cm of the test-hole and a square-formed reinforced concrete top plug were cast. After hardening, the concrete plug was prevented from heaving, due to bentonite swelling and water pressure, by use of two steel beams, which were fixed by 4 rock bolts (Figure 4-2). The sensor and heater cables were connected to measuring and regulating equipment placed in cabinets on top of the test hole, and the cabinets were covered by a simple drip shelter. The measuring equipment was connected to computers in a hut at about 10 m distance. These computers were in turn connected to the general backup system at the Äspö HRL.

4.2 Heating phase

4.2.1 Temperature control

There are in principle two main options to control the temperature in this kind of test, i.e. regulation of the heater power to a fixed value or regulation of the power to provide a defined temperature at a certain position. Constant power best simulates the heat production of spent fuel and constant temperature limits the risk for overheating. The power was first turned on February 2, 2000, and regulated to give a constant maximum temperature of 50°C. The mean value of three thermocouples (A008T1, A014T1 and A020T1) was initially used to govern the power in order to prevent overheating. The maximum temperature target was thereafter increased in steps of 10°C. On April 19, 2000 the regulation was changed to a fixed power of 480 W. The power was thereafter increased in steps to a final power of 850 W which was reached on June 17, 2000.

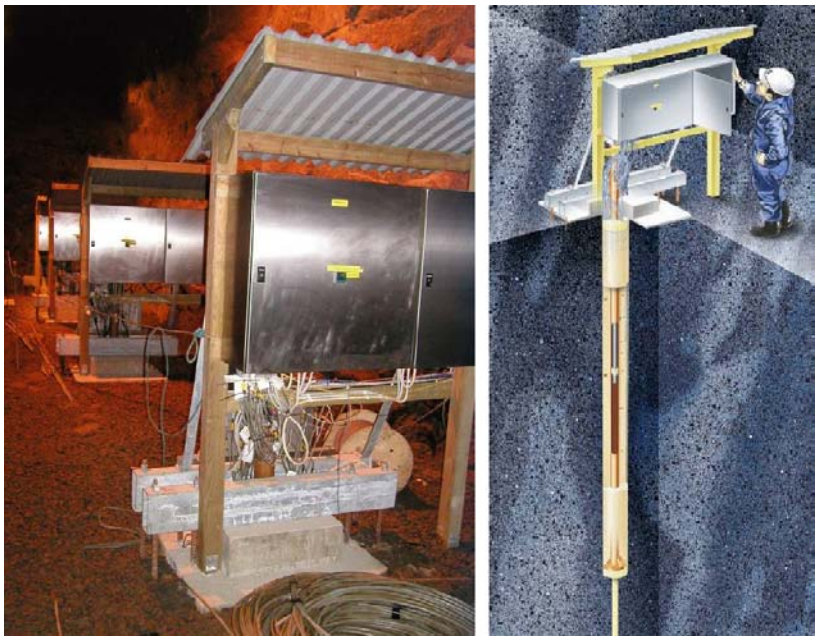

Figure 4-2. *Left: Picture of the test site including 4 test parcels and local data collecting device. The data collecting computers were placed in a hut behind the photographer. Right: Schematic drawing of the final appearance of a test parcel after installation.*

4.2.2 Water supply

The slot between the clay column and the rock was slowly filled with water on February 2, 2000, in parallel with the onset of heating. Ground-water from the water bearing fracture intersecting borehole HG0038B01 was injected through a closed titanium tubing system to the titanium tube and bottom filter (tube no. 4) placed in the sand below the parcel. The valve connected to the bottom filter was closed when there was an outflow in the tunnel of ground-water from the uppermost filters in block 32, which were initially open to atmosphere (Figure 3-3). At this point, the 3 axial tubes with filters were connected to the ground-water supply, and kept open during the entire field exposure time. The 3 tubes were evenly placed along the outside of the parcel (separation angle of 120°). Three titanium filters with a length of 3 cm were welded along the tubes outside blocks 5, 18 and 32, respectively. The 3 water inlet points at each level may be seen as simulating a water bearing fracture at each level. This construction was motivated by the need for a substantial degree of water saturation of the bentonite during the relatively short field exposure time.

4.3 Field results

4.3.1 General

The field regulating and measuring systems worked well during the period of operation, and no malfunction of importance occurred. Most important was that no overheating or unplanned temperature drop took place. Minor incidents with logging units and service stops in logging can be seen in the various results.

4.3.2 Temperature

The temperature recordings were of special importance as this parameter is critical for the reaction rate of chemical processes. The large number (25 thermocouples) of sensors gave a clear picture of the temperature distribution within the parcel. Figure 4-3 shows the measured temperature evolution in the warmest section (blocks 08, 14 and 20). The uppermost curve shows the temperature closest to the copper tube, and the underlying curves show the temperatures of points successively closer to the rock. The lowest curve in each diagram represents a point approximately 1 cm from the rock.

Figure 4-4 (left) shows the temperature distribution in the parcel on October 1, 2001 which is representative for the major part of the field exposure period (cf. Figure 4-3), and Figure 4-4 (right) shows the distribution in the cooled parcel seven days after power termination.

4.3.3 Total and water pressure

The two types of pressure sensors, i.e. optical sensors in blocks 08 and 20 and vibrating wire sensors in block 14, show that the total pressure build up is not finalized at test termination, which is in agreement with the fact that the water pressure has not reached the applied ground-water pressure level of approximately 1.2 MPa (Figure 4-5).

4.3.4 Moisture

High quality moisture measurements are difficult to perform over long time, especially in the very harsh environment in bentonite at high temperature. At full water saturation of the bentonite the fragile moisture sensors normally get contaminated by the saline ground-water. This commonly leads to subsequent erroneous results, which however is a good indicator of full water saturation. Figure 4-6 shows the results from three moisture and accessory temperature sensors from blocks A008, A014 and A020, respectively. All sensors indicate a rather fast increase in humidity to over 90% within a month. A complete failure of the moisture sensors took place in blocks 08 and 14 after approximately 9 months, which indicates full water saturation at their positions. The moisture sensor in block 20 was functioning almost the entire test period, but indicated almost 100% relative humidity, i.e. close to full water saturation. These results are consequently not in full agreement with the indications from the pressure sensors, which indicate an increasing total pressure. The explanation is likely that the moisture measurements represent the local condition at the measuring points, while the results are affected by the conditions in a larger volume including the dryer part closer to the copper tube.

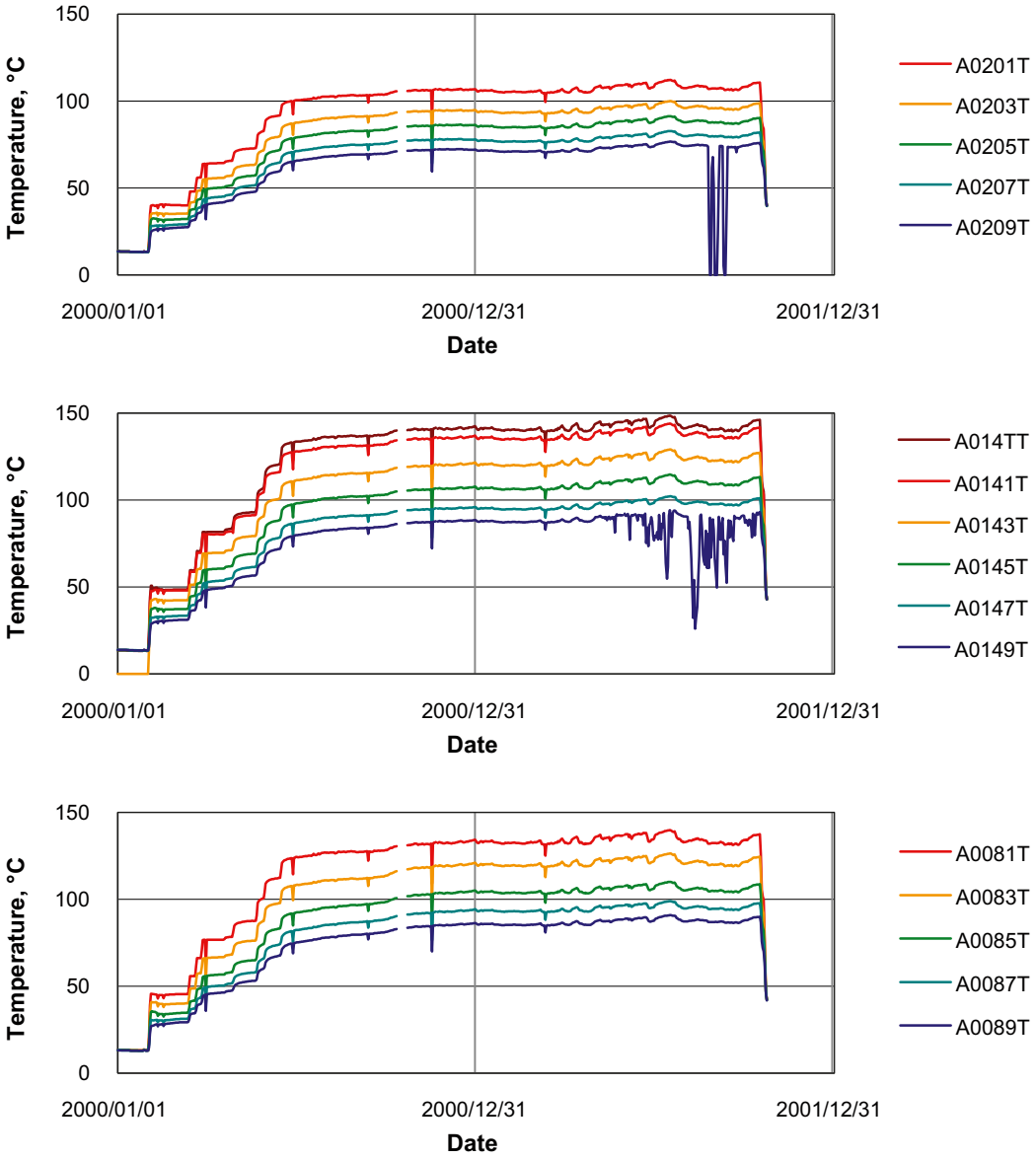

Figure 4-3. *Temperature evolution in blocks 08, 14 and 20. TT in the legend represents temperature of the copper tube surface, 1T represents points approximately 1 cm from the Cu-tube and the underlying curves show the temperatures of points successively 2 cm closer to the rock. The lowest curve represents a point approximately 1 cm from the rock. The large scatter in the thermocouples A0149T and A0209T was due to malfunction of the sampling equipment and do consequently not represent the actual temperatures.*

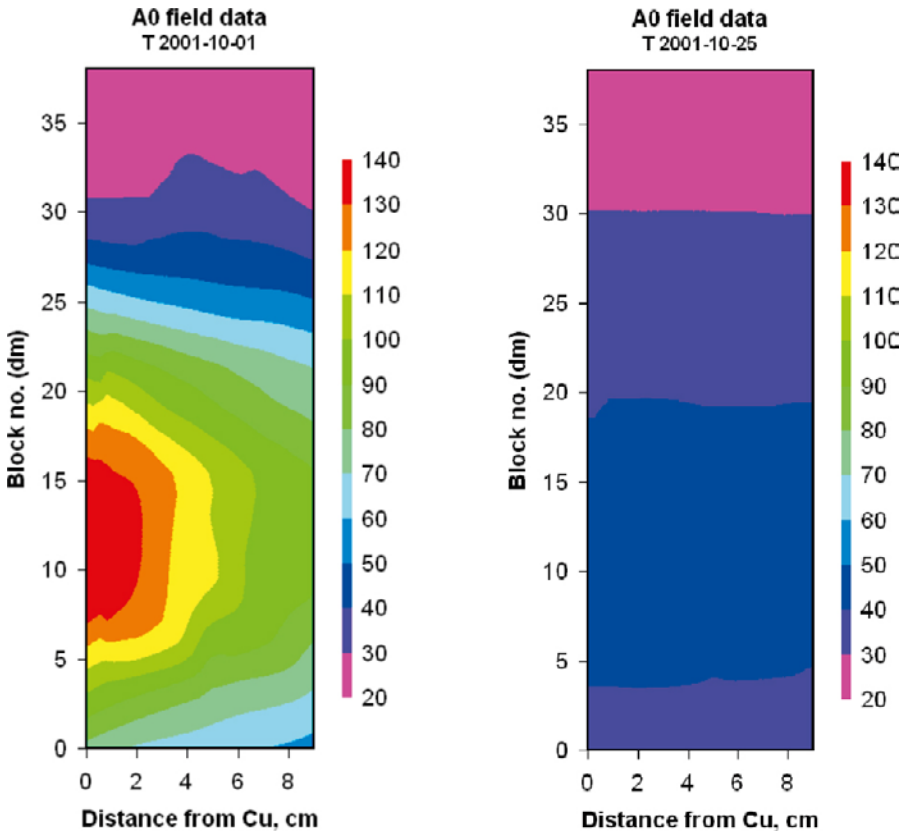

Figure 4-4. *Temperature distribution shortly before termination of the heating, which is also representative for the major part of the field exposure time (left), and temperature distribution one week after power shut off (right).*

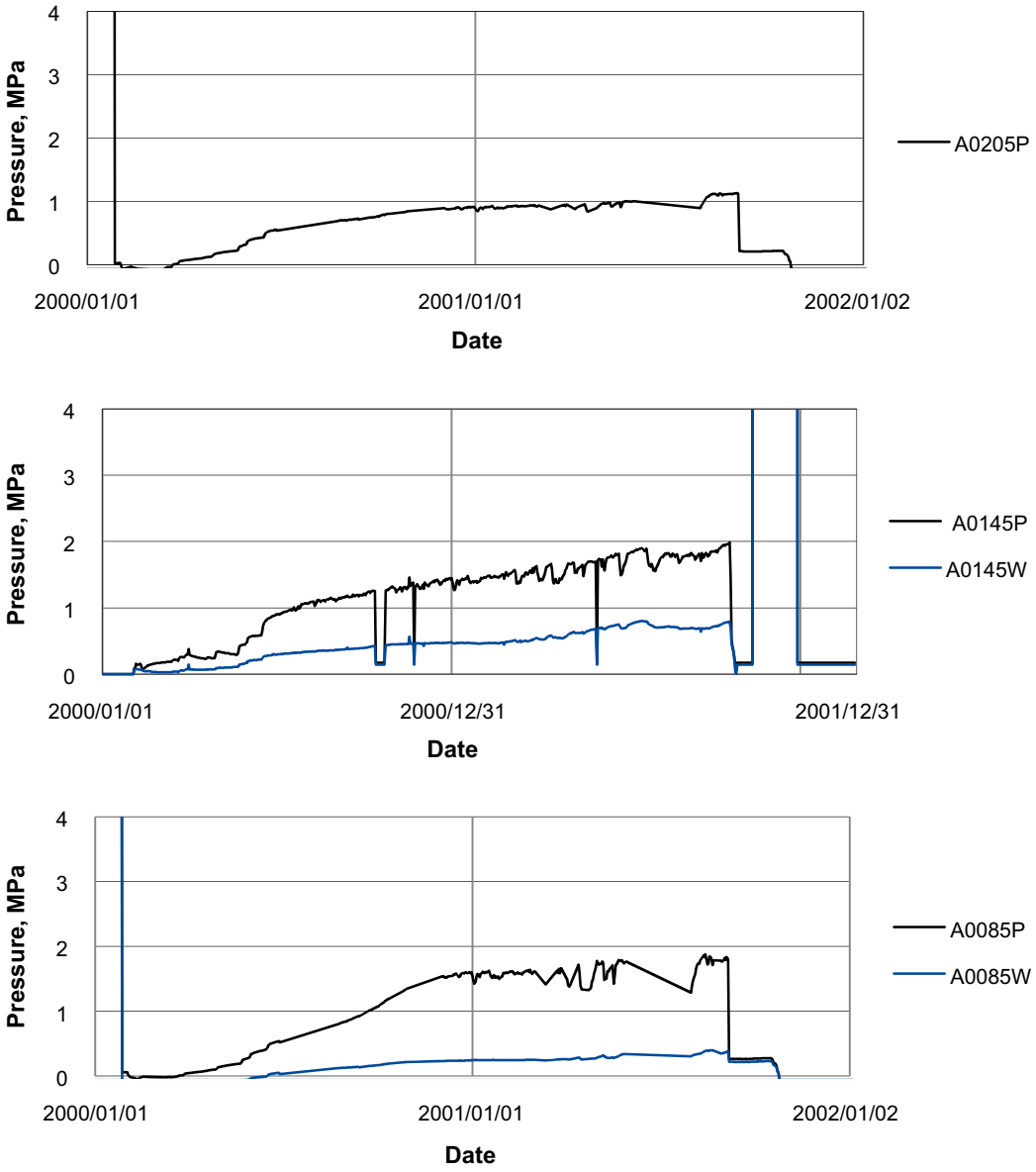

Figure 4-5. *Total pressure (black lines) and water pressure (blue lines) versus time in block 8 (lower) and in block 14 (mid) and total pressure in block 20 (upper), in radial position 5, i.e. at mid position between the copper tube and the rock.*

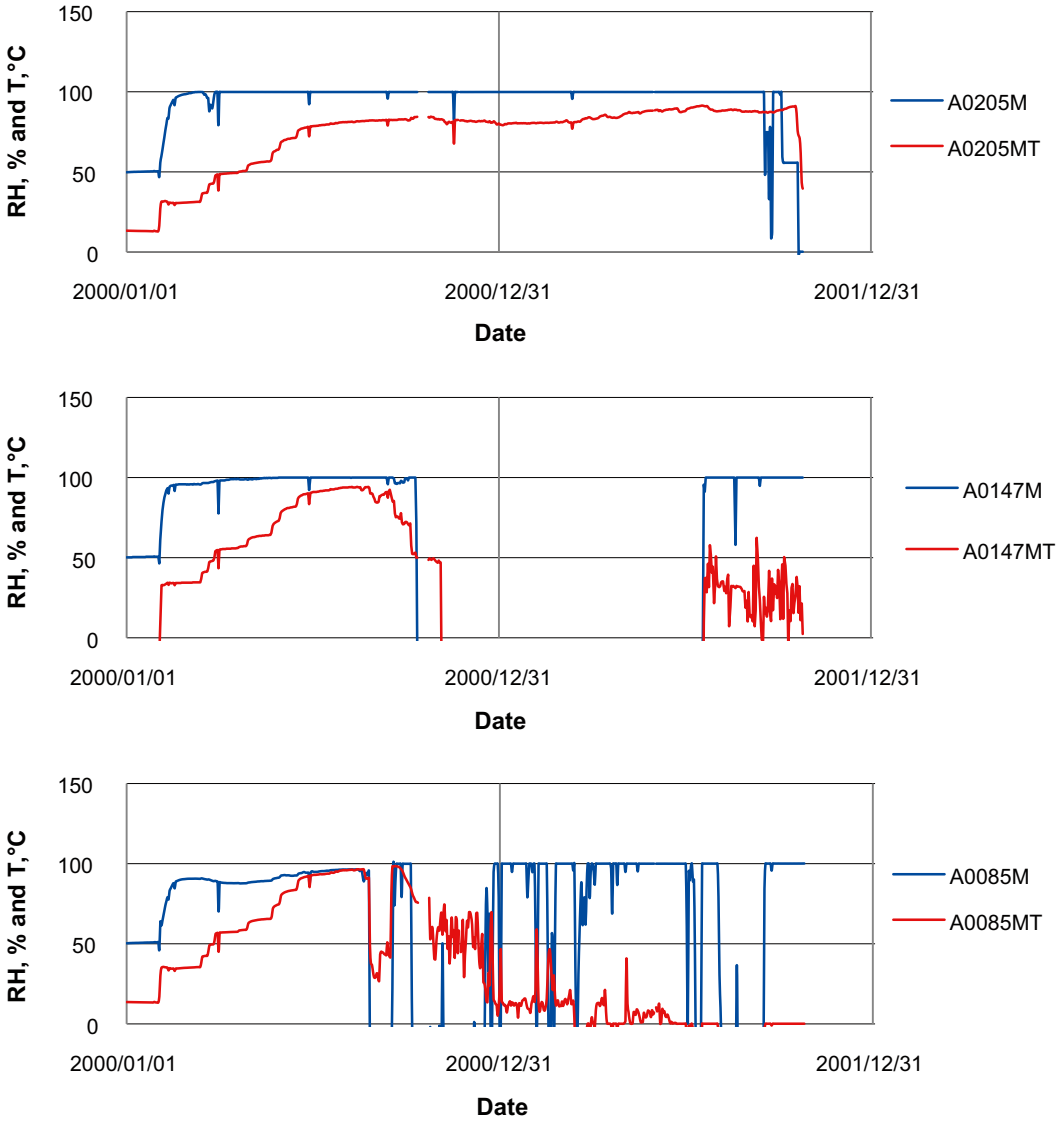

Figure 4-6. *Results from the Vaisala moisture sensors showing temperature (red lines) and the in situ relative humidity (blue lines) in equilibrium with the bentonite in blocks A008, A014 and A020. Large scatter indicates sensor malfunction, which is expected at full water saturation.*

4.4 Termination of the field activity

4.4.1 Termination, drilling and uplift

The heater power was reduced to zero on October 23, 2001. The temperature dropped relatively fast and was below 50°C within one week (Figure 4-4, right). The recovery operation is described in the Äspö HRL activity plan AP TD F62-02-041.

In short, the test parcel was partly released by overlapping percussion drilling in the surrounding rock. The diameter of the boreholes was 76 mm diameter and the depth was around 4.5 m. The boring of the slit was not free of problems, and especially ridges of remaining rock in the bottom of the slit caused a delay of a few days. The final part of the circumference was core drilled with a diameter of 300 mm. The choice of percussion technique was motivated partly by economic reasons, but mostly by the fact that no cooling water was necessary. The core drilling technique was used to finalize the slot around the parcel, since the rock support normally is poor at this stage which makes the steering of a percussion boring head cumbersome. The large diameter of the core drilled holes was motivated by the wire sawing equipment which was used to release the bottom of

the rock column. The released column, containing the test parcel and the rock-cover, was lifted by a crane lorry and transported to a dry niche for examination and sampling. The total weight of the rock/parcel column was around 4,000 kg, and the diameter was around 65 cm, i.e. the rock cover of the test parcel was more than 15 cm in average (Figure 4-7).

4.4.2 Partitioning of the parcel

The removal of the rock cover and subsequent sampling operation started on November 27, 2001 and was finalized after two days of intense work. In short, the surrounding rock was successively removed in approximately 0.5 m long pieces by sawing, wedging, and otherwise exploiting natural weaknesses in the rock (Figure 4-7). The approximate position of the original block interfaces was identified in the exposed bentonite by use of the tubes going in to defined positions and by measuring. The bentonite blocks were cut by sawing and successively removed from the copper tube where this technique was possible. In some parts of the bentonite, the low degree of water saturation resulted in spontaneous breakage of the material resulting in irregular pieces. The blocks and pieces were successively marked and placed in plastic bags. Air was evacuated by use of a vacuum pump, and the bags were closed and placed in plastic boxes. The main part of the material was transported to Clay Technology's laboratory in Lund for analyses and further distribution to the involved laboratories. Special care was taken in handling the blocks aimed for water analyses at VTT and the bottom 6 blocks aimed for ^{134}Cs and ^{57}Co tracer analyses at KTH. The VTT blocks were placed in metal containers, and air was replaced by a nitrogen atmosphere in order to prevent redox reaction during transport. The KTH bottom part of the parcel was placed in a special box for prompt transport to the Department of Nuclear Chemistry at KTH, Stockholm. The blocks containing copper coupons were sealed and delivered to Studsvik AB for analyses after most of the clay analyses were performed at Clay Technology.

Figure 4-7. *Upper left: Placement of the entire parcel on a lorry for transport to a dry niche. Upper right: Removal of the first piece of covering rock. Lower left: Radioactivity check of the uncovered bentonite in the lower part of the parcel. Lower right: Partly water unsaturated bentonite exposed during the sampling of the upper part of the parcel.*

5 Laboratory analyses – general

5.1 Test philosophy

Reference material and material from defined positions in the A0 parcel material were tested and analyzed. The results were compared with respect to changes in physical properties and mineralogy. Since highly accurate quantitative data are difficult to obtain for some of the properties, the aim has been to reveal possible systematic discrepancies between the reference material and parcel material from different positions.

5.2 Test material

The six bottom blocks for the tracer analyses were only analyzed at KTH, Stockholm and the results are presented in Appendix 1. The main part of the blocks was transported to Clay Technology's laboratory, and selected blocks were divided by use of an electric band saw in order to produce test material according to Figure 3-2. The rough partitioning of the clay at the test site enabled a relatively fast and precise sampling of the bentonite. The partition was made within a few days in order to reduce redistribution of elements in the material. The sawn samples were made large enough to admit several tests from a specific position. In other words, material with the same specimen denomination was used for several different kinds of tests and analyses. The denomination of a specific point (center of a volume) was according to the following example:

08ASE3 where

08 block number (counted from the bottom of the parcel),

A vertical level in the block,

SE direction of compass in the test hole (south east in this example),

3 radial distance in centimeters from the previous copper contact surface to the center of the specimen.

6 Basic geotechnical properties

6.1 Test principles

Basic geotechnical properties were determined for a large number of positions in the test material in order to give a general picture of especially density and the water distribution. Block no. 9 and every second block above were analyzed with respect to water-to-solid mass ratio (w). Bulk density (D_b) was measures in 9 blocks. No specific preparation of the test material was made except for sawing specimens to a suitable size with a typical mass of 10 grams or more. The relatively large samples and quick handling after sawing were used in order to minimize drying artifacts.

The main series were taken from the north-western side but duplicates were also taken from the south-eastern side of the blocks. The sample bulk density (D_b = total mass/total volume) was determined by weighing the material in air and submerged in paraffin oil. The bulk density was thereafter calculated according to:

$$D_b = \frac{m \cdot D_{paraffin}}{m_{paraffin}} \qquad \text{Equation 6-1}$$

where m is the mass of the specimen, $D_{paraffin}$ is the density of the paraffin oil, and $m_{paraffin}$ is the mass of displaced paraffin oil, measured as the weight difference between the specimen in air and in paraffin oil. All bulk density results are compiled in Table 6-1.

The water-to-solid mass ratio (w) was determined by drying the material in a laboratory oven at 105°C for 24 h, and the water-to-solid mass ratio was calculated according to:

$$w = \frac{m - m_d}{m_d} \qquad \text{Equation 6-2}$$

where m_d is the mass of the dry sample. All water-to-solid mass ratio results are compiled in Table 6-2.

The degree of saturation (S_r) was calculated from sample density (D_b) and water-to-solid mass ratio (w) according to:

$$S_r = \frac{w \cdot D_b \cdot D_s}{D_w(D_s(w+1) - D_b)} \qquad \text{Equation 6-3}$$

where D_s is the mean grain density, D_w is the water density. A mean grain density of 2,750 kg/m^3 was used for the bentonite (Karnland et al. 2006). All results of calculated degree of saturation are compiled in Table 6-3.

6.2 Results

The results show that there was a significant variation in bentonite density within the parcel. The lower part close to the hot copper tube had the highest density and the uppermost outer part had the lowest density. The bulk density in the warmer part was still significantly lower than the KBS-3 target density due to the relatively low water content in this position. The effects on water saturation of the water supplying filter in blocks 18 and 32 are clearly indicated in the water content results (Figure 6-1 and Table 6-2).

The raw and calculated data are stored in Excel files and transferred to the SICADA database. The individual specimens were denominated according to the general description scheme. A typical denomination of a specimen is consequently A038BNW1b, where A0 is the parcel, 38 is the block number, B is the mid height in the block, NW is the north-western direction, 1 is the radial position, and finally the b denotes that it concerns the bulk material.

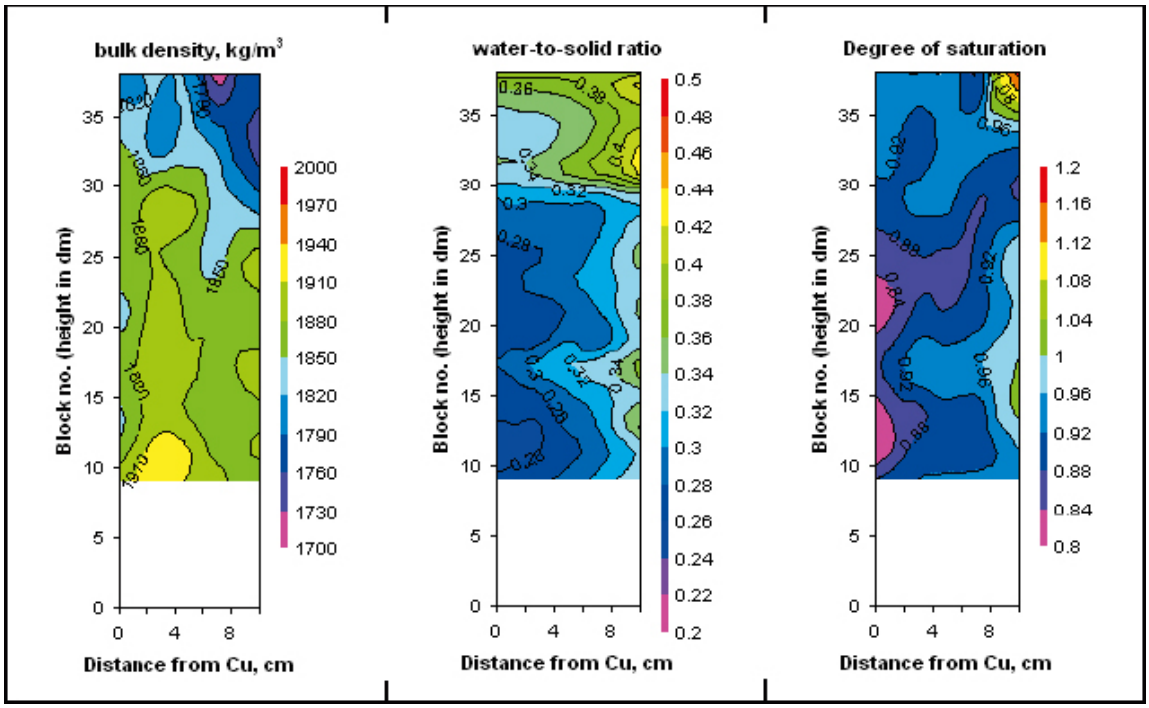

Figure 6-1. *Bulk density (left), water-to-solid mass ratio (center) and degree of water saturation (right) in the LOT A0 parcel.*

Table 6-1. Measured bulk density in kg/m³ of blocks 09 to 37 in parcel A0.

Block no.	Position, in cm from Cu tube				
	1	3	5	7	9
37	1,815	1,819	1,819	1,736	1,771
33	1,844	1,803	1,832	1,812	1,765
29	1,870	1,891	1,885	1,838	1,814
25	1,876	1,880	1,862	1,841	1,878
21	1,852	1,902	1,876	1,869	1,871
17	1,880	1,898	1,884	1,874	1,882
13	1,866	1,900	1,886	1,856	1,874
11	1,886	1,932	1,914	1,873	1,877
9	1,913	1,925	1,908	1,891	1,861

Table 6-2. Measured water-to-solid mass ratio of blocks 09 to 38 in parcel A0.

Block no.	Position, in cm from Cu tube				
	1	3	5	7	9
38	0.396	0.391	0.390	0.386	0.390
37	0.364	0.366	0.373	0.388	0.412
35	0.337	0.339	0.347	0.362	0.383
33	0.336	0.333	0.348	0.368	0.403
31	0.336	0.346	0.366	0.384	0.404
29	0.303	0.302	0.305	0.306	0.324
27	0.291	0.294	0.293	0.296	0.318
25	0.272	0.278	0.287	0.306	0.333
23	0.277	0.289	0.297	0.310	0.325
21	0.268	0.269	0.281	0.298	0.330
19	0.272	0.273	0.298	0.281	0.317
17	0.285	0.307	0.319	0.331	0.349
15	0.269	0.279	0.298	0.309	0.329
13	0.261	0.260	0.286	0.301	0.341
11	0.249	0.259	0.273	0.289	0.313
9	0.268	0.274	0.288	0.304	0.325

Table 6-3. Calculated degree of saturation of blocks 09 to 37 in parcel A0.

Block no.	Position, in cm from Cu tube				
	1	3	5	7	9
37	0.94	0.95	0.95	0.89	1.09
33	0.93	0.89	0.94	0.94	0.93
29	0.91	0.93	0.93	0.88	0.88
25	0.86	0.88	0.88	0.88	0.96
21	0.84	0.89	0.88	0.90	0.95
17	0.89	0.94	0.95	0.95	0.99
13	0.84	0.87	0.90	0.89	0.97
11	0.83	0.90	0.90	0.89	0.93
9	0.90	0.92	0.92	0.93	0.93

7 Sealing properties

7.1 Test principles

The hydraulic conductivity and swelling pressure were determined in combined tests on material chosen from strategic positions within the test parcel and on the corresponding reference material. The test series included the following sub-series, and all the samples are summarized in Table 7-1:

- Reference material, air-dried and compacted, Äspö-water, 5 samples.
- Parcel material, air-dried and crushed to a grain size similar to the original MX-80 powder and re-compacted to a density of 2,000 kg/m^3, Äspö-water, 5 samples.
- Parcel material, naturally saturated, sawn and trimmed to fit the test cells, and the tested samples thus had a slightly lower density than the field value. Äspö-water, 5 samples.

Five purpose-built swelling pressure test cells were used (Figure 7-1). The samples were confined by cylinder rings with a diameter of 20 mm and stainless steel filters at the top and bottom. The test volumes were sealed by o-rings placed between the bottom plates and the cylinder rings, and between the pistons and the cylinder rings. At test start the height of the test volumes was fixed to 10 mm by the flanges on the moveable pistons. The axial force from a sample was determined by the transducer placed between the piston and the upper lid.

The Äspö test solution was initially circulated below the lower filter in order to let air out through the upper filter during the saturation. The water uptake was indirectly monitored by the force transducer (Figure 7-1). The solution was circulated also above the upper filter when the swelling pressure had stabilized, which normally took place within 1 week. At this point a water pressure of maximum 50% of the measured swelling pressure was applied in the bottom filter in order to establish percolation. The volumes of the percolated water solution were registered daily by visual observations of the water/air interface meniscus until stable flow conditions were reached, typically 7 days. The water pressure was thereafter reduced to zero and the tests were terminated when the recorded axial forces had stabilized.

The swelling pressure P_s (Pa) was calculated from the measured force at zero water pressure according to:

$$P_s = \frac{F}{A} \qquad \text{Equation 7-1}$$

where F is the axial force (N) and A is the sample area acting on the piston (m^2). The accuracy of the measured values is governed by the force transducers which were calibrated against a standard force ring before and after each test.

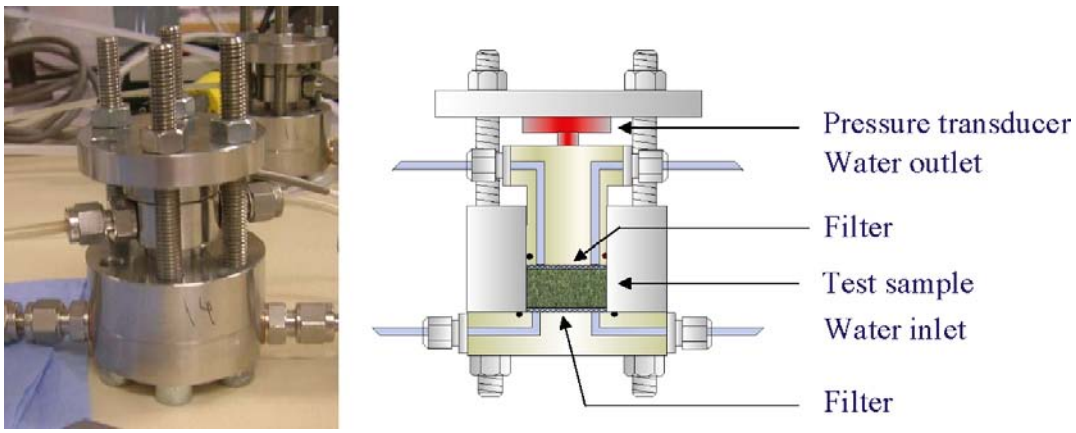

Figure 7-1. *Photo and schematic drawing of the test cell used for determination of swelling pressure and hydraulic conductivity.*

The hydraulic conductivity k (m/s) was evaluated from the percolated water volume according to Darcy´s law:

$$k = \frac{V \cdot l}{A \cdot h \cdot t}$$ Equation 7-2

where V is the percolated volume (m^3), l is the sample length (m), A is the sample area (m^2), h is the water pressure difference over the sample expressed as water column (m) and t is the time (s).

At test termination, the samples were split in two halves and the sample bulk density (D_b) and water-to-solid mass ratio (w) were determined by the technique described in Section 6.1. The samples may be considered fully water saturated due to the test conditions, and the dry density, void ratio and porosity can be calculated since the grain density is known.

7.2 Results

Measured swelling pressures and hydraulic conductivities are presented in Table 7-1.

The scatter in density of the sawn and trimmed samples are likely due to the preparation technique and are not directly related to the previous field conditions (Figure 7-2). No differences were found in the results for samples from warm positions compared to those from the upper cool positions or from the reference material. The results for the A0 parcel are also in good agreement with previously measured results for the A1 parcel and reference material (Karnland et al. 2000).

There is a minor but significant shift in hydraulic conductivity as a function of density between trimmed and re-compacted samples (Figure 7-3). There is, however, no significant difference between samples from different positions in the parcel. The slightly lower conductivity in the trimmed samples can consequently not be related to temperature or temperature gradients.

The raw and calculated data have been stored in Excel files and transferred to the SICADA database. The test series was termed LA0OE and the individual specimens were denominated according to the general scheme, e.g. LA011SW8.

Table 7-1. Results from swelling pressure and hydraulic conductivity tests. Äspö ground-water from bore-hole HG0038B01 was used in all tests.

Test material	Preparation	Water-to-solid mass ratio, w	Bulk Density, D_b	Swelling pressure, P_s	Hydraulic conductivity, C_h
LA0R	air-dry	0.86	1,594	20	1.54E–10
LA0R	air-dry	0.44	1,792	520	1.22E–12
LA0R	air-dry	0.36	1,906	2,200	3.01E–13
LA0R	air-dry	0.27	1,988	8,100	8.78E–14
LA0R	air-dry	0.23	2,055	18,400	5.91E–14
LA011SW2	re-compacted	0.30	1,973	4,410	1.29E–13
LA011SW8	re-compacted	0.30	1,951	4,690	1.39E–13
LA015SW2	re-compacted	0.30	1,964	4,540	1.29E–13
LA015SW8	re-compacted	0.29	1,966	5,270	1.15E–13
LA033SW2	re-compacted	0.29	2,001	4,980	1.31E–13
LA011SW2	trimmed	0.33	1,957	3,500	1.61E–13
LA011SW8	trimmed	0.37	1,889	2,250	1.64E–13
LA015SW2	trimmed	0.33	1,951	2,800	1.84E–13
LA015SW8	trimmed	0.36	1,900	2,900	1.56E–13
LA033SW2	trimmed	0.36	1,900	2,200	1.74E–13

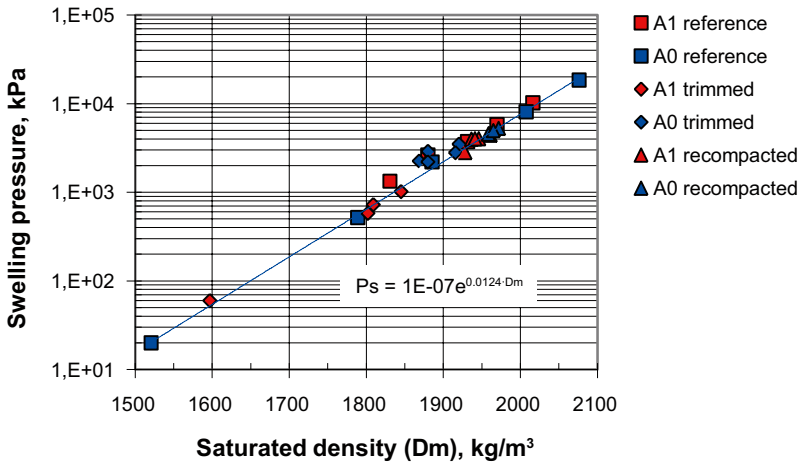

Figure 7-2. *Measured swelling pressure results from the A0 parcel material, reference material and from the previous A1 test material (Karnland et al. 2000). The blue line indicates the Excel generated best fit line for the A0 reference results. Ps indicates swelling pressure and Dm indicate saturated sample density.*

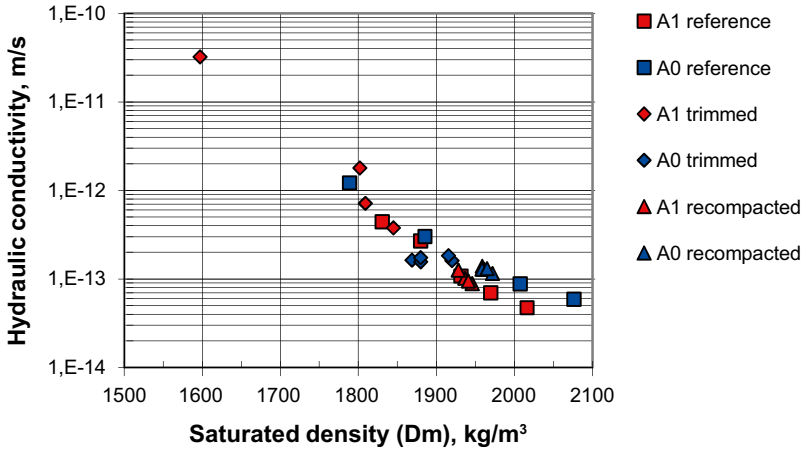

Figure 7-3. *Measured hydraulic conductivity results for the A0 parcel material, reference material and the previously reported A1 material (Karnland et al. 2000).*

8 Mineralogy and chemical composition

8.1 Materials and methods

8.1.1 Sampling and sample nomenclature

Two blocks, 11 and 15, from the hot section and block 33 from the cool section of the parcel have been analyzed. The position of the blocks within the parcel is shown in Figure 3-3. The entire volume of blocks 11 and 15 has been exposed to temperatures > 80ºC, and the innermost 4 centimeters to temperatures exceeding 100ºC. Block no. 33 was never exposed to temperatures exceeding 35ºC. The temperature evolution in the hot zone during the test period is shown in Figure 4-3.

The blocks were sampled contiguously at five positions along the radius at mid height in the blocks (B-level) according to Figure 3-2 by use of a band saw. Bentonite used for and stored since the fabrication of the blocks has been used as reference material.

The analytical test protocol is summarized in Table 8-1, where individual samples have been given an identity code according to the general nomenclature, e.g. A011BSE1b means that the sample is from the LOT **A0** parcel, block no. **11**, level **B** of the **S**outh-**E**astern sector of the block, radial position **1,** and the **b**ulk of the material has been analyzed (**c** is used if the material analyzed is the clay fraction). The identity code of the corresponding reference sample is A011Rb (A011Rc for the clay fraction).

8.1.2 Sample preparation

Both the bulk material and the clay fraction (< 2 μm) of the bentonite samples have been analyzed when relevant (cf. Table 8-1). The bulk material was not subject to any pre-treatments prior to the analyses, apart from drying at 60ºC and grinding.

The fraction < 2 μm was separated by centrifuged sedimentation. Approximately 10 g of the bulk material was dispersed in 1 L deionized water by stirring and ultrasonic treatment. After dispersion of the bentonite, the suspension was left to rest for 10 minutes to allow sedimentation of the coarsest particles. The supernatant was thereafter collected in centrifuge bottles and centrifuged at 850 revolutions/minute, i.e. rpm, for 5 minutes. The centrifugation time and speed required for sedimentation of particles > 2 μm was calculated by use of the integrated form of Stokes´ Law. After centrifugation the supernatants were collected in plastic containers and concentrated by evaporation at 60°C in a ventilated oven.

8.1.3 Chemical analysis of the bentonite

The chemical composition of the reference and the parcel bentonite was determined by ICP emission spectrometry (AES) and ICP mass spectrometry (MS) at an ISO 9001 certified laboratory (ACME Analytical Laboratories, Canada), using standard techniques for silicate analysis (fusion with $LiBO_2$ followed by nitric acid digestion). These analyses include major (Si, Al, Fe, Ca, Mg, K, Na, Mn, P, Ti), minor and trace elements (Ba, Co, Cr, Cu, Mo, Nb, Ni, S, Sc, Sn, Sr, V, W, Y, Zn, Zr). Loss on ignition (LOI) was determined as the difference in weight of the dried (105ºC) and ignited (1,000ºC) sample.

Total carbon and sulfur were determined by evolved gas analysis (EGA) at the same laboratory by combustion of the samples in a Leco furnace, equipped with IR-detectors for CO_2 and SO_2.

All samples were ground, dried at 105ºC and stored in desiccators prior to the analysis, i.e. all analytical results are expressed in wt% (major oxides) or ppm (trace elements) of the dry mass of the sample. The data have been stored as Excel files in a matrix in which concentration values are given for each parcel position using an identity code according to the general nomenclature and transferred to the SICADA database.

Table 8-1. Sample nomenclature and analytical test protocol for reference material and the blocks 11, 15, and 33 of the LOT A0 parcel.

	Chemical analysis	Cation exchange capacity	Exchangeable cations	X-ray diffraction analysis		Aqueous leaching
SICADA test code b=bulk;c=clay fraction	LA0EA b/c	LA0CEC b/c	LA0EC b	LA0XRD b/c		LA0WA b
Sample identity				random	oriented	
Reference bentonite samples						
A011Rb	X	X	X	X		X
A011Rc	X	X			X	
A015Rb	X	X	X	X		X
A015Rc	X	X			X	
A033Rb	X	X	X	X		X
A033Rc	X	X			X	
Block samples						
A011BSE1b	X	X	X	X		X
A011BSE1c	X	X			X	
A011BSE3b	X	X	X	X		X
A011BSE3c	X	X			X	
A011BSE5b	X	X	X	X		X
A011BSE5c	X	X			X	
A011BSE7b	X	X	X	X		X
A011BSE7c	X	X			X	
A011BSE9b	X	X	X	X		X
A011BSE9c	X	X			X	
A015BSE1b	X	X	X	X		X
A015BSE1c	X	X			X	
A015BSE3b	X	X	X	X		X
A015BSE3c	X	X			X	
A015BSE5b	X	X	X	X		X
A015BSE5c	X	X			X	
A015BSE7b	X	X	X	X		X
A015BSE7c	X	X			X	
A015BSE9b	X	X	X	X		X
A015BSE9c	X	X			X	
A033BSE1b	X	X	X	X		X
A033BSE1c	X	X			X	
A033BSE3b	X	X	X	X		X
A033BSE3c	X	X			X	
A033BSE5b	X	X	X	X		X
A033BSE5c	X	X			X	
A033BSE7b	X	X	X	X		X
A033BSE7c	X	X			X	
A033BSE9b	X	X	X	X		X
A033BSE9c	X	X			X	

8.1.4 Cation exchange capacity (CEC) and exchangeable cations (EC)

The cation exchange capacity (CEC) of bulk materials and of clay fractions was determined by exchange with Cu(II)-triethylenetetramine following the procedure of (Meier and Kahr 1999) slightly modified. The ground sample (400 mg), dried at 70ºC, was dispersed in 50 ml deionized water by ultrasonic treatment and shaking overnight. 20 ml of 15 mM Cu(II)-triethylenetetramine solution was added to the suspension, which was left to react for 30 minutes on a vibrating table. After centrifugation the absorbance at 620 nm of the supernatant was measured using a double-beam spectrophotometer (Perkin Elmer Lambda 3). CEC was calculated on the basis of the uptake of Cu by the clay and is presented in milliequivalents per 100 g (meq/100 g). All CEC determinations were duplicated.

The exchangeable cations of the bulk bentonite were also extracted into alcoholic ammonium chloride solution (0.15 M NH_4Cl in 80% ethanol) according to a procedure originally recommended for CEC determinations of gypsiferous/calcareous soils (e.g. Belyayeva 1967, Jackson 1975). An alcoholic solution is used to minimize dissolution of gypsum and calcite, which are soluble or relatively soluble in aqueous solutions. Ideally, i.e. when the dissolution of easily soluble salts such as chlorides and carbonates of alkali metals is low, the sum of cations extracted should be equivalent to the CEC of the sample.

0.8 g of the ground sample, dried at 70ºC, was shaken for 30 minutes in approximately one third of a total volume of 50 ml of the extractant. After centrifugation the supernatant was collected in a volumetric flask. The treatment was repeated three times. The concentration of Ca, Mg, Na and K in the extracts was determined by use of an ICP-AES equipment at the Department of Ecology, Lund University. The concentration of exchangeable cations is presented in milliequivalents per 100 g (meq/100 g).

The results have been delivered in Excel files from the laboratories involved as a matrix in which calculated CEC values/exchangeable cation concentrations are given for each parcel position using an identity code according to the general scheme and transferred to the SICADA database.

8.1.5 Aqueous leachates

Aqueous leaching of the bulk samples was used to obtain information about the pore water composition and the spatial distribution of soluble/sparingly soluble salts within the blocks. The ground and dried (105ºC) bentonite was dispersed in deionized water (solid:solution ratio 1:100) by ultrasonic treatment for 30 minutes and stirring overnight. The suspension was left for 5 days at room temperature to allow equilibration. The supernatant was collected in centrifuge bottles and centrifuged at 3,000 rpm for two hours prior to analysis. Major cations were determined by ICP-AES and anions by use of ion chromatography (IC) at the Department of Ecology, Lund University. The results have been delivered from the laboratory in Excel files in which concentration values are given for each parcel position and transferred to the SICADA database.

8.1.6 X-ray diffraction analysis

The mineralogical composition was determined by X-ray diffraction analysis of two different types of preparations, one type consisting of unsorted and randomly oriented powders of the bulk materials, the other type consisting of aggregates of the fraction < 2 μm with maximized preferred orientation of the clay minerals.

The random powder produces reflections of all crystalline minerals and is needed for a general characterization of the material. Also the distinction between di- and trioctahedral types of clay minerals by measurements of d(060) requires an X-ray diffraction profile of a randomly oriented sample.

The bulk material was ground in an agate mortar to a grain-size < 10 μm and the powders were stored at room temperature at ambient relative humidity prior to X-ray scanning. The random powders were scanned with a step size of 0.02º 2θ in the 2θ interval 2–66°.

The oriented specimen of the clay fraction gives strongly enhanced basal (*00l*) reflections, and little or no evidence of the hk reflections of clay minerals. This type of preparation is useful for identification of the clay minerals and is used for tests of the swelling properties of the clay after the clay has been solvated with a polyalcohol, such as ethylene glycol. However, the diffraction characteristics of smectites both in the air-dried and the ethylene glycol solvated state depend on the type of charge-balancing cations. Therefore, in order to give unambiguous diffraction characteristics, all clay samples were saturated with one single cation (Mg) prior to the X-ray scanning.

The clay fractions were deflocculated in deionized water, saturated with Mg (0.5M $MgCl_2$) and thereafter washed free of excess salt by centrifuge-washing with water. Oriented aggregates were prepared of the clay slurry by the "smear-on-glass" method (Moore and Reynolds 1989) and dried at room temperature. The oriented mounts were X-ray scanned with a step size of 0.02º 2θ in the 2θ interval 3–10°. In order to test the swelling properties the samples were re-scanned after solvation with ethylene glycol (EG) at 60ºC for 48 hours.

A Seiffert 3000 TT X-ray diffractometer equipped with automatic slits and a Cu-tube operated at 50kV/30mA was used for the X-ray diffraction analyses.

The results have been stored as Excel files in which the intensity values and the corresponding 2θ values are listed and transferred to the SICADA database. The code for the sample positions follows the general scheme.

8.2 Results

8.2.1 Aqueous leachates

The chemical data on non-reactive solutes and water-soluble salts are given in Table 8-2 together with the concentration of major anions and cations of the groundwater in the borehole used for water supply (HG0038B01), sampled in 2000 and 2001. Focus is laid on the major anions, chloride and sulfate, since the concentration of the cations is strongly affected by the exchange reactions that take place when divalent cations are released from dissolving minerals during the contact with water. Moreover, some of the cations included in the analysis originate from suspended ultra-fine clay particles which did not settle during centrifugation. Evidence for this contribution is a strong correlation between elements existing in the clay mineral structure (e.g. R^2=0.92 between Al and Fe) and also the fact that their concentrations are at a minimum in samples with maximum sulfate concentrations, because dissolution of salts during the extraction promoted flocculation and sedimentation of clay particles.

The radial concentration profiles of chloride and sulfate, expressed as the molar concentration of the pore water, are presented in Figure 8-1. The water-to-solid ratios given in Table 6-2 were used to calculate these concentrations. Chloride displays a fairly regular distribution in all three blocks but the concentration has increased compared with the chloride concentration of the reference bentonite. Thus, the groundwater is the essential source of chloride, but the concentration in the pore water is lower than that of the groundwater at Äspö.

In contrast, the sulfate concentration of the pore water in all blocks is significantly higher than that of the Äspö groundwater. Accordingly, the essential source must be the inventory of calcium sulfate initially present in the parent bentonite MX-80 as gypsum. The concentration in the cool block no. 33 is fairly constant and in the same range as that of the reference bentonite. Both hot blocks display an irregular distribution pattern with maxima 2-4 cm from the central heater and minima in the peripheral parts of the blocks, where the concentration is lower than that of the reference samples. Thus, it is evident that sulfate has been redistributed along the thermal gradient in the hot blocks. The spatial distribution pattern is confirmed by other chemical data (8.2.4) and by the XRD analysis (8.2.5), which shows that the re-precipitated sulfate in the hot zone is anhydrite ($CaSO_4$).

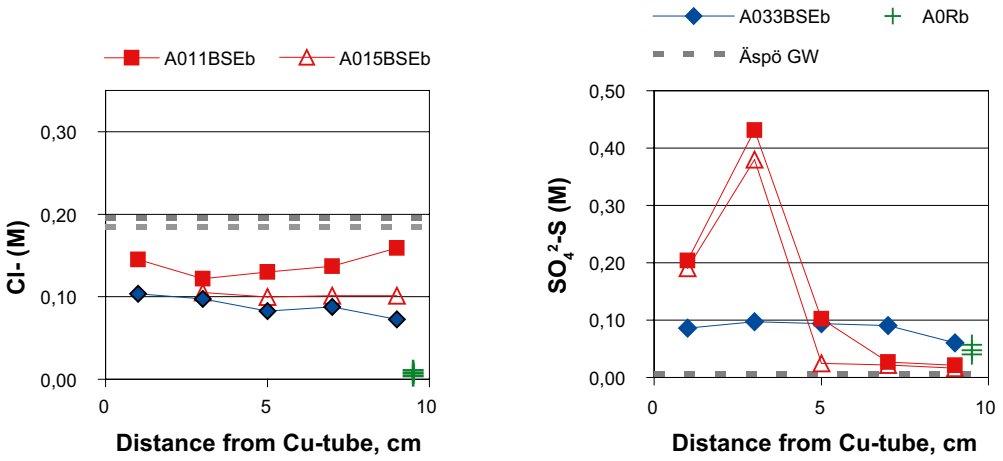

Figure 8-1. *The radial distribution of Cl –and SO_4^{2-}S (in M) in water extracts of bulk samples from blocks 11, 15 and 33 of the LOT A0 parcel. The concentration in three reference samples (A0Rb) is shown at position 9.5 cm. Broken lines show the concentration in the groundwater at Äspö.*

Table 8-2. Major anions and cations (mg/g dry clay) extracted by dispersion of bentonite in deionized water in a solid to liquid ratio of 1:100. Data for blocks 11, 15 and 33 from the LOT A0 parcel together with the corresponding reference samples. Included is also the concentration of major anions and cations in Äspö groundwater sampled in borehole HG0038B01 in 2000 and 2001.

Sample id	Al	B	Ba	C-inorg.	C-org	Ca	Cl^-	Cu	Fe	K	Mg	Mn	Mo	Na	NO_3^--N	Ni	P	PO_4^{3-}-P	Pb	S	SO_4^{2-}-S	Si	Sr	Ti	Zn	$[HCO_3^-]$
	mg/g dry clay																									mM
A011BSE1	8.7	0.05	0.00	0.41	0.28	0.50	1.38	0.06	2.25	0.23	1.46	0.00	0.01	5.02	0.01	0.00	0.01	0.00	0.00	1.86	1.75	15.12	0.02	0.05	0.01	0.41
A011BSE3	6.7	0.03	0.00	0.41	0.17	0.69	1.24	0.00	1.65	0.37	1.10	0.00	0.00	7.82	0.01	0.00	0.00	0.00	0.00	4.42	3.97	12.18	0.02	0.04	0.00	0.37
A011BSE5	18.0	0.09	0.03	0.74	0.26	1.09	1.27	0.00	4.27	0.32	2.57	0.01	0.00	5.82	0.01	0.01	0.00	0.00	0.00	0.92	0.90	31.58	0.05	0.11	0.01	0.73
A011BSE7	24.3	0.12	0.00	0.69	0.30	1.20	1.48	0.00	5.92	0.37	3.41	0.01	0.00	6.11	0.01	0.01	0.00	0.00	0.00	0.27	0.26	43.94	0.04	0.14	0.01	0.66
A011BSE9	25.9	0.13	0.01	0.91	0.48	1.36	1.84	0.01	6.25	0.39	3.59	0.02	0.00	6.32	0.01	0.02	0.00	0.00	0.01	0.22	0.22	47.34	0.04	0.16	0.01	0.79
A015BSE1	5.5	0.02	0.00	0.47	0.09	0.30	0.00	0.05	1.18	0.16	0.77	0.00	0.00	4.47	0.00	0.00	0.02	0.01	0.00	1.52	1.52	12.44	0.01	0.03	0.00	0.39
A015BSE3	5.3	0.02	0.00	0.39	0.14	0.43	0.97	0.01	1.19	0.26	0.75	0.00	0.00	6.18	0.00	0.00	0.00	0.00	0.00	3.17	3.15	11.91	0.01	0.03	0.00	0.38
A015BSE5	15.1	0.06	0.00	0.68	0.18	0.66	0.96	0.00	3.25	0.21	1.94	0.01	0.00	3.78	0.01	0.00	0.01	0.00	0.00	0.22	0.22	32.27	0.02	0.08	0.00	0.61
A015BSE7	16.9	0.07	0.01	0.85	0.17	0.78	1.04	0.00	3.68	0.22	2.11	0.01	0.00	4.46	0.00	0.01	0.01	0.00	0.00	0.20	0.20	37.66	0.03	0.09	0.00	0.79
A015BSE9	15.8	0.07	0.01	0.79	0.18	0.77	1.12	0.00	3.46	0.22	2.08	0.01	0.00	4.15	0.01	0.01	0.01	0.00	0.00	0.16	0.16	35.45	0.03	0.09	0.00	0.78
A033BSE1	24.9	0.12	0.02	1.04	0.23	1.68	1.23	0.04	5.16	0.44	3.69	0.01	0.00	6.21	0.01	0.01	0.02	0.00	0.01	1.04	0.92	57.73	0.05	0.15	0.01	1.08
A033BSE3	23.2	0.11	0.01	1.06	0.19	1.55	1.15	0.00	4.81	0.38	3.30	0.01	0.00	6.16	0.01	0.01	0.01	0.01	0.01	1.13	1.04	53.41	0.05	0.13	0.01	1.18
A033BSE5	23.3	0.10	0.01	0.96	0.18	1.40	1.02	0.00	4.42	0.35	3.03	0.01	0.00	6.13	0.01	0.01	0.01	0.00	0.01	1.09	1.05	54.15	0.05	0.12	0.01	1.03
A033BSE7	25.4	0.10	0.01	1.04	0.19	1.42	1.15	0.00	4.48	0.37	3.09	0.01	0.00	7.61	0.01	0.01	0.01	0.00	0.01	1.20	1.07	58.48	0.05	0.12	0.01	1.10
A033BSE9	27.1	0.10	0.01	0.99	0.30	1.40	1.04	0.02	4.68	0.32	3.15	0.01	0.00	6.78	0.01	0.02	0.02	0.00	0.01	0.79	0.78	64.18	0.05	0.13	0.01	1.01
A011R	7.9	0.03	0.00	0.71	0.15	0.38	0.13	0.00	1.54	0.15	0.97	0.00	0.00	2.94	0.01	0.00	0.00	0.00	0.00	0.53	0.51	18.04	0.01	0.04	0.00	0.64
A015R	8.1	0.03	0.00	0.72	0.17	0.38	0.09	0.00	1.52	0.12	0.97	0.00	0.00	3.05	0.02	0.00	0.00	0.00	0.00	0.64	0.63	18.61	0.01	0.04	0.00	0.72
A033R	7.5	0.03	0.00	0.67	0.16	0.35	0.06	0.00	1.43	0.12	0.93	0.00	0.00	2.66	0.01	0.00	0.00	0.01	0.00	0.53	0.52	17.17	0.01	0.04	0.00	0.66

Äspö GW	Na	K	Ca	Mg	HCO_3	Cl	SO_4	SO_4-S	Br	F	Si	Fe_{tot}	Fe(II)	Mn	Li	Sr	pH	Conduct.	DOC	NH_4-N
year	mg/L	mg/L	mg/L	mg/L	mg/L	mg/L	mg/L	mg/L	mg/L	mg/L	mg/L	mg/L	mg/L	mg/L	mg/L	mg/L		mS/m	mg/L	mg/L
2001	2,380	9.6	1,990	52.2	43	6,940	475	172	49.3	2.5	5.5	0.14	0.14	0.40	1.42	34.9	7.4	1,930	1.9	0.09
2000	2,270	9.2	1,740	53.8	52	6,560	465	152	40.3		5.0				1.33	29.2	7.4	1,750		

The Cu concentration in the water extracts of the reference samples is below the analytical detection limit but measurable amounts of Cu are extracted from some of the block samples. As expected, the maximum concentrations are found in extracts of those samples that have been in contact with the Cu-tube, but an increase in Cu is seen also in some of the peripheral samples. In this case the source of Cu is the thermocouple tubings of Cu-Ni alloy that were aligned on the outer surface of the block during the field test (cf. 8.2.4). The water-extractable amount of Cu is a few percent of the total available Cu content (cf. chemical data on the solid bentonite in Table 8-5).

8.2.2 Exchangeable cations

Data on the cations extracted by exchange with ammonium in alcoholic solutions are given in Table 8-3. There is generally a poor match between the sum of cations and the CEC of the sample (Table 8-4) and variations in the cation sum within and between the blocks are larger than variations in CEC and display no clear tendencies. This fact probably reflects some of the problems inherent with extraction methods for exchangeable cations: non-reactive solutes taken up from the groundwater will necessarily contribute to the extractable cation pool. No correction has been made for this contribution.

The concentration of the major exchangeable cations, K, Na, Mg and Ca, has been plotted against the distance from the Cu-tube in Figure 8-2 together with the ratios Na/Ca, Na/Mg, and Ca/Mg. Sodium makes up approximately 70%, calcium 20%, magnesium 5% and potassium 2% of the pool of exchangeable cations in the reference samples. In relation to the references, the potassium concentration has remained more or less constant in all blocks, whereas Ca has decreased somewhat and sodium has increased, in particular in the cooler parts of the parcel. A small but general increase (1.5–2 meq/100 g dry clay) is seen also in exchangeable magnesium in the hot blocks. The redistribution of calcium sulfate must have exerted a chemical control on the porewater in hot blocks affecting the relative proportions of exchangeable Na and Ca, but there is no obvious explanation of the increase in exchangeable Mg. It seems, however, to be paralleled by a redistribution of non-exchangeable Mg (See Section 8.2.4). A tendency of elevated exchangeable magnesium concentrations in the warmer part of the buffer was observed also in the investigation of parcels A1 and S1 (Karnland et al. 2000) and parcel A2 (Karnland et al. 2009).

Table 8-3. Exchangeable cations of the samples of blocks 11, 15 and 33 from the LOT A0 parcel and of three reference samples. Cations extracted by exchange with NH_4^+ in alcoholic solution.

Sample id	Ca meq/100g	Ca %	K meq/100g	K %	Mg meq/100g	Mg %	Na meq/100g	Na %	Sum meq/100g
A011BSE1b	13	19	1.6	2.2	6.0	8.3	51	71	72
A011BSE3b	13	16	1.5	1.9	5.3	6.5	61	75	81
A011BSE5b	14	19	1.6	2.2	5.3	7.2	53	72	73
A011BSE7b	13	18	1.5	2.1	4.6	6.4	53	74	72
A011BSE9b	12	17	1.4	2.1	4.7	6.8	51	74	70
Block mean	*13*	*18*	*1.5*	*2.1*	*5.2*	*7.0*	*54*	*73*	*74*
A015BSE1b	11	17	1.5	2.2	5.0	7.6	48	74	65
A015BSE3b	12	17	1.5	2.3	4.9	7.3	49	73	67
A015BSE5b	13	18	1.4	2.1	5.3	7.6	50	72	70
A015BSE7b	12	12	1.4	1.4	4.9	5.0	80	81	99
A015BSE9b	14	15	1.4	1.5	5.8	6.3	70	77	91
Block mean	*12*	*16*	*1.4*	*1.9*	*5.2*	*6.8*	*60*	*75*	*78*
A033BSE1b	13	13	1.4	1.5	3.4	3.6	76	81	93
A033BSE3b	12	15	1.4	1.9	3.1	3.9	61	79	78
A033BSE5b	12	14	1.4	1.6	3.1	3.6	72	81	88
A033BSE7b	12	11	1.4	1.4	3.3	3.1	87	84	104
A033BSE9b	17	22	1.4	1.8	4.6	5.9	55	70	78
Block mean	*13*	*15*	*1.4*	*1.6*	*3.5*	*4.0*	*70*	*79*	*88*
A011Rb	16	21	1.7	2.3	3.8	5.0	51	68	75
A015Rb	14	20	1.6	2.2	3.2	4.5	51	70	72
A033Rb	16	21	1.7	2.3	3.6	4.8	51	68	75
Reference mean	*15*	*21*	*1.7*	*2.2*	*3.5*	*4.8*	*51*	*69*	*74*

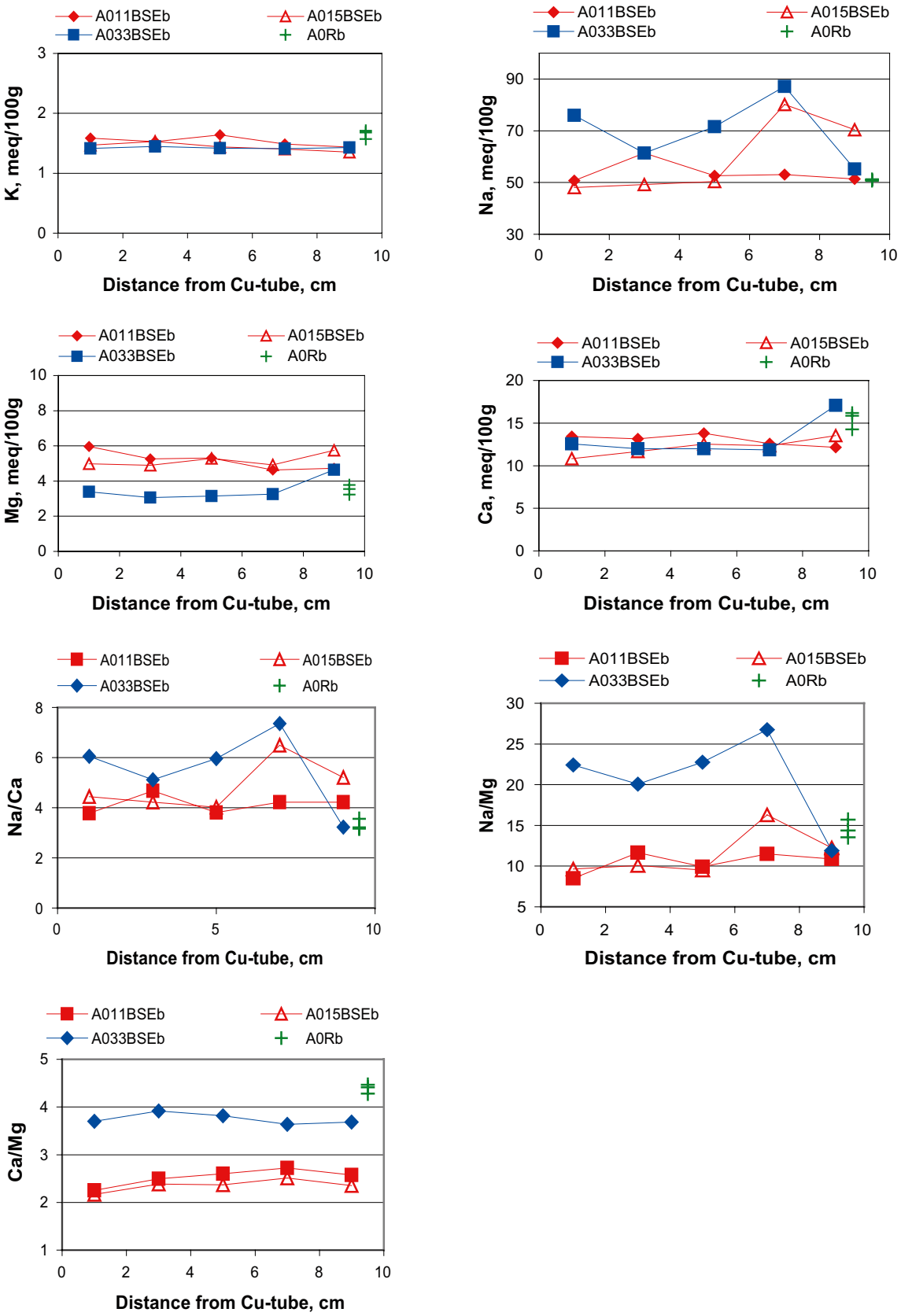

Figure 8-2. *Plots of exchangeable K, Na, Mg and Ca, and the ratios Na/Ca, Na/Mg, and Ca/Mg versus the distance from the Cu-tube for blocks 11, 15 and 33 of the LOT A0 parcel. Values of three reference samples (A0Rb) are shown at position 9.5 cm.*

8.2.3 CEC

The data on the cation exchange capacity (Cu-CEC) of the bulk samples and of the clay fractions are compiled in Table 8-4 and are plotted against the distance from the Cu-tube in Figure 8-3.

The mean CEC value of the three LOT A0 reference bentonites, 76 meq/100 g, is somewhat lower than the CEC value reported for the bentonite MX-80 used in the A1 and S1 parcels (80 meq/100 g (Karnland et al. 2000)). The CEC values are, however, not directly comparable since different reference temperatures, 70 and 105ºC, have been used for dry mass in the two investigations. Although most of the water is lost up to 70ºC, somewhat lower CEC values should therefore be expected for the A0 samples.

The samples from the A0 parcel have CEC values within the same range (mean CEC for the parcel is 75 meq/100 g, std. dev. 0.95) as the reference samples. There is no significant tendency in CEC evident between reference and block samples and small variations within or between the blocks are probably within the analytical error of the method.

The CEC of the clay fractions of both block samples and references is in general 8–9% higher than the CEC of the corresponding bulk samples. Again, no clear tendencies can be seen within or between the blocks. Sample 3 from block 15 has one of the lowest CEC of the sample population but it is uncertain whether analytical artifacts may arise due to the high calcium sulfate content of this sample (cf. Section 8.2.4).

Table 8-4. Cation exchange capacity (CEC) in meq/100 g of bulk samples (left) and of clay fractions (right) from blocks 11, 15 and 33 together with three reference samples for the LOT A0 parcel. CEC determined by exchange with the Cu(II)-triethylenetetramine complex.

Sample id.	Bulk sample CEC 1 meq/100 g	CEC 2 meq/100 g	CEC mean meq/100 g	Sample id.	< 2 µm CEC 1	CEC 2	CEC mean meq/100 g
A011BSE1b	74	76	75	A011BSE1c	82	82	82
A011BSE3b	78	75	77	A011BSE3c	82	84	83
A011BSE5b	73	73	73	A011BSE5c	–	82	82
A011BSE7b	74	71	73	A011BSE7c	83	83	83
A011BSE9b	75	76	76	A011BSE9c	82	82	82
Block mean			*75*				*82*
A015BSE1b	74	77	76	A015BSE1c	80	84	82
A015BSE3b	73	73	73	A015BSE3c	77	78	78
A015BSE5b	76	75	76	A015BSE5c	83	81	82
A015BSE7b	75	75	75	A015BSE7c	83	82	83
A015BSE9b	73	76	75	A015BSE9c	81	82	82
Block mean			*75*				*81*
A033BSE1b	74	75	75	A033BSE1c	77	78	78
A033BSE3b	74	75	74	A033BSE3c	79	80	79
A033BSE5b	74	74	74	A033BSE5c	77	81	79
A033BSE7b	74	75	74	A033BSE7c	79	79	79
A033BSE9b	72	75	74	A033BSE9c	81	78	80
Block mean			*74*				*79*
A011Rb	77	75	76	A011Rc	78	81	80
A015Rb	75	73	74	A015Rc	81	83	82
A033Rb	79	76	78	A033Rc	79	83	81
Reference mean			*76*				*81*

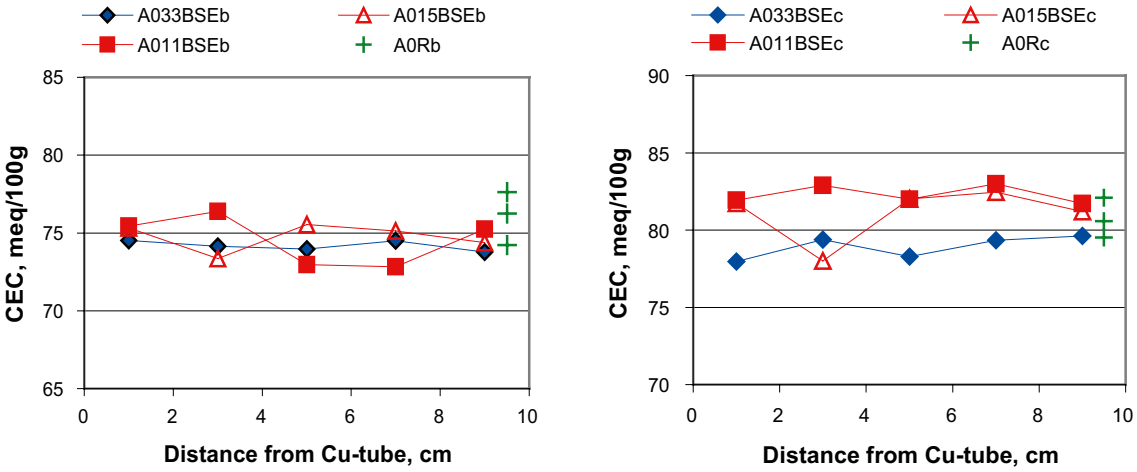

Figure 8-3. *Plot of the CEC of bulk samples (left) and of clay fractions (right) versus radial distance for blocks 11, 15 and 33 of the LOT A0 parcel. Values for the three reference samples (A0R) are shown at position 9.5 cm.*

8.2.4 Chemical composition of the bentonite

The chemical composition of the bentonite samples is given in Table 8-5 (bulk samples) and Table 8-6 (clay fractions). In figures the data are presented on an ignited basis when relevant, in order to minimize artifacts that may arise due to variable moisture and volatile content in the samples.

Cu and Ni

The radial Cu-distribution within the blocks (Figure 8-4) clearly shows that copper has been incorporated into the bentonite matrix proximal to the Cu-tube at all temperatures, although the concentration in the contact samples of the hot blocks is significantly higher than in the cool block. An increase in Cu, which is paralleled by an increase in Ni (cf. Table 8-5) in the peripheral samples suggests that in this case Cu originates from the thermocouple tubing of Cu-Ni alloy that were aligned on the mantle surface of the block during the field test.

Minor and major elements

The sulfate and carbonate minerals are trace constituents (< 2%) in the parent bentonite MX-80 but attention should be paid to these minerals because of their temperature-dependant solubility - that is, the solubility decreases with increasing temperature.

Under non-isothermal conditions with steep temperature gradients salts may accumulate in the warmer parts of the buffer, which would affect the rheology of the bentonite. Furthermore, dissolution/re-precipitation of salts will exert a chemical control on the evolution of the pore water in the buffer, and this fact may explain some of the changes in the pool of the exchangeable cations that are indicated in Figure 8-2.

Table 8-5. Chemical composition of the bulk bentonite samples of blocks 11, 15 and 33 together with three reference samples of the LOT A0 parcel. Analysis by ICP-AES and MS, C and S by evolved gas analysis (Leco furnace).

Sample id.	SiO_2 %	Al_2O_3 %	Fe_2O_3 %	CaO %	MgO %	K_2O %	Na_2O %	MnO %	P_2O_5 %	TiO_2 %	Cr_2O_3 %	LOI %	Sum %	S_{tot} %	C_{tot} %	Ba ppm	Co ppm	Cu ppm	Mo ppm	Nb ppm	Ni ppm	Sc ppm	Sn ppm	Sr ppm	V ppm	W ppm	Y ppm	Zn ppm	Zr ppm
A011BSE1b	58.8	17.6	4.55	1.19	2.36	0.46	1.97	0.02	0.05	0.13	0.006	12.6	99.8	0.35	0.23	332	1.5	1,297	9.5	27	< 20	5	6	244	< 5	0.5	42	80	177
A011BSE3b	58.5	17.5	3.78	1.64	2.27	0.45	1.95	0.02	0.04	0.13	0.003	13.6	99.9	0.51	0.25	350	1.8	11.7	3.1	27	< 20	5	6	320	< 5	0.4	41	105	169
A011BSE5b	59.0	17.7	3.99	1.49	2.18	0.46	1.98	0.02	0.04	0.13	0.003	12.8	99.8	0.33	0.3	512	1.8	5.7	1.7	27	< 20	5	6	366	< 5	0.3	40	93	164
A011BSE7b	61.3	18.5	4.11	1.24	2.19	0.47	2.06	0.02	0.06	0.14	0.002	9.7	99.8	0.19	0.29	268	1.9	4.9	1	31	< 20	5	7	235	6	0.3	44	108	183
A011BSE9b	62.2	18.7	4.04	1.28	2.20	0.47	2.19	0.02	0.04	0.14	0.001	8.6	99.9	0.19	0.42	338	2.2	80.4	1.1	32	64	5	8	232	< 5	0.3	44	99	188
A015BSE1b	60.7	18.2	3.79	1.31	2.39	0.45	1.98	0.01	0.06	0.13	0.003	10.6	99.7	0.39	0.27	298	1.2	1,917	8	29	< 20	5	7	256	< 5	0.6	43	88	177
A015BSE3b	60.8	18.1	4.0	2.03	2.28	0.46	2.14	0.02	0.04	0.13	0.004	9.9	99.9	0.70	0.27	334	1.5	12.1	3.6	31	< 20	5	6	421	< 5	0.5	44	122	179
A015BSE5b	61.7	18.6	4.04	1.24	2.26	0.48	2.07	0.02	0.04	0.14	0.005	9.3	99.9	0.17	0.3	360	2	6	1.5	30	< 20	5	8	217	< 5	0.3	45	121	178
A015BSE7b	60.8	18.1	4.19	1.29	2.21	0.45	2.07	0.02	0.03	0.13	0.003	10.6	99.9	0.18	0.29	316	1.3	5.7	1.2	29	< 20	5	7	215	< 5	0.4	43	93	173
A015BSE9b	60.9	18.4	3.9	1.25	2.21	0.44	2.01	0.02	0.02	0.13	0.004	10.6	99.9	0.20	0.32	326	1.5	25.9	1.3	30	< 20	5	7	235	< 5	0.5	45	92	182
A033BSE1b	61.6	18.4	3.94	1.34	2.31	0.44	1.96	0.01	0.04	0.13	0.004	9.7	99.9	0.31	0.33	299	1.5	74.6	2.7	31	< 20	5	7	271	< 5	0.3	43	106	172
A033BSE3b	61.7	18.7	3.89	1.32	2.24	0.46	2.02	0.02	0.03	0.14	0.003	9.2	99.8	0.29	0.3	341	1.9	6.5	2.5	30	< 20	6	7	279	< 5	0.6	45	87	178
A033BSE5b	61.3	18.6	3.94	1.42	2.2	0.44	2.07	0.02	0.03	0.14	0.004	9.8	99.9	0.32	0.3	352	2.4	5.5	2.3	30	< 20	5	7	281	< 5	0.1	44	102	174
A033BSE7b	61.0	18.5	3.88	1.32	2.19	0.45	1.99	0.02	0.04	0.14	0.005	10.3	99.8	0.30	0.3	330	1.8	5.1	2.3	32	< 20	5	7	289	< 5	0.3	45	98	185
A033BSE9b	60.6	18.5	4.0	1.28	2.17	0.44	1.96	0.02	0.03	0.14	0.004	10.8	99.9	0.23	0.34	335	1.7	41.4	2.2	30	48	5	8	257	< 5	0.4	43	95	176
A011Rb	60.8	18.5	3.75	1.18	2.28	0.44	1.97	0.01	0.03	0.13	0.002	10.8	99.9	0.28	0.29	293	1.8	4.1	2.3	30	< 20	5	7	238	6	0.3	44	82	177
A015Rb	60.5	18.5	4.13	1.22	2.29	0.44	1.98	0.02	0.04	0.13	0.002	10.5	99.8	0.27	0.29	352	1.7	4.3	2.4	30	< 20	5	6	249	7	0.5	43	101	169
A033Rb	60.7	18.4	4.6	1.22	2.29	0.41	2.03	0.02	0.03	0.13	0.001	10.0	99.9	0.27	0.28	295	1.5	4.9	2.4	30	22	5	7	236	5	0.4	43	73	181

Table 8-6. Chemical composition of the fraction < 2 µm of samples from blocks 11, 15 and 33 together with three reference samples of the LOT A0 parcel. Analysis by ICP-AES and MS, C and S by evolved gas analysis (Leco furnace).

Sample id.	SiO_2 %	Al_2O_3 %	Fe_2O_3 %	CaO %	MgO %	K_2O %	Na_2O %	MnO %	P_2O_5 %	TiO_2 %	Cr_2O_3 %	LOI %	Sum %	S %	C_{tot} %	Ba ppm	Co ppm	Cu ppm	Mo ppm	Nb ppm	Ni ppm	Sc ppm	Sn ppm	Sr ppm	V ppm	W ppm	Y ppm	Zn ppm	Zr ppm
A011BSE1c	60.5	18.85	4.10	1.02	2.55	0.18	1.79	0.01	0.04	0.12	< .001	10.6	99.8	0.24	0.17	88	1	1,136	5.2	27	< 20	5	8	252	< 5	0.8	39	51	139
A011BSE3c	60.8	18.68	3.73	1.43	2.43	0.19	1.77	0.01	0.03	0.13	< .001	10.7	99.9	0.39	0.17	116	1.6	11.4	1.8	28	< 20	5	9	345	< 5	0.2	41	49	139
A011BSE5c	61.7	19.12	3.83	1.1	2.38	0.18	1.89	0.01	0.02	0.12	< .001	9.6	99.9	0.19	0.19	223	1.7	4.5	0.8	28	< 20	5	8	337	< 5	0.3	40	28	142
A011BSE7c	61.8	19.5	4.12	0.9	2.41	0.11	2.02	0.01	< .01	0.12	0.001	8.9	99.9	0.05	0.17	29	1.9	3.7	0.5	26	< 20	5	9	221	< 5	0.3	34	20	141
A011BSE9c	61.5	19.44	3.95	0.88	2.43	0.11	2.05	0.01	0.02	0.12	< .001	9.3	99.8	0.06	0.18	73	1.6	83.3	0.5	25	68	5	9	223	< 5	0.1	33	23	134
A015BSE1c	60.8	18.57	3.81	1.19	2.53	0.19	1.72	0.01	0.03	0.12	< .001	10.7	99.6	0.29	0.2	100	0.9	1,458	4	29	< 20	5	8	266	< 5	0.1	42	57	145
A015BSE3c	60.8	18.51	3.72	1.57	2.44	0.2	1.68	0.01	0.02	0.13	< .001	10.7	99.8	0.45	0.19	127	1.3	52	1.5	29	< 20	5	8	410	< 5	< .1	42	48	141
A015BSE5c	60.9	19.43	3.87	0.9	2.45	0.13	2.06	0.01	< .01	0.12	< .001	9.9	99.8	0.04	0.17	63	1.2	4.0	0.7	27	< 20	5	9	205	< 5	< .1	33	20	140
A015BSE7c	61.2	19.39	3.99	0.9	2.41	0.11	2.03	0.01	0.02	0.12	0.001	9.7	99.8	0.06	0.17	77	1.4	2.9	0.5	25	< 20	5	9	201	< 5	< .1	31	18	132
A015BSE9c	61.3	19.15	4.06	0.94	2.49	0.1	2.04	0.01	0.02	0.12	< .001	9.7	100	0.06	0.17	83	0.8	29.4	0.6	24	< 20	5	8	205	< 5	< .1	30	18	136
A033BSE1c	61.7	19.08	3.87	1.04	2.57	0.11	1.93	0.01	< .01	0.12	< .001	9.5	99.9	0.15	0.18	76	1.6	84.3	1.1	24	< 20	5	7	244	< 5	0.4	31	19	135
A033BSE3c	61.6	19.06	4.04	1.07	2.55	0.12	1.96	0.01	< .01	0.12	0.001	9.4	100	0.14	0.17	72	1.4	3.4	0.9	25	< 20	5	7	268	< 5	0.1	32	18	140
A033BSE5c	61.6	19.18	3.96	1.06	2.57	0.09	1.92	0.01	< .01	0.12	< .001	9.4	100	0.13	0.15	72	1.0	7.7	0.9	25	< 20	5	8	265	< 5	0.1	32	21	138
A033BSE7c	61.6	19.26	3.89	1.09	2.53	0.1	1.99	0.01	0.01	0.12	0.001	9.3	99.9	0.14	0.16	80	1.3	2.8	1.1	25	< 20	5	9	259	< 5	0.4	29	20	138
A033BSE9c	61.6	19.39	4.09	1.01	2.57	0.09	1.96	0.01	< .01	0.12	0.001	9.1	100	0.08	0.21	78	1.0	47	0.9	25	38	5	8	235	< 5	0.1	31	20	132
A011Rc	62.0	19.53	3.9	0.96	2.46	0.13	2.02	0.01	< .01	0.12	< .001	8.8	99.9	0.13	0.19	81	1.5	3.1	1.7	27	< 20	5	10	247	< 5	0.2	37	20	136
A015Rc	61.7	19.53	4.12	0.93	2.43	0.13	1.92	0.01	< .01	0.12	< .001	9	99.9	0.15	0.19	95	1.4	3.0	1.6	27	< 20	5	10	247	< 5	0.2	37	21	135
A033Rc	61.5	19.63	4.04	0.88	2.37	0.13	1.96	0.01	0.02	0.12	< .001	9.3	99.9	0.12	0.17	71	1.5	3.0	1.3	28	< 20	5	10	234	< 5	0.6	38	18	141

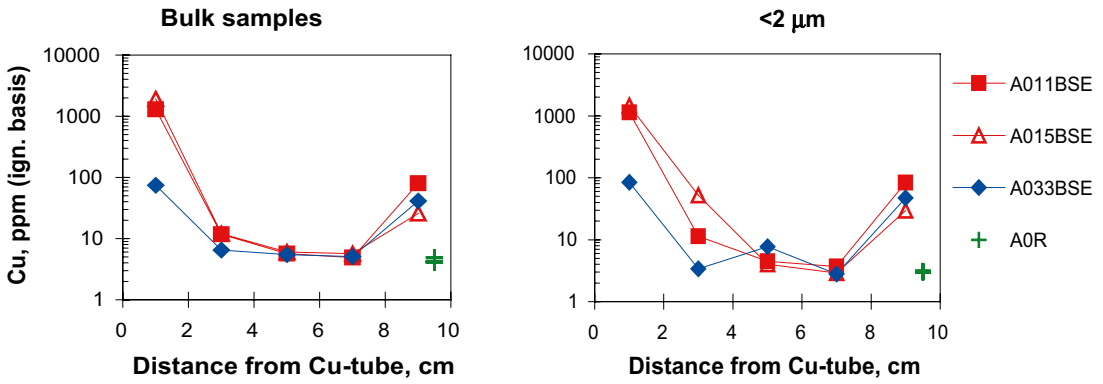

Figure 8-4. Plot of the Cu concentration in bulk samples (left) and clay fractions (right) versus the distance from the Cu-tube for blocks 11, 15 and 33 of the LOT A0 parcel. Values for three reference samples (A0R) are shown at position 9.5 cm.

The mean concentration of total carbon in the reference samples is 0.29% C (N=3). The distribution of total carbon (Figure 8-5), which includes organic and inorganic carbon, indicates a loss in the bulk bentonite proximal to the Cu-tube in the hot blocks but the change in carbon concentration is close to the detection limit of the analysis (DL=0.02%).

The mean concentration of total sulfur in the reference samples is 0.27% S (N=3; DL=0.02%). The major fraction of sulfur in MX-80 is derived from water-soluble minerals, mainly gypsum, ($CaSO_4 \cdot 2H_2O$). Iron sulfide (pyrite FeS_2) is generally the predominant insoluble sulfur-bearing mineral in the MX-80 bentonite.

The distribution of total sulfur in the blocks (Figure 8-6 left) matches the results of the analysis of aqueous leachates (Figure 8-1). Thus, the cool block has a regular distribution of sulfur in the same concentration range as the references. In the hot blocks the total sulfur content has increased in the interval 0–4 cm from the heater where anhydrite ($CaSO_4$) has accumulated (cf. XRD data), whereas the peripheral parts are depleted in sulfur. Accordingly, maxima in calcium coincide with maxima in sulfur in the hot blocks (Figure 8-6). If all S is allocated to anhydrite, the maximum sulfur concentration, 0.7% S at 3 cm distance in block 15, corresponds to ca. 3% $CaSO_4$.

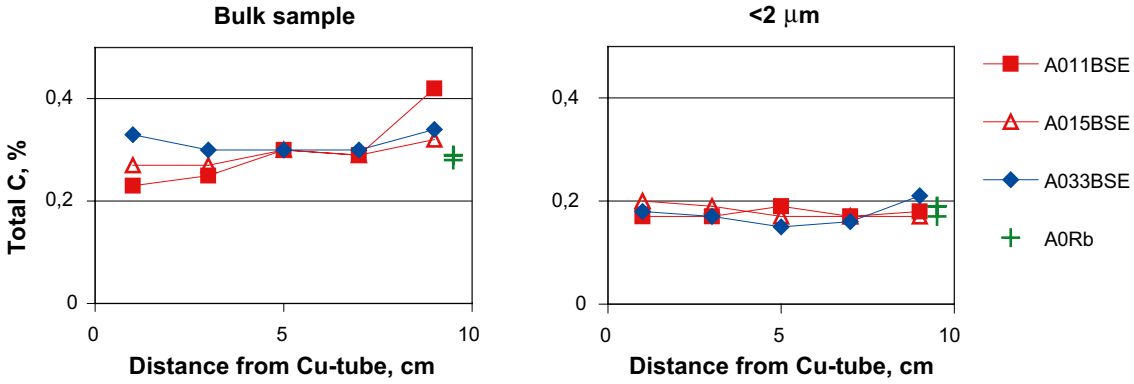

Figure 8-5. The distribution of total carbon in the bulk sample (left) and in the clay fraction (right) of samples of blocks 11, 15 and 33 of the LOT A0 parcel. Values for three reference samples (A0Rb) are shown at position 9.5 cm.

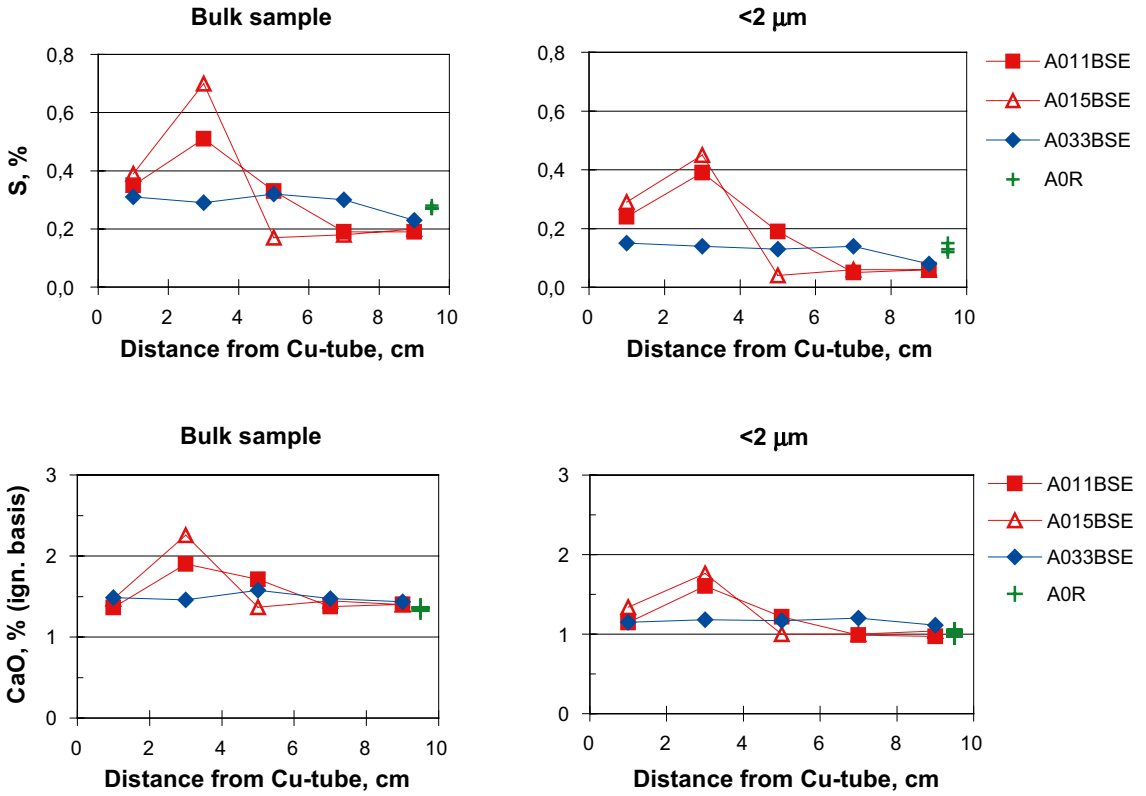

Figure 8-6. *The distribution of total sulfur and calcium in the bulk sample (left) and in the clay fraction (right) of samples of blocks 11, 15 and 33 of the LOT A0 parcel. Values for three reference samples (A0Rb) are shown at position 9.5 cm.*

The chemical data on the clay fraction of these sulfate-rich samples (cf. Table 8-6) clearly show that some calcium sulfate still exists after the separation by size. Dissolution of calcium sulfate during the fractionation procedure will necessarily lead to replacement of interlayer sodium, which will promote flocculation and sedimentation of the clay minerals. This is clear in the data on the aqueous leachates (Table 8-2) which show that the concentration of elements (e.g. Al and Fe) originating from suspended ultra-fine clay particles in the water extracts is at a minimum in samples with maximum sulfate concentrations. It cannot be excluded that this difference in the dispersion behaviour among the samples has resulted in artifactual differences in the particle size spectra of the extracted < 2 µm fractions. A skewness in the particle-size spectra to the coarse side would result in a relative excess of coarse-grained accessory minerals, and, accordingly, in a change of the average chemical composition of the extracted clay fraction. As shown in Table 8-7, which gives the chemical composition of different Na-saturated particle-size fractions of MX-80, the concentration of elements like Ti, P, Sr and K, is significantly higher, and e.g. Al lower, in the coarse fractions due to the preferential equivalent diameter of the major source minerals. As illustrated in Figure 8-7 and seen in Table 8-6, the clay fractions of the hot block display small but fairly abrupt changes in several of these elements in the sulfate-zone (all data compared on an ignited basis). Also the sodium concentration of the clay fraction decreases in the innermost 4 cm of the hot blocks but in this case the Na-Ca cation exchange contributes to the change.

Table 8-7. Chemical composition of different grain size fractions of MX-80. The proportion of each size fraction in % of the < 2 µm fraction is also given.

Grain size fraction		< 2 µm	1–2 µm	< 1 µm	0.2–1 µm	<0.2 µm
% of < 2 µm		100	4	96	21	75
SiO_2	%	63.7	68.4	62.8	64.1	62.9
Al_2O_3	%	22.7	16.2	22.6	21.7	22.9
Fe_2O_3	%	4.23	3.55	4.23	4.15	4.27
CaO	%	< 0.1	0.29	< 0.1	< 0.1	< 0.1
MgO	%	2.83	1.79	2.77	2.49	2.87
K_2O	%	0.079	0.771	0.085	0.160	0.151
Na_2O	%	2.87	2.25	2.87	2.58	2.97
MnO	%	0.004	0.008	0.004	0.004	0.005
P_2O_5	%	0.048	0.129	0.043	0.063	0.035
TiO_2	%	0.155	0.239	0.153	0.201	0.136
Σ excl. LOI	%	96.6	93.6	95.6	95.4	96.2
LOI	%	5.8	7.5	6.6	6.8	6.2
Ba	ppm	19	294	12.9	45.9	< 2
Be	ppm	1.86	1.84	1.9	2.05	1.87
Cr	ppm	< 10	26.4	< 10	< 10	< 10
Nb	ppm	26.7	53.7	24.8	43	19.2
Ni	ppm	< 10	< 10	< 10	< 10	< 10
Sc	ppm	8.0	7.0	8.0	8.5	7.8
Sr	ppm	12.9	61.1	13.9	23.7	13.4
V	ppm	6.3	9.48	6.08	4.68	6.62
W	ppm	< 60	< 60	< 60	< 60	< 60
Y	ppm	38.8	177	32.6	84.7	15.9
Zr	ppm	177	253	174	247	151

No clear tendencies can be seen in the distribution of iron and silicon (Figure 8-8) and the concentration ranges in block samples are the same as in the references.

In contrast, the magnesium content in both the bulk sample and the clay fraction (Figure 8-8) displays a clear gradient towards the Cu-tube, in particular in the hot blocks. In the bulk samples the concentration has increased from 2.56% (mean of three reference bulk samples on ignited basis) to 2.70% in the innermost high temperature samples, whereas the peripheral parts of the blocks seem to be depleted in magnesium. This apparent redistribution of magnesium is paralleled by an increase of the exchangeable Mg concentration (Se Section 8.2.2). No water-soluble Mg-bearing phase has been identified in the XRD-analysis (See Section 8.2.5) but the detection limit of this method may be too poor to detect trace minerals, and depends, among other things, on the crystallinity of the phase.

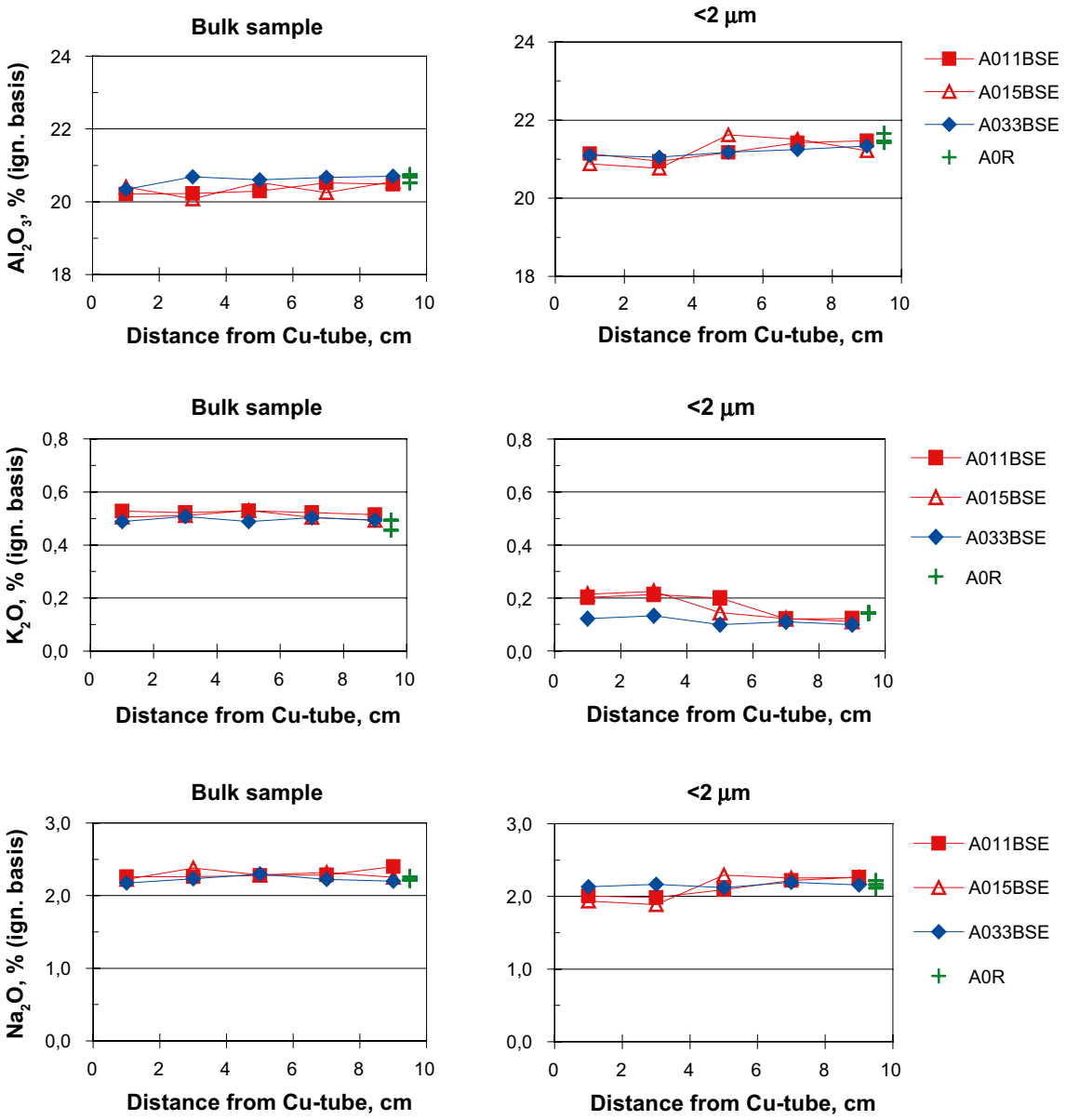

Figure 8-7. *Plot of the Al_2O_3, K_2O and Na_2O content (on ignited basis) of the bulk samples (left) and of <2 µm fractions (right) versus the distance from the Cu-tube for blocks 11, 15 and 33 of the LOT A0 parcel. Values for three reference samples are indicated at the position 9.5 cm.*

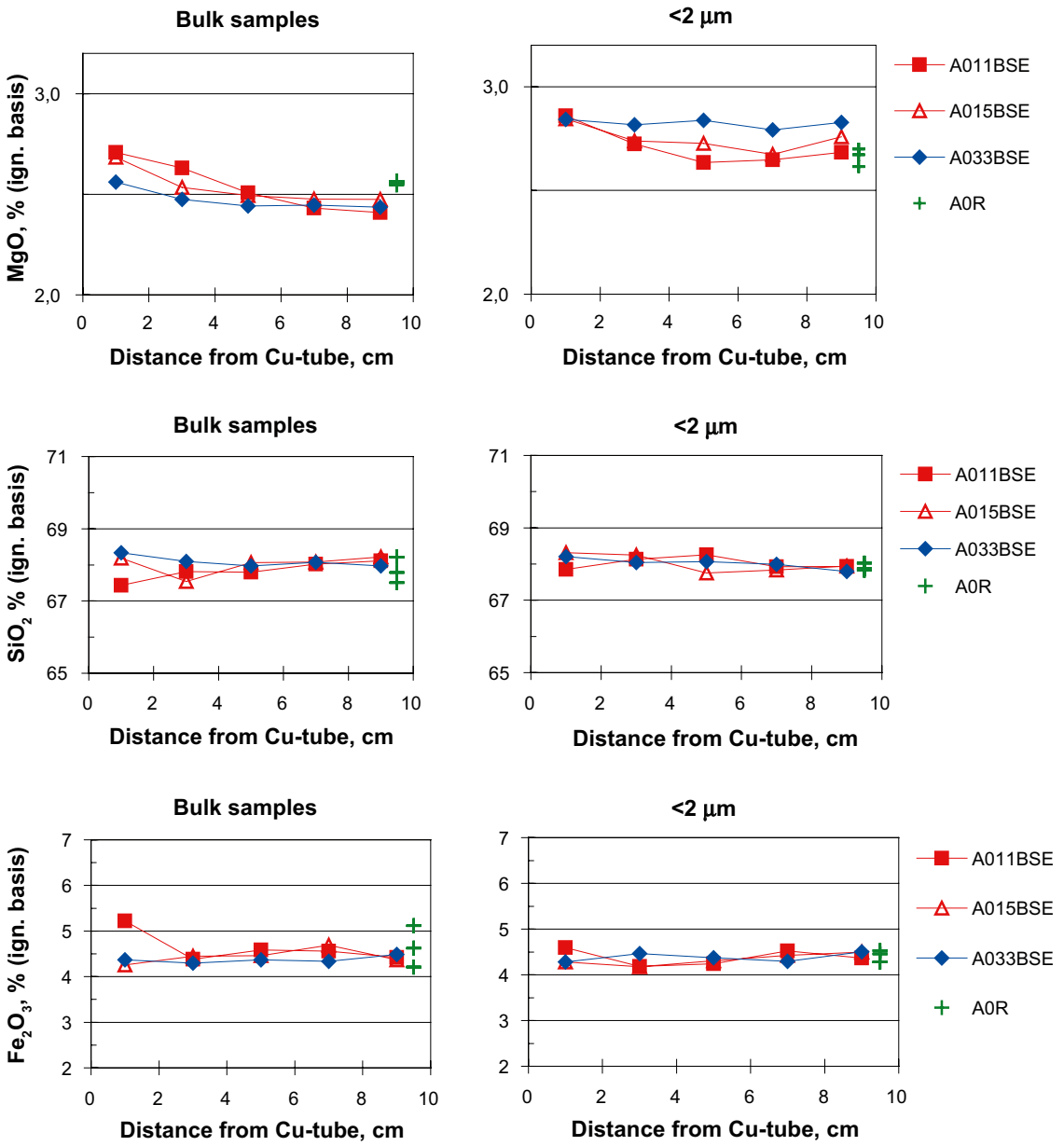

Figure 8-8. *Plot of the SiO_2, Fe_2O_3 and MgO content (on ignited basis) of the bulk samples (left) and of <2 µm fractions (right) versus the distance from the Cu-tube for blocks 11, 15 and 33 of the LOT A0 parcel. Values for three reference samples are indicated at the position 9.5 cm.*

8.2.5 Bentonite mineralogy

The reference bentonite

The XRD-profiles of random powders of the bulk material of three LOT A0 reference samples and their mean profile are shown in Figure 8-9. The strongest peaks of the major non-phyllosilicates, i.e. quartz, cristobalite and feldspars (K-feldspar and Na-plagioclase), have been labeled in the figure. Traces of gypsum are generally found in MX-80 bentonite, used for the LOT A0 parcel, and peak positions for gypsum are also indicated in Figure 8-9, but according to the chemical data the maximum amount of gypsum that can exist in the reference bentonite (i.e. all sulfur, 0.27% S, is allocated to $CaSO_4 \cdot 2H_2O$) is approximately 1.5%, which is close to the detection limit of the XRD analysis. Also calcite has been found in MX-80 (e.g. Karnland et al. 2000), and one of the reference samples has a peak of low intensity at the position of the most intense reflection of calcite, but the identification is uncertain since no other calcite reflections are detectable.

In the XRD-profiles of Figure 8-9 also the strongest basal reflections (*00l*) and the two-dimensional hk-bands of montmorillonite are indicated. The position of the first order basal reflection (ca. 12.5 Å) is typical of the monolayer hydrate of Na-montmorillonite, which is stable at a relative humidity below 65–70% (Brindley and Brown 1980).

In Figure 8-9 also the position of the so called (060)-peak is labelled. This reflection is useful for recognizing di- and trioctahedral sub-groups of clay minerals since it includes the b cell dimension, which is more sensitive to the size of the cations and to site occupancy in the octahedral sheet than are the a or c cell dimensions. For smectites this peak is distinct enough to allow an estimate of the b parameter to an accuracy of approximately ±0.5% (cf. Brindley and Brown 1980). The indicated d(060) value of 1.49–1.50 Å (62º 2θ) is typical of the dioctahedral sub-group of smectites, to which montmorillonite belongs.

Micaceous minerals, which have their (001) reflection at 10 Å, occur in such small quantities that basal peaks would barely be detectable in the XRD-trace of a good preparation of a randomly oriented powder. No peaks can be detected with certainty in the mean XRD-profile of the references in Figure 8-9 but, depending on the degree of accidental orientation, individual samples may display a peak of low intensity in the 10 Å-region, which indicates that trace amounts of mica/illite occur.

The low angle region 3–10º 2θ of the XRD-profiles of oriented aggregates of the Mg-saturated < 2 μm fraction in the air-dried and EG-solvated state are shown in Figure 8-10.

The homo-ionic Mg-clay has a basal spacing of approximately 15 Å when air-dried (RH 50±10%) and expands to 16.9–17 Å upon ethylene glycol treatment (EG). As can be seen in the diffractograms of the EG-solvated sample A015Rc-EG the peak position deviates somewhat from this value and the peak intensity is anomalously low, which is an effect seen in preparations with poor preferred orientation.

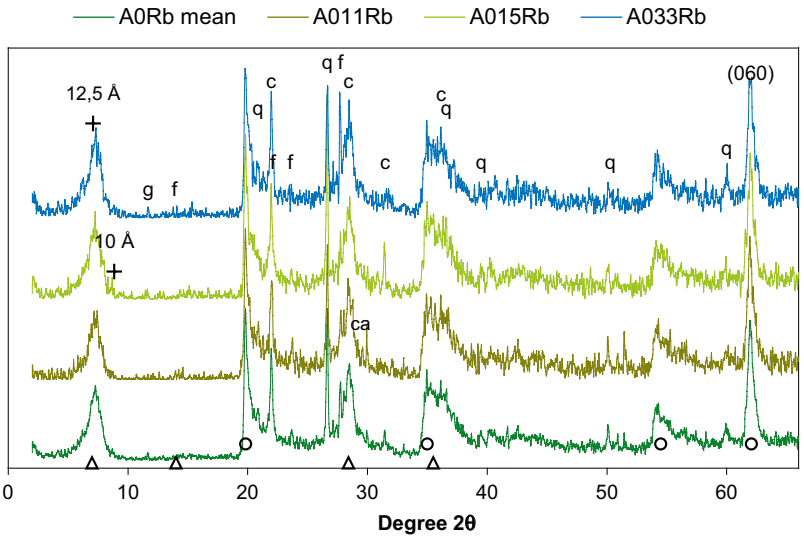

Figure 8-9. *XRD-profiles of random powders of the bulk of three reference samples for the LOT A0 parcel together with the mean profile. Peak positions for calcite (ca), cristobalite (c), feldspars (f), gypsum (g) and quartz (q) are indicated. Δ=positions of the basal reflections of smectite; o= positions of the hk-reflections of smectite. CuKα radiation.*

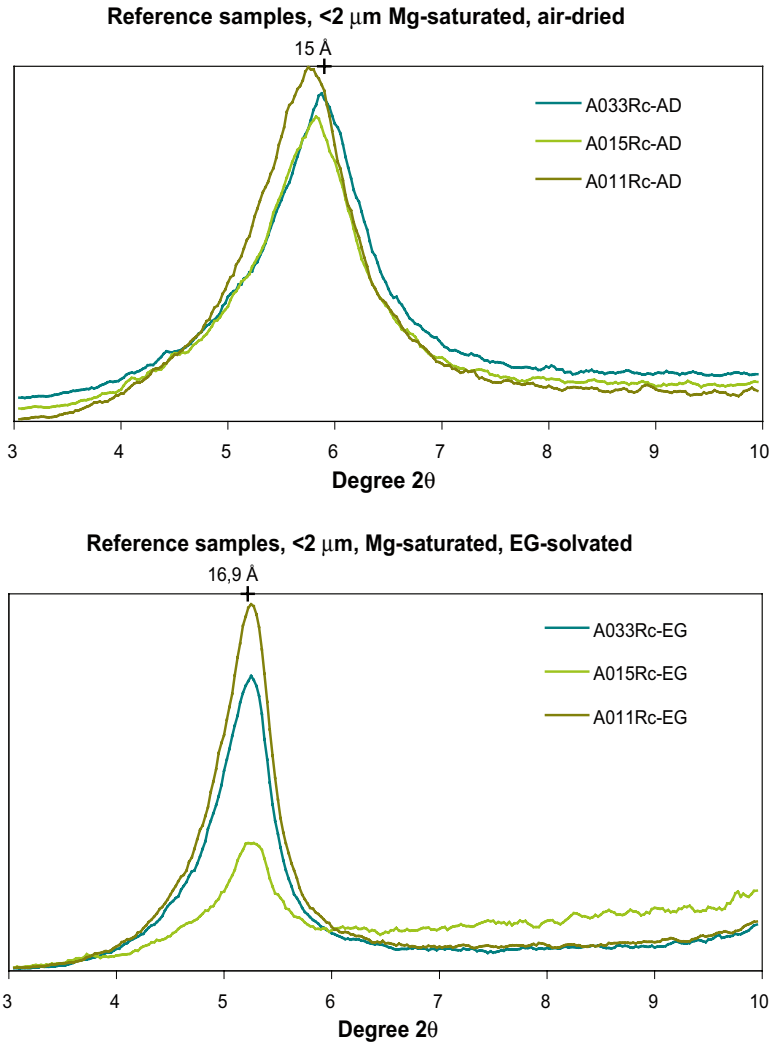

Figure 8-10. *The position of the first order basal reflection of montmorillonite in the air-dried and EG-solvated state. Oriented aggregates of Mg-saturated clay fraction of three reference samples for LOT A0. CuKα radiation.*

No discrete mica/illite can be seen in the diffractograms but judged by the chemical data on the < 2 µm fraction, some illitic layers may exist as interlayers in the smectite structure. The amount of non-exchangeable potassium (0.13% K_2O; Table 8-6) would correspond to 1.5–2% illitic layers and such small amount of interlayering in the smectite structure cannot be detected by the routine XRD analysis applied.

In summary, the XRD analysis of the reference bentonite shows that:

- The bulk bentonite contains montmorillonite, quartz, cristobalite, feldspars and traces of gypsum and mica/illite. One of the reference samples has a weak peak at the position of the most intense reflection of calcite, but the identification is uncertain since no other calcite reflections are detectable.
- The clay fraction is almost pure montmorillonite and no discrete 10 Å phase, i.e. mica/illite, can be detected. Judged by the chemical data on the clay fraction, some illitic layers may, however, exist as interlayers in the smectite structure.
- Montmorillonite in the "as-received state", i.e. saturated predominantly with Na, has a basal spacing of 12.5 Å at an RH of around 60% but the 001-peak tends to be broad and asymmetrical. The air-dried, homoionic Mg-exchanged clay fraction has a basal spacing of ca. 15 Å, and expands to 16.9–17 Å on EG-solvation, which is typical of smectites.

Bentonite of the LOT A0 parcel

The XRD-profiles of the bulk samples from blocks 33, 15 and 11 are presented in Figure 8-11 to Figure 8-13. The cool block 33 (Figure 8-11) displays no significant changes compared with the reference samples, neither with respect to the type nor to the peak intensities of accessory minerals. A variation of the intensity of the feldspar peaks can be seen among the samples, but both the excellent {010} and {001} cleavage of feldspars, which promotes preferred orientation, and the coarse grain size of feldspars, may give a random variation in the peak intensities.

Similarly, depending on the degree of random orientation of the preparation, some but not all samples display a 10 Å peak of low intensity produced by mica.

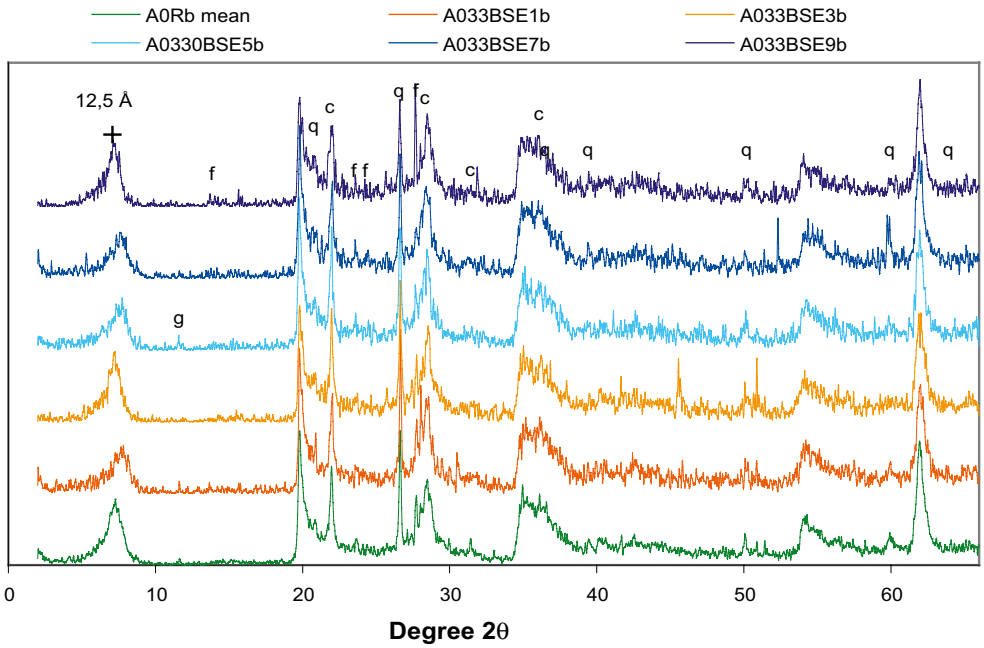

Figure 8-11. *XRD-profiles of samples 1 to 9 from block 33 of the LOT A0 parcel. Green curve: mean XRD-profile of three reference samples. The positions of the strongest peaks of the major non-clay minerals are labeled: c=cristobalite, f=feldspars, g=gypsum and q=quartz. The (001) peak of Na-smectite at 12.5 Å is also indicated. Random powders of bulk samples; CuKα radiation.*

The position, shape and width of the (001) basal reflection of montmorillonite varies somewhat among the samples, which is probably an effect of variable rehydration after drying due to the lack of humidity control during sample handling. However, like the references, most samples have the maximum peak intensity around 12.5 Å, which is typical of the monolayer hydrate of a Na-montmorillonite and consistent with the data on the composition of the exchangeable cation pool, showing that sodium is by far the most abundant cation in block 33 (Table 8-3).

The most conspicuous mineralogical change in the hot blocks is the appearance of moderately intense peaks of anhydrite ($CaSO_4$) in samples 1 and 3, which represent the innermost 4 cm adjacent to the heater (Figure 8-12 and Figure 8-13). Accordingly, the mineralogical data confirms the chemical data (Section 8.2.1 and 8.2.4), which clearly shows that Ca-sulfate has been redistributed along the thermal gradient in the hot blocks. In some of the samples the re-precipitated Ca-sulfate phase may include also the hemi-hydrate (bassanite).

Several of the samples from block 15 produce broad and indistinct first order basal smectite reflections of low intensity with a mean spacing smaller than 12.5 Å. A probable explanation for this is that the rehydration of the smectite was incomplete due to the lack of strict control of humidity and as a consequence, smectite of mixed hydration states occur in the samples.

The samples from block 11 produce fairly well-defined first order basal smectite reflections. There is no clear shift of the basal spacing (i.e. from 12.5 towards 15 Å), which would be consistent with a replacement of interlayer Na by divalent cations. However, peaks tend to be asymmetrical or resolved towards the low-angle side, a feature generally seen in mixed Na-Ca (Mg) smectite if conditions are such that the layers with divalent cations have two interlayer water layers and the Na-layers only one layer.

A close-up of the region 60–64º 2θ (i.e. scan resolution is not changed) of the XRD-profiles of the parcel and reference samples (Figure 8-14) shows that the d-value of the (060) peak is almost identical in all samples (ca. 1.50 Å). Those variations that may exist appear to be random and independent of the position of the sample in the parcel. Thus, the available XRD-data provide no evidence of any significant change of the b cell dimension of the clay mineral, which would be an expected effect of, for instance, a change of the cations or the site occupancy in the octahedral sheet, or of a change of the amount of Al in tetrahedral coordination.

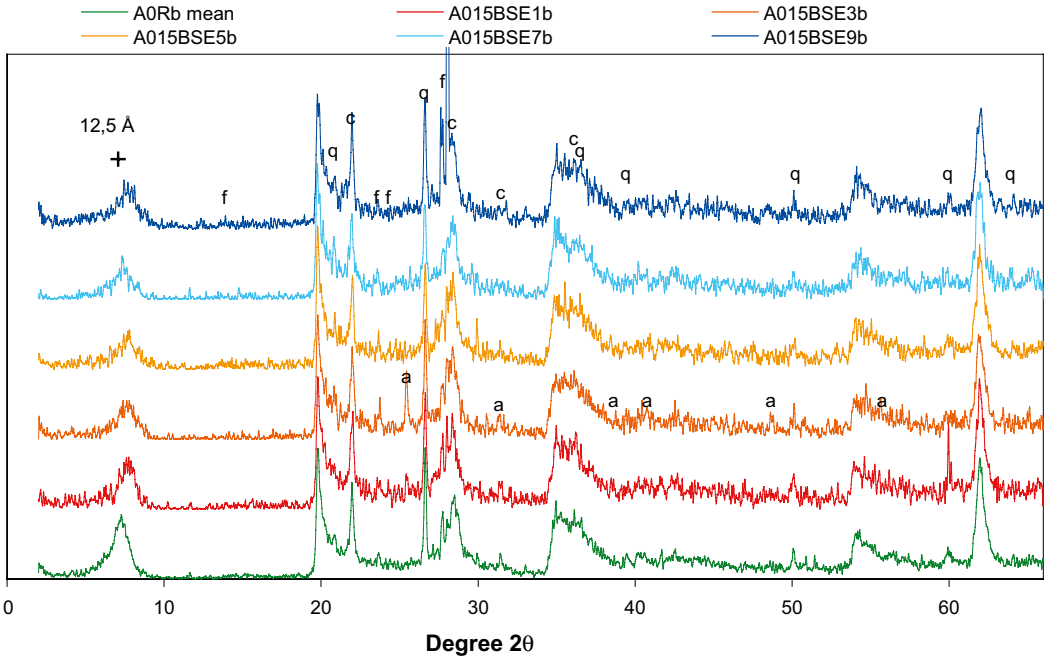

Figure 8-12. *XRD-profiles of samples 1 to 9 from block 15 of the LOT A0 parcel. Green curve: mean XRD-profile of three reference samples. The positions of the strongest peaks of the major non-clay minerals are labelled: a=anhydrite ($CaSO_4$), c=cristobalite, f=feldspars, q=quartz. The (001) peak of Na-smectite at 12.5 Å is also indicated. Random powders of bulk material; CuKα radiation.*

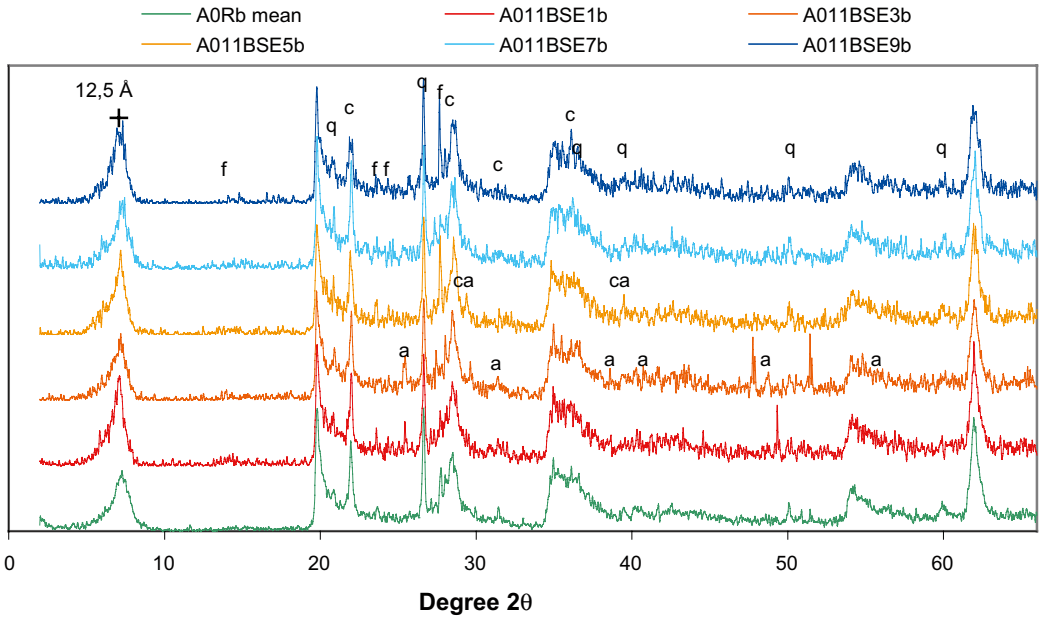

Figure 8-13. *XRD-profiles of samples 1 to 9 from block 11 of the LOT A0 parcel. Green curve: mean XRD-profile of three reference samples. The positions of the strongest peaks of the major non-clay minerals are labelled: a=anhydrite ($CaSO_4$), ca=calcite, c=cristobalite, f=feldspars, q=quartz. Random powders of bulk material; CuKα radiation.*

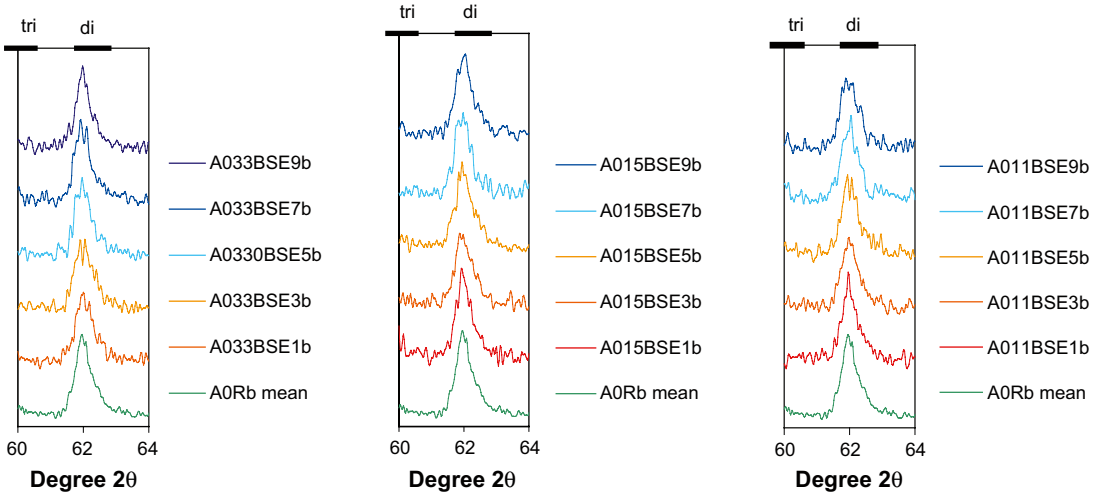

Figure 8-14. *Close-up of the (060)-peak position. XRD-profiles of samples 1 to 9 from blocks 33, 15 and 11 of the LOT A0 parcel. Green curve: Mean XRD-profile of three reference samples. The indicated d-value (1.50 Å) of the (060)-peak is typical of dioctahedral smectites. The position of the (060)-peak of trioctahedral smectites is also indicated. CuKα radiation.*

XRD-profiles of oriented mounts of the Mg-exchanged clay fraction of the individual samples from the A0 parcel are shown in Figure 8-15 (air-dried clay) and Figure 8-16 (EG-solvated clay) together with the XRD profiles of the corresponding reference samples.

The basal spacing of the air-dried, homo-ionic Mg-clay is ca. 15 Å (relative humidity 50±10%) and the smectite expands to ca. 16.9 Å upon EG-solvation, which is typical of Mg-saturated montmorillonite. Those small variations that can be seen in the close-up of the 17 Å region of the XRD-profiles (Figure 8-16) appear to be random and independent of the position of the sample in the parcel.

In summary, the available XRD-data provide no evidence of any structural change or change of the expansion behavior of the montmorillonite of the LOT A0 parcel.

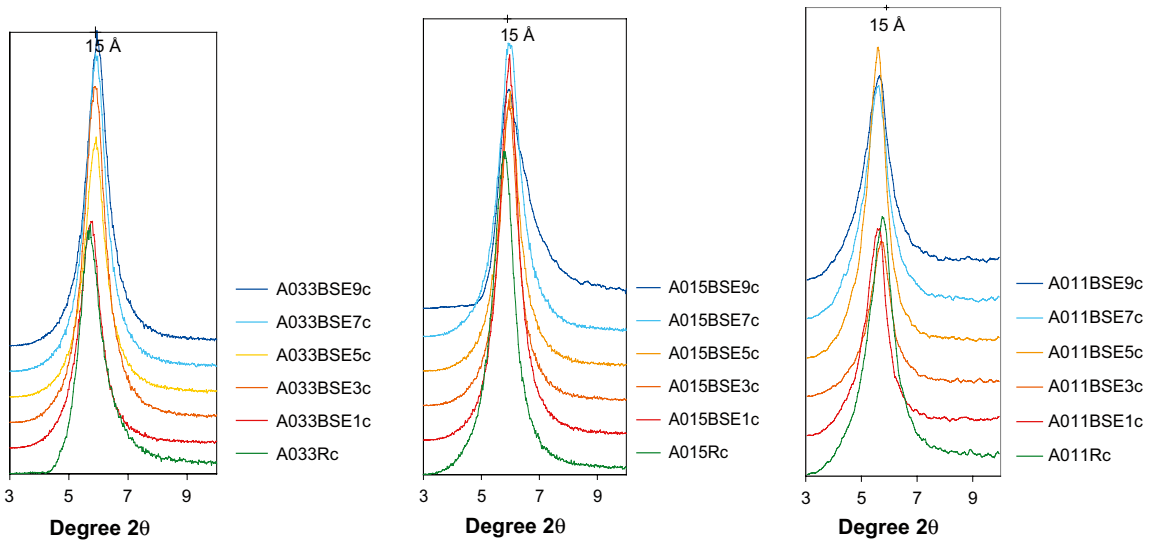

Figure 8-15. *Close-up of the 15 Å region of air-dried, Mg-saturated clay fractions from the LOT A0 parcel. XRD-profiles of samples 1 to 9 from blocks 33, 15 and 11. Green curve: XRD-profile of the reference sample. CuKα radiation.*

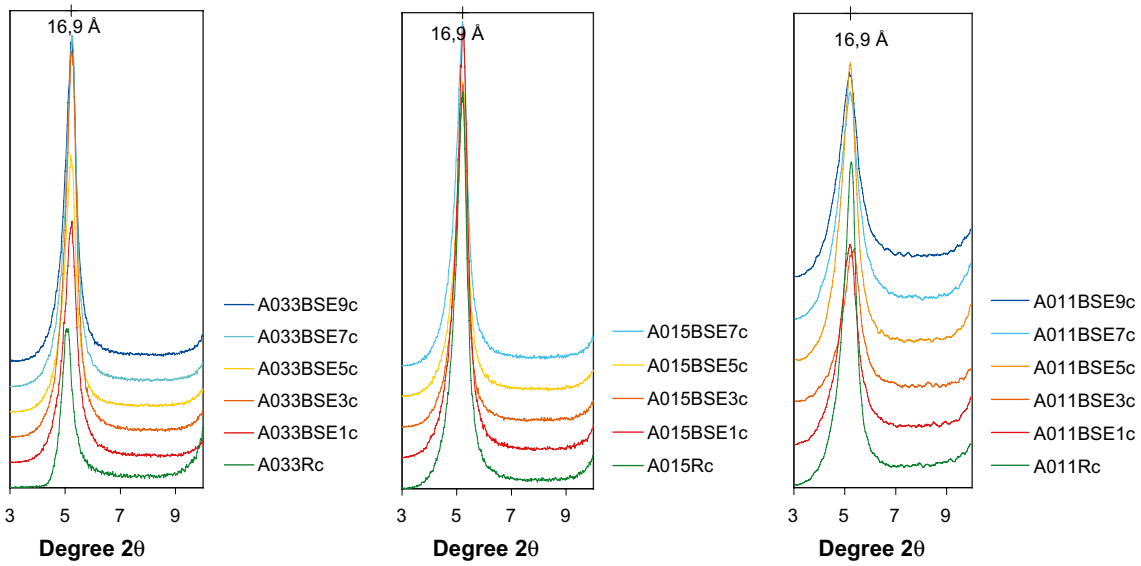

Figure 8-16. *Close-up of the 17 Å region of EG-solvated, Mg-saturated clay fractions from the LOT A0 parcel. XRD-profiles of samples 1 to 9 from blocks 33 and 11, and of samples 1 to 7 of block 15. Green curve: XRD-profile of the reference sample. CuKα radiation.*

8.3 Summary and conclusions

The chemical and mineralogical investigation of the bentonite of the standard blocks 11, 15 and 33 from the LOT A0 parcel indicates that

- *Calcium sulfate has been redistributed* along the thermal gradient in hot blocks. Anhydrite has accumulated 0–4 cm from the heater, whereas the peripheral parts of the blocks are depleted in sulfates.
- *Cu has been incorporated in the bentonite matrix* proximal to the Cu-tube in *all* blocks but the concentration is significantly higher in the hot blocks. The form in which copper has been incorporated has not been identified, but the major fraction is not readily soluble or accessible for cation exchange.
- The redistribution of calcium sulfate must have exerted a chemical control on the pore water in hot blocks affecting the relative proportions of exchangeable Na and Ca, but there is no obvious explanation of the *increase in exchangeable Mg in the hot parts of the parcel*. It seems, however, to be *paralleled by an increase in non-exchangeable Mg* towards the heater whereas the peripheral parts of the bentonite blocks appear to be depleted in Mg. The source of Mg has not been identified and remains to be established.
- *CEC displays no clear tendency* within or between the blocks.
- The available XRD-data provide *no evidence of a structural change of the montmorillonite*. Both the expansion behavior and the *b* cell dimension of the clay mineral are typical of montmorillonite and similar to that of the reference material. However, the resolution of the XRD-technique may be inadequate for detecting very small-scaled changes.

9 References

SKB's (Svensk Kärnbränslehantering AB) publications can be found at www.skb.se/publications.

Abercrombie H J, Hutcheon I E, Bloch J D, de Caritat P, 1994. Silica activity and the smectite-to-illite reaction. Geology, v. 22, p 539–542.

Belyayeva N I, 1967. Rapid method for the simultaneous determination of the exchange capacity and content of exchangeable cations in solonetzic soils. Soviet Soil Science, 3, pp 1409–1413.

Birgersson M, Karnland O, 2009. Ion equilibrium between montmorillonite interlayer space and an external solution – Consequences for diffusional transport. Geochimica et Cosmochimica Acta, 73, doi:10.1016/j.gca.2008.11.027.

Boles J R, Frank S G, 1979. Clay diagenesis in the Wilcox sandstones of southwest Texas. Journal of Sedimentary Research, 49, pp 55–70.

Brindley G W, Brown G (eds), 1980. Crystal structures of clay minerals and their X-ray identification. London: Mineralogical Society. (Mineralogical Society Monograph 5).

Börgesson L, Johannesson L-E, Sandén T, Hernelind J, 1995. Modelling of the physical behaviour of water saturated clay barriers. SKB TR 95-20, Svensk Kärnbränslehantering AB.

Coulson J M, Richardson J F, 1977. Chemical Engineering, Volume 1, Fluid flow, heat transfer and mass transfer. 3rd ed. Oxford: Pergamon Press.

Couture R A, 1985. Steam rapidly reduces the swelling capacity of bentonite. Nature, 318, pp 50–52.

Crank J, 1975. The mathematics of diffusion. 2nd ed. Oxford: University Press.

Dimmock N A, Settle C, Webber H M, 1979. The use of ferrozine for the absorptiometric determination of iron in boiler-feed water. Laboratory note no RD/L/N41/79, Central Electricity Research Laboratories.

Eberl D D, Velde B, McCormic T, 1993. Synthesis of illite-smectite from smectite at earth surface temperatures and high pH. Clay Minerals, 28, pp 49–60.

Eriksen T E, Jansson M, 1996. Diffusion of I^-, Cs^+ and Sr^{2+} in compacted bentonite. Anion exclusion and surface diffusion. SKB TR 96-16, Svensk Kärnbränslehantering AB.

Eriksen T E, Jansson M, Molera M, 1999. Sorption effects in cation diffusion in compacted bentonite. Engineering Geology, 54, pp 231–236.

Hower J, Eslinger E V, Hower M E, Perry E A, 1976. Mechanism of burial metamorphism of argillaceous sediments. Geological Society of America Bulletin, 87, pp 725–737.

Huang W-L, Longo J M, Pevear D R, 1993. An experimentally derived kinetic model for smectite-to-illite conversion and its use as a geothermometer. Clays and Clay Minerals, 41, pp 162–177.

Hökmark H, Fälth B, 2003. Thermal dimensioning of the deep repository. Influence of canister spacing, canister power, rock thermal properties and nearfield design on the maximum canister surface. SKB TR-03-09, Svensk Kärnbränslehantering AB.

Jackson M L, 1975. Soil chemical analysis: advanced course. 2nd ed. Madison, WI: Parallel Press.

Jansson M, Eriksen T E, 1998. CHEMLAB – in situ diffusion experiments using radioactive tracers. Radiochimica Acta, 82, pp 153–156.

Johannesson L-E, Börgesson L, Sandén T, 1995. Compaction of bentonite blocks. Development of technique for industrial production of blocks which are manageable by man. SKB TR 95-19, Svensk Kärnbränslehantering AB.

Karnland O, 1999. Äspö Hard Rock Laboratory. Test plan. Long term test of buffer material. SKB IPR-99-01, Svensk Kärnbränslehantering AB.

Karnland O, Birgersson M, 2006. Montmorillonite stability. With special respect to KBS-3 conditions. SKB TR-06-11, Svensk Kärnbränslehantering AB.

Karnland O, Sandén T, Johannesson L-E, Eriksen T E, Jansson M, Wold S, Pedersen K, Motamedi M, Rosborg B, 2000. Long term test of buffer material. Final report on the pilot parcels. SKB TR-00-22, Svensk Kärnbränslehantering AB.

Karnland O, Olsson S, Nilsson U, 2006. Mineralogy and sealing properties of various bentonites and smectite-rich clay materials. SKB TR-06-30, Svensk Kärnbränslehantering AB.

Karnland O, Olsson S, Nilsson U, Sellin P, 2007. Experimentally determined swelling pressure and geochemical interactions of compacted Wyoming bentonite with highly alkaline solutions. Physics and Chemistry of the Earth, 32, 275–286.

Karnland O, Olsson S, Dueck A, Birgersson M, Nilsson U, Hernan-Håkansson T, Pedersen K, Nilsson S, Eriksen T E, Rosborg B, 2009. Long term test of buffer material at the Äspö Hard Rock Laboratory, LOT project – Final report on the A2 test parcel. SKB TR-09-29, Svensk Kärnbränslehantering AB.

Laaksoharju M, Smellie J, Nilsson A-C, Skårman C, 1995. Groundwater sampling and chemical characterization of the Laxemar deep borehole KLX02. SKB TR 95-05, Svensk Kärnbränslehantering AB.

Meier L P, Kahr G, 1999. Determination of the cation exchange capacity (CEC) of clay minerals using the complexes of copper(II) ion with triethylenetetramine and tetraethylenepentamine. Clays and Clay Minerals, 47, pp 386–388.

Moore D M, Reynolds R C, 1989. X-ray diffraction and the identification and analysis of clay minerals. Oxford: Oxford University Press.

Muurinen A, 1994. Diffusion of anions and cations in compacted sodium bentonite. Ph.D. thesis. Espoo: Technical Research Centre of Finland. (VTT Publications 168).

Muurinen A, 2001. Development and testing of analysis methods for bentonite porewater. Posiva Working Report 2001-07, Posiva Oy, Finland.

Muurinen A, Lehikoinen J, 1999. Porewater chemistry in compacted bentonite. Posiva 99-20, Posiva Oy, Finland.

Müller-Vonmoos M, Kahr G, 1983. Mineralogische Untersuchungen von Wyoming Bentonit MX-80 und Montigel. NAGRA Technisher Bericht 83-12, Nationale Genossenschaft für die Lagerung radioaktiver Abfälle, Switzerland.

Perry E A, Hower J, 1970. Burial diagenesis in Gulf Coast pelitic sediments. Clays and Clay Minerals, 18, pp 165–178.

Pusch R, Karnland O, Lajudie A, Lechelle J, Bouchet A, 1993. Hydrothermal field test with French candidate clay embedding steel heater in the Stripa mine. SKB TR 93-02, Svensk Kärnbränslehantering AB.

Rendahl B, 1998. Avlägsnande av korrosionsprodukter på koppar (utkast II 98-08-18). KI Rapport 65 221, Korrosionsinstitutet (The Swedish Corrosion Institute). (In Swedish).

Rosborg B, 1998. Exposure of copper samples in bentonite. STUDSVIK/M-98/76, Studsvik Material AB, Sweden.

Ruotsalainen P, Snellman M, Helenius J, Keinonen M, Vaahtera V, Kuusela H, Oksa M, 1994. TVO:n vesinäytteenoton kenttätyöohje. (TVOs field working guide to water sampling). Working report PATU-94-28, Teollisuuden Voima Oy, Finland. (In Finnish).

Silbey R J, Alberty R A, 2001. Physical chemistry. 3rd ed. New York: John Wiley & Sons.

SKB, 1999. Äspö Hard Rock Laboratory. Annual report 1998. SKB TR-99-10, Svensk Kärnbränslehantering AB.

Slaughter M, Early J W, 1965. Mineralogy and geological significance of the Mowry bentonites, Wyoming. New York: Geological Society of America. (Special Paper 83).

Weaver C E, 1959. The clay petrology of sediments. Clays and Clay Minerals, 6, pp 154–187.

Wersin P, Bruno J, Spahiu K, 1993. Kinetic modelling of bentonite-canister interaction. Implications for Cu, Fe and Pb corrosion in a repository for spent nuclear fuel. SKB TR 93-16, Svensk Kärnbränslehantering AB.

Wersin P, Spahiu K, Bruno J, 1994. Kinetic modelling of bentonite-canister interaction. Long-term predictions of coper canister corrosion under oxic and anoxic conditions. SKB TR 94-25, Svensk Kärnbränslehantering AB.

Yu W J, Neretnieks I, 1997. Diffusion and sorption properties of radionuclides in compacted bentonite. SKB TR 97-12, Svensk Kärnbränslehantering AB.

Appendix A

Cation diffusion

Mats Jansson, Trygve E Eriksen and Kjell Svärdström

KTH

A1 Introduction

The diffusion of cations in bentonite clay has been studied extensively in laboratory by for instance Muurinen (1994), Eriksen and Jansson (1996), Yu and Neretnieks (1997). Apparent and effective diffusivities as well as sorption coefficients (K_d-values) are known for a wide range of elements present in spent nuclear fuel. However, field data for diffusion of ions in bentonite clay are not as abundant as laboratory data, and the quite unique conditions that the LOT experiments offer (larger scale, initially dry bentonite subjected to water saturation, high temperature and temperature gradient across the buffer during the experiments) are enticing.

The cations Cs^+ and Co^{2+} with tracers ^{134}Cs and ^{57}Co, respectively, were chosen for the experimental study since they reasonably well fulfill the following criteria:

- Diffusion behavior at different chemical conditions should be well characterized.
- Dependence of sorptive behavior and sorption mechanisms on pH and water solution composition should be known.
- The dominant sorption mechanism for the cations should preferably be different, *i.e.* ion exchange for Cs^+ and surface complexation for Co^{2+}.
- The half-life of the tracers should be sufficiently long to allow at least a two-year experimental study.
- The retardation of the ions should be sufficient to keep the ions from diffusing out of the bentonite blocks.

The results of the diffusion experiment in the first two LOT test parcels (S1 and A1) deviated from what was expected (Karnland et al. 2000), complementary laboratory experiments with similar conditions as those in LOT (tracer placed in dry bentonite, then exposed to water saturation and heating) were therefore carried out.

A2 Experimental performance

The experimental technique chosen in the field test was to add the diffusants (carriers and tracers), contained in pre prepared plugs of dry bentonite compacted to the desired dry density, to well defined positions in the bentonite parcel immediately before lowering the parcel into the borehole. Two identical bentonite plugs doped with ^{57}Co and ^{134}Cs were prepared in laboratory using 20 mm long cylindrical plugs with 20 mm diameter. A 5 mm diameter hole was drilled into the center of each plug and a few cubic millimeters of dry bentonite, ion exchanged to contain 1 MBq of each tracer, was placed at the bottom of the hole. The remaining volume was refilled with inactive bentonite and compacted to the original density. The plugs were inserted in two diametrically opposite holes in the fifth bentonite block from the bottom of the test parcel (see Figure 3-3 in the LOT A0 main report). The holes in the block were sealed with undoped bentonite plugs.

The radionuclides were left in the bentonite parcel for the whole experimental period and thus exposed to the water saturation and heat treatment described in section 4 in the main report. When the groundwater on water saturation of the bentonite parcel reached the radionuclides, the diffusion started and continued for the rest of the experimental period.

A2.1 Laboratory studies

Two laboratory experiments were performed in a cylindrical cell equipped with a heating plate at one end and a filter at the other end, see Figure A-1. A few cubic millimeters of dry bentonite, ion exchanged to contain the desired caesium activity, were placed 0.5 cm from the bottom and close to bottom of the cell in Experiments 1 and 2, respectively. Additional bentonite was then added and the clay compacted to 1,800 kg m^{-3} dry density.

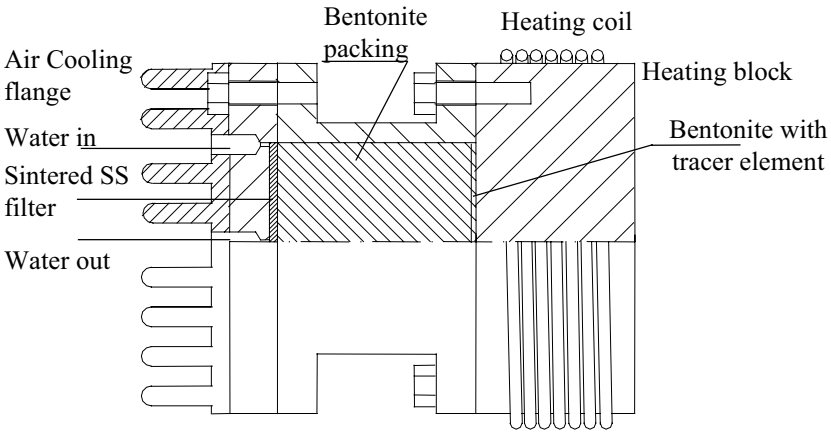

Figure A-1. *Drawing of the cell used in the laboratory experiments.*

Water was pumped through the inlet channel of the filter during the whole experiment. Whereas the clay was water saturated for 63 days before turning on the heater in Experiment 1 the heater was turned on at the start of water saturation in Experiment 2. The temperatures used were 70 and 90°C in Experiment 1 and 2, respectively. When the experiments were terminated after 95 days, the bentonite plug was sliced into thin sections, dried, weighed and analyzed by γ-counting using a germanium detector and multi-channel analyzer.

A3 Analyses

The whole A0 parcel was recovered from the deposition hole in the rock by a technique called "over-lapping core drilling", see further sections 4.4.1 in the A0 main report for retrieval and portioning detailes. The lower part of the A0 parcel was taken to the radiochemical laboratories of Nuclear Chemistry at KTH, Stockholm. The block was cut into slices and the slices were scanned with a GM-detector equipped with a collimator. Spot samples were taken at selected positions and on approaching the maximum specific activity the sample volumes were reduced and the sampling more frequent. Altogether about 100 samples were taken from the A0 parcel. Each sample was weighed and analyzed by γ-counting.

Figure A-2. *Test parcel A0 after the successful uptake.*

A4 Data evaluation

A4.1 Field experiment

From the A0 analyses, activity values from approximately 100 positions in the bentonite parcel were obtained. Since one doped bentonite plug was inserted at each side of the copper tube, the samples were divided into two groups depending on which side of the tube the sample was taken from. The two groups were then treated separately. A coordinate system was applied to each side of the copper tube, putting the origin in the point where the activity maximum was found. The distance to the origin was calculated for each point to create a one-dimensional activity profile. The profile was then examined to see whether it looked different in different directions from the origin. This was done by studying six 1 cm thick planes in different directions in space. The examination showed that the profiles for both cobalt and caesium appeared to be the same in all planes on both sides of the copper tube.

Scooping calculations showed that with the diffusivities and K_d-values obtained in a similar environment, the radionuclides would not diffuse out of the bentonite block. The system could therefore be described as diffusion from a source into an infinite medium. The cylinder containing the radionuclides was approximated to be a sphere. The concentration at distance r could then be obtained from Equation A-1 (Crank 1975).

$$C(r,t) = \frac{1}{2}C_0\left\{\operatorname{erf}\frac{a+r}{2\sqrt{(Dt)}} + \operatorname{erf}\frac{a-r}{2\sqrt{(Dt)}}\right\} - \frac{C_0}{r}\sqrt{\left(\frac{Dt}{\pi}\right)}\left\{e^{\frac{(a+r)^2}{4Dt}} - e^{\frac{(a-r)^2}{4Dt}}\right\} \qquad \text{Equation A-1}$$

where C_0 is the initial concentration, a is the radius of the sphere and D the diffusivity, or as in this case, the apparent diffusivity, D_a.

A4.2 Laboratory experiments

The initial activity distribution was treated as an infinitely thin layer and the apparent diffusivity was calculated from the slopes in ln(C) versus x^2 plots. The slope, k is then equal to (Crank 1975):

$$k = -\frac{1}{4D_a t} \qquad \text{Equation A-2}$$

where D_a is the apparent diffusivity and t the time. The time required to reach water saturation was estimated to be 50 days.

A5 Results and discussion

Water molecules are sorbed between the montmorillonite layers when bentonite swells. Initially, the amount of water in the LOT experiments corresponds to one layer of water molecules, which increases to around three layers of water molecules at full water saturation. One can argue that the diffusion starts with a low apparent diffusivity and that the apparent diffusivity increases as the water layers build up between the montmorillonite layers. Consequently, the diffusivities obtained from this kind of field experiments are less controlled than those performed in the laboratory.

A5.1 Field experiment

Cobalt

The A0 activity profile for cobalt is presented in Figure A-3. From the plot it is obvious that the cobalt did not move much at all, which was to be expected from the relatively high K_d -values and low diffusivities found in earlier laboratory and CHEMLAB investigations. As can be seen from the calculated profiles, the apparent diffusivity, D_a, is about $2.5 \cdot 10^{-13}$ m^2 s^{-1}, which is in good agreement with diffusivities obtained in the laboratory (Eriksen and Jansson 1996) as well as CHEMLAB experiments (Jansson and Eriksen 1998).

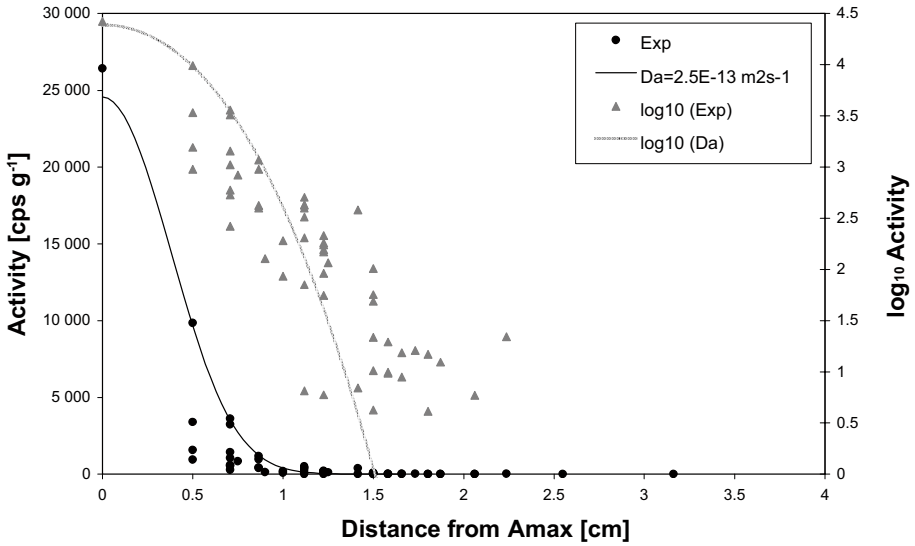

Figure A-3. *Experimentally determined and calculated results for cobalt in the A0 test parcel.*

Caesium

The results from the previous LOT experiment (A1) revealed an unexpected caesium distribution. However, when the experiment was repeated in test parcel A0, a more "normal" activity profile was obtained, as can be seen in Figure A-4. The obtained apparent diffusivity, D_a, is about $1 \cdot 10^{-12}$ m^2 s^{-1}, which is in good agreement with data obtained in previous investigations (Eriksen and Jansson 1996, Jansson and Eriksen 1998, Eriksen et al. 1999) as well as in the laboratory experiments with increased temperature, see Table A-1.

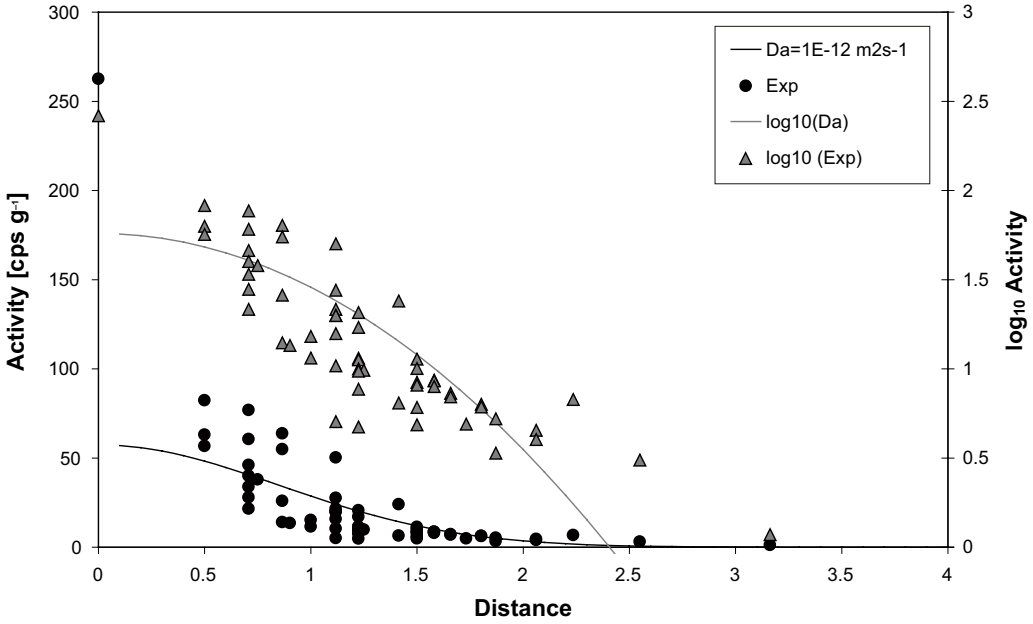

Figure A-4. *Experimentally determined and calculated results for caesium in the A0 test parcel.*

Table A-1. Obtained apparent diffusivities for Cs^+ and Co^{2+} in this study, in the laboratory (Eriksen and Jansson 1996) and in the CHEMLAB (*in situ*) experiments (Jansson and Eriksen 1998). All units are $m^2\ s^{-1}$.

Cation	A0[a]	Laboratory (70°C)[a]	Laboratory (20°C)[b]	CHEMLAB (15°C)[b]
Co^{2+}	~$2.5\cdot10^{-13}$	$8\cdot10^{-14}$	$(2 \pm 1)\cdot10^{-13}$	$4.4\cdot10^{-13}$
Cs^+	~$1\cdot10^{-12}$	$8.7\cdot10^{-12}$	$(2 \pm 1)\cdot10^{-12}$	$2\cdot10^{-12}$

[a] Temperature gradient over the clay

[b] No temperature gradient over the clay

A5.2 Laboratory experiments

In the high temperature experiment (90ºC), the heater was turned on from the beginning of the experiment. The analyses revealed that the cations had not moved much at all, indicating that water saturation was not sufficient at the activity. No conclusions were hence drawn from the high temperature laboratory experiment.

Figure A-5 displays the results from the caesium experiment. As can be seen, the experimental data fit nicely to a line which corresponds to an apparent diffusivity of about $8.7\cdot10^{-12}$ $m^2\ s^{-1}$, which is slightly higher than diffusivities obtained in laboratory and CHEMLAB experiments performed at room temperature with no temperature gradient over the clay. It is obvious that the caesium has not moved further than expected, which was found to be the case in the previous LOT experiment (Karnland et al. 2000).

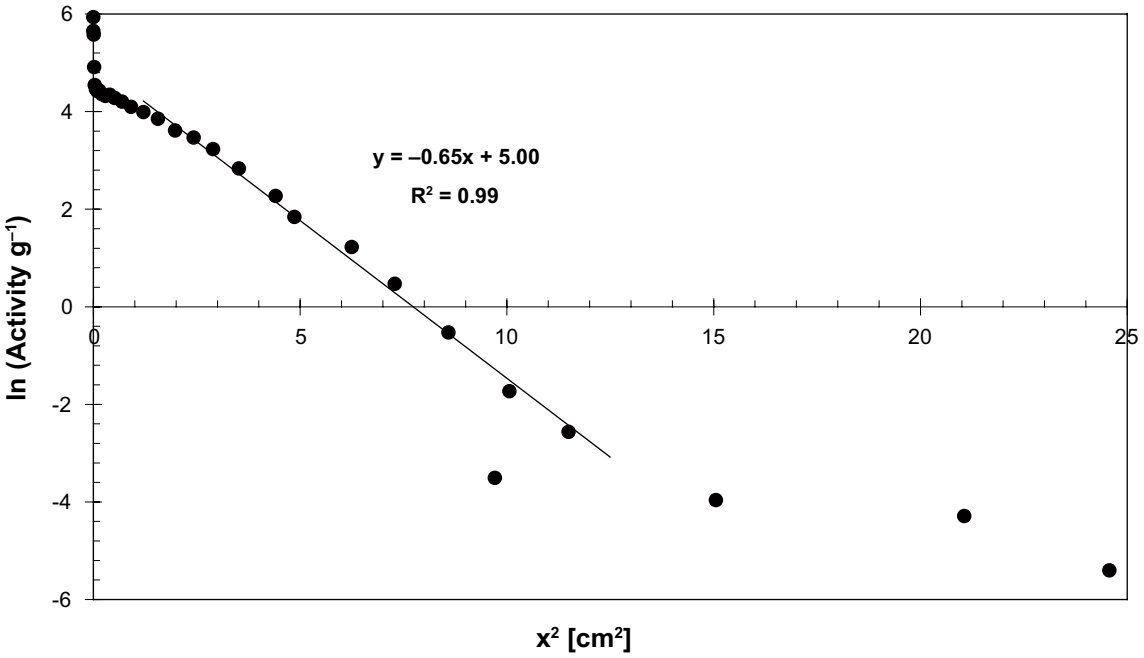

Figure A-5. *Laboratory results for caesium at 70ºC plotted as x^2 vs ln (specific activity). The least square fitted line gives an apparent diffusivity of $8.7\cdot10^{-12}$ $cm^2\ s^{-1}$.*

A5.3 Discussion

The diffusivity is proportional to the absolute temperature, T, and indirectly proportional to a friction factor f according to (Silbey and Alberty 2001)*;*

$$D = \frac{RT}{N_A f}$$ Equation A-3

where R is the gas constant and N_A Avagadro's number. The friction factor can for spherical particles with radius r be described as

$$f = 6\pi\eta r$$ Equation A-4

where η is the viscosity.

The viscosity of water is approximately 1 mN s m^{-2} at room temperature, while it is about 0.35 mN s m^{-2} at 70ºC (Coulson and Richardson 1977). The diffusivity in pure water is thus approximately three and a half times greater at 70ºC as compared to 20ºC, which agrees well with the diffusivities obtained for caesium. However, the effect of high temperature on the sorption of cations and on the behavior of bentonite is extremely difficult to quantify, and the agreement for cesium in obtained diffusivities and estimated diffusivities in pure water may be purely incidental.

Appendix B

Post test examination of copper coupons from LOT test parcel A0 regarding corrosion

Bo Rosborg, Studsvik Nuclear AB

B1 Summary

Coupons of pure copper have been exposed in bentonite blocks 22 and 30 in LOT test parcel A0 at the Äspö Hard Rock Laboratory from December 1999 to November 2001 (in total 498 days at full temperature). The conditions for the coupons have been similar to the conditions anticipated in an early phase in a KBS-3 repository. Objective: Determine nature and extent of copper corrosion.

This report documents the post-test examination of copper coupons A022A and A030C. The coupons had milled surfaces but for one polished side, and contained a micro hardness indentation on the latter.

The copper coupons showed about the same weight loss, in spite of the fact that coupon A022A has been exposed at about 80°C and coupon A030C at about 35°C, and the average corrosion rate was estimated to be less than 4 µm/year.

The nature of the corrosion can be classified as a somewhat uneven general attack; the corrosion attack is on the micro scale somewhat uneven and different corrosion products are formed along the surfaces of the coupons, however, any obvious signs of pitting cannot be claimed.

B2 List of contents

B3 Background information

The test series “Long Term Test of Buffer Material” (LOT) has been initiated at the Äspö Hard Rock Laboratory comprising conditions similar to those in an early phase in a KBS-3 repository (Karnland et al. 2000). The main purpose is to study the behaviour of the bentonite clay. Wyoming bentonite with the commercial name MX-80 has been used. However, additional testing has been included, and the investigation of corrosion on copper coupons exposed in bentonite blocks is the subject of this report.

Objective Determine nature and extent of copper corrosion.

Attempt “Quantitative information about the mean corrosion rate. Qualitative information about pit corrosion and corrosion products” (Karnland 1999).

Hypothesis The average corrosion rate is less than 7 µm per year (Wersin et al. 1994).

A pilot test series has earlier been performed and evaluated (Karnland et al. 2000). The average corrosion rate of a copper coupon in LOT test parcel S1 exposed at about 50°C was estimated to less than 3 µm/year (Rosborg 1998).

The present investigation concerns LOT test parcel A0 (Karnland 1999). The copper coupons exposed in bentonite blocks no A022 and A030 were handed over by Ulf Nilsson, Clay Technology AB, at Äspö on September 6, 2002. The two coupons in bentonite block A022, copper coupons A022A and A022B, were already loose from the bentonite block, however, copper coupons A030C and A030D were still inside an intact bentonite block.

The copper coupons were manufactured from plate material of canister quality (99.99% Cu with a deliberate addition of 50 ppm P). All but one side was left in the as-machined milled condition, and one side was also polished (FEPA P# 500). The nominal dimensions of the coupons were 60·15·1.5 mm. For actual dimensions, surface area and original weight before exposure, see Table B-1. Each coupon was marked with a capital letter in one end on the polished side. (The complete notification used in reporting is comprised of the test parcel identification followed by the bentonite block number and this letter, as an example A022A.) Copper coupons A022A and A030C contained a micro hardness indentation on the polished side. (Intention: Photographing of the same area before and after exposure.)

Test parcel A0 was emplaced on December 16, 1999. Power to the heater was first turned on February 2, 2000. Full temperature lasted from June 16, 2000, up to October 18, 2001. The bentonite blocks no 22 and 30 have been exposed at temperatures of about 80°C and 35°C respectively. The test parcel was retrieved on November 27, 2001. The total time of exposure is 710 days and the time of exposure at full temperature is 498 days.

Table B-1. Copper coupons in LOT test parcel A0.

Coupon	Length mm	Width mm	Thickness mm	Surface area mm^2	Weight g	Micro hardness indentation
A022A	60.03	14.98	1.51	2,025	11.8634	x
A022B	60.08	15.03	1.50	2,031	11.9023	
A030C	59.99	15.00	1.50	2,025	11.8469	x
A030D	60.10	14.99	1.51	2,029	11.8745	

B4 Experimental procedure

The sequence of actions performed during investigation of the copper coupons were:

Item Action

0 Origin.

1 Photographing of the received copper coupon A022A in a bentonite piece.

2 Photographing of the received bentonite block A030 containing copper coupons A030C and A030D.

3 Breaking loose copper coupon A030C.

4 Photographing of copper coupon A030C with bentonite pieces.

5 Exposure of copper coupons A022A and A030C separately in deionised water overnight followed by flushing with deionised water.

6 Drying and weighing of the copper coupons.

7 Photographing of polished and milled side of ditto.

8 Ultrasonic cleaning of the copper coupons in deionised water during 5 min.

9 Drying and weighing.

10 Photographing.

11 Ultrasonic cleaning during another 55 min.

12 Drying and weighing.

13 Photographing.

14 Exposure in 10% H_2SO_4 solution during 10 min + another 5 min with ultrasonic cleaning in the same solution.

15 Drying and weighing.

16 Photographing.

17 Scanning electron microscopy.

This sequence of actions was elaborated in the investigation of copper coupons from LOT test parcel S1 (Rosborg 1998).

Copper coupon A022A was photographed in its bentonite piece as received (item 1), see Figure B-1 on page 5. (Coupon A022B was archived in its plastic container for later transport to Clay Technology.)

Copper coupon A030C was removed from bentonite block 30 by first sawing loose "a piece of cake" and then breaking loose the coupon from this part (item 3), see Figure B-2. (The remaining part of the block was archived for later transport to Clay Technology.)

The coupons went first through a few steps of cleaning in deionised water. (The water from each cleaning step were saved for possible later examination of loose corrosion products.) In the previous investigation a reference coupon was selected to follow the exposed coupons through all cleaning procedures for the purpose of comparison (Karnland et al. 2001). However, this time no reference coupon was used, but saved for later investigations of copper coupons within the LOT project.

The main reason for exposure of the coupons in water overnight was to get rid of adhesive bentonite. When the coupons were removed from the water, they were flushed with water which was also saved.

The coupons were stored in a desiccator before each weighing operation and a control weight was used.

Finally the coupons were exposed to 10% H_2SO_4 solution, first dipped in the solution for 10 min and then ultrasonically cleaned in the same solution during another 5 min (Rendahl 1998). After treatment in this solution the copper coupons were examined in a scanning electron microscope (SEM).

B5 Corrosion rates

The weight changes of the copper coupons after the different cleaning steps are compiled in Table B-2.

Table B-2. Weight changes during the cleaning procedure (in g).

Item	Condition	Coupon A022A	Coupon A030C
0	Original weight	11.8634	11.8469
6	After exposure in water over night	11.8737	11.8106
9	After 5 min ultrasonic cleaning in water	11.8614	11.7976
12	After 60 min ultrasonic cleaning in water	11.8470	11.7902
15	After 15 min in 10% H_2SO_4 solution	11.7775	11.7638
	Total weight loss	85.9 mg	83.1 mg

The average corrosion rate of the copper coupons has been calculated from the following data and is given in Table B-3:

weight loss – from Table B-2

surface area – 20.25 cm^2 for both; the actual sample dimensions deviated somewhat from the nominal, however, they gave the same surface area

density of copper – 8.94 g/cm^3

time of exposure – 498 days at full temperature (in total 710 days).

Table B-3. Weight loss data and estimated average corrosion rate.

Coupon	Original weight g	Final weight g	Weight loss mg	Corrosion rate µm/year
A022A	11.8634	11.7775	86	3.5
A022B	11.9023			
A030C	11.8469	11.7638	83	3.4
A030D	11.8745			

The average corrosion rate of the copper coupons is thus less than 4 µm per year (conservatively based on the time of exposure at full temperature). The copper coupons revealed about the same corrosion rate in spite of the fact that coupon A022A was exposed at the higher temperature of about 80°C compared to about 35°C for coupon A030C.

B6 Observations

Macro photographs taken after the different steps of cleaning in deionised water and 10% H_2SO_4 solution are found in Figures B-1 through B-4. Microphotographs from scanning electron microscopy are found in Figures B-5 through B-8.

After breaking loose the copper coupons from the bentonite, corrosion products could be seen on parts of the bentonite surfaces facing the copper coupons, see for instance the right photograph in Figure B-1. The weight changes in Table B-2 reveal possible differences in adherence of the corrosion products to the coupons; after 5 min ultrasonic cleaning in water (item 9) the weight of coupon A022A is for instance about the same as its original weight, while coupon A030C has about 50 mg lower weight. Exposure to sulphuric acid was needed to remove most of the corrosion products on coupon A022A. Both brownish (cuprite) and blue-green corrosion products were seen on the coupons. The former covered the entire surface. The latter reveal the presence of bivalent copper and were present on part of the surface.

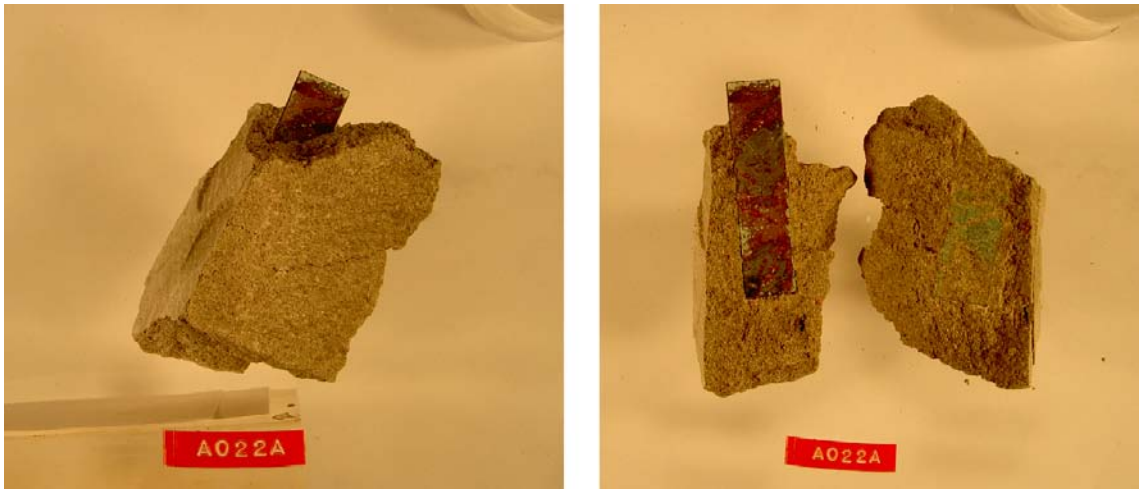

Figure B-1. *The received copper coupon A022A in its bentonite piece to the left and after breaking apart the bentonite piece to the right (item 1). The dimensions of the copper coupon were 60·15·1.5 mm.*

Figure B-2. *The received bentonite block A030 to the left and copper coupon A030C visible after breaking apart the bentonite block to the right (item 2).*

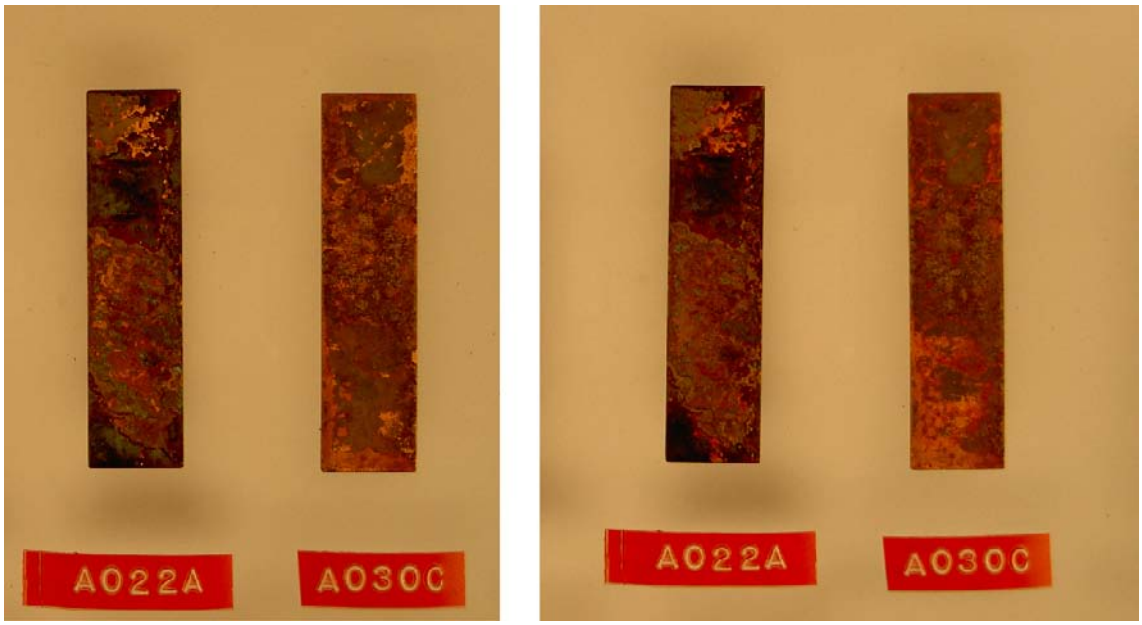

Figure B-3. *The polished side of the copper coupons after 5 min ultrasonic cleaning in water (item 10) to the left and after 60 min ditto (item 13) to the right.*

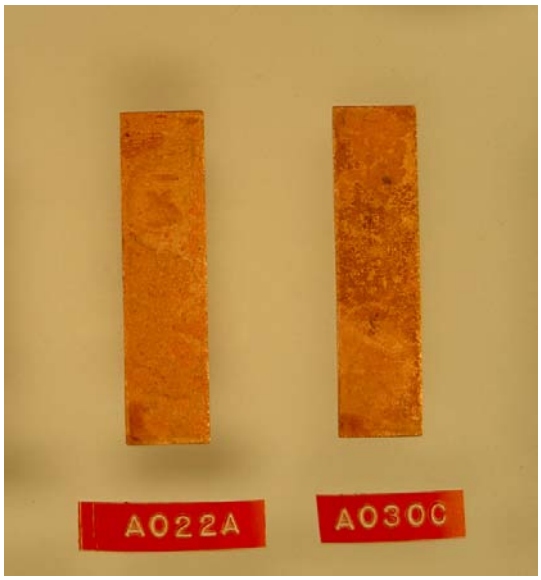

Figure B-4. *The polished side of the copper coupons after treatment in 10% H_2SO_4 solution (item 16).*

Examination of the coupons in stereo and scanning electron microscopes revealed a somewhat uneven corrosion attack. However, any signs of active pits could not be found.

Surprisingly enough it was not easy to find the micro hardness indentation mark on the polished side of the coupons after exposure, in spite of the fact that the average corrosion rate was estimated to be less than 4 µm/year and that the indentation marks were more than an order of magnitude larger, see Figures B-5 and B-6. However, the milling marks were still quite clear after exposure, see Figures B-7 and B-8.

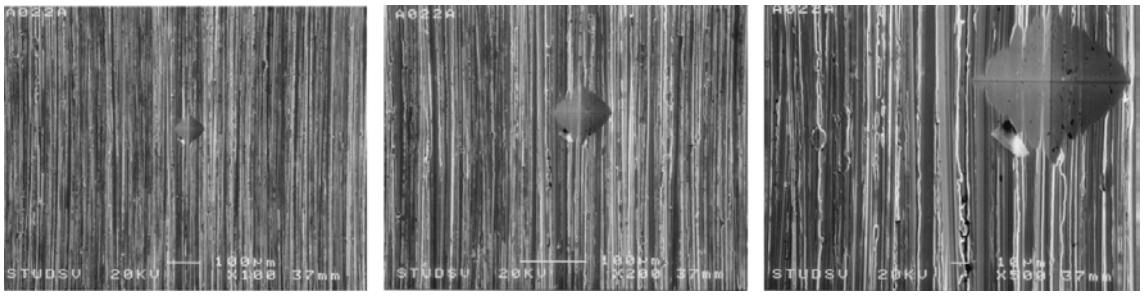

Figure B-5. *The polished surface of copper coupon A022A with micro hardness indentation before exposure (item 0).*

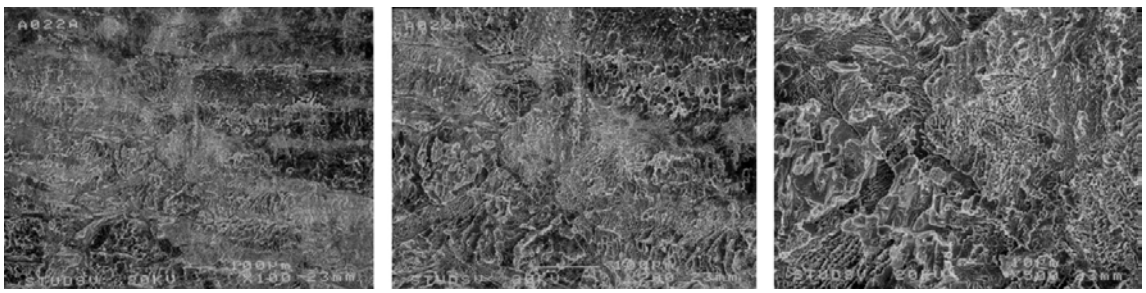

Figure B-6. *The polished surface of copper coupon A022A after exposure (item 17).*

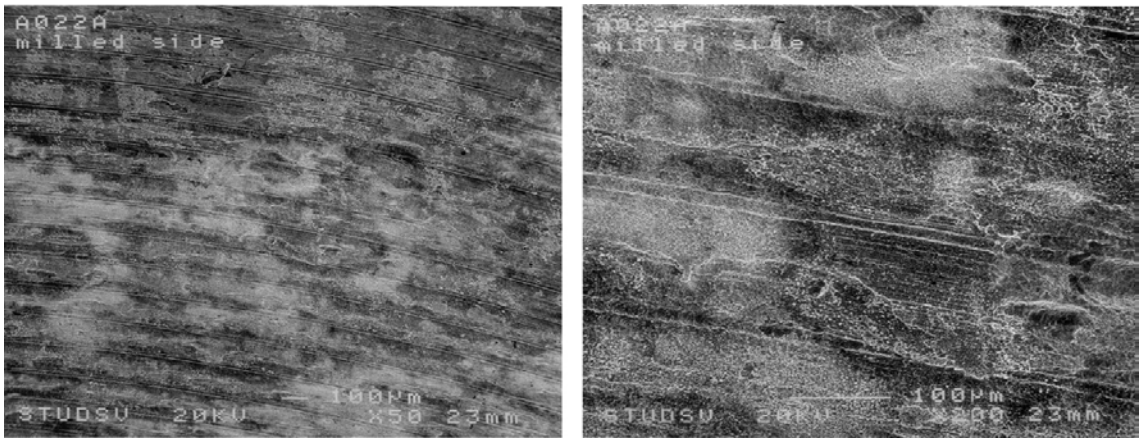

Figure B-7. *The milled surface of copper coupon A022A after exposure (item 17).*

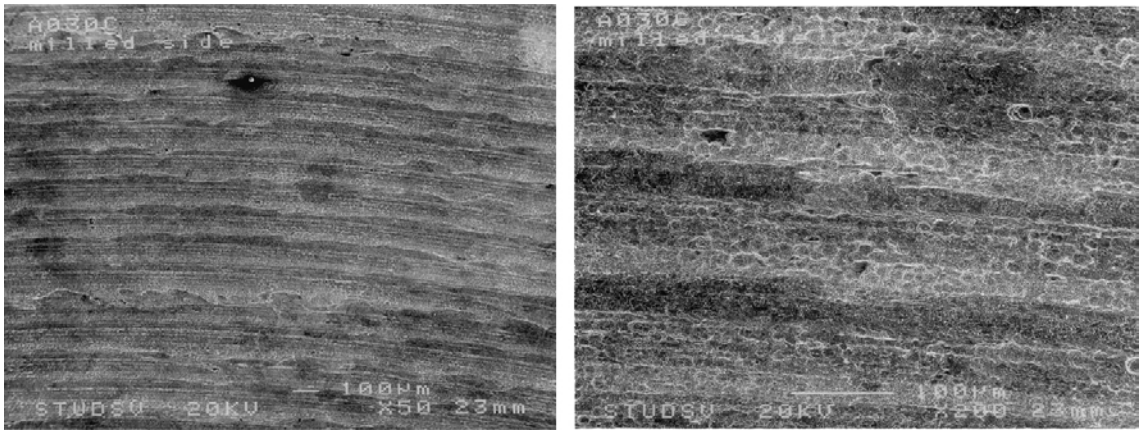

Figure B-8. *Milled surface of copper coupon A030C after exposure (item 17).*

In summary, the nature of the corrosion can be classified as a somewhat uneven general attack; the corrosion attack is on the micro scale somewhat uneven and different corrosion products are formed along the surfaces of the coupons, however, any obvious signs of pitting cannot be claimed.

B7 Acknowledgements

The contributions from Hans Ericsson (weighing and macro photography) and Roger Lundström (scanning electron microscopy) at Studsvik Nuclear AB are gratefully acknowledged.

Appendix C

Bentonite block and sensor configuration

Ola Karnland, Clay Technology

Instrument	Designation	Remark
Thermocouple	A0020T	J026369
	A0024T	J0263521
	A0028T	J026370
	A0080T	J026367
	A0082T	J026314
	A0084T	J026302
	A0086T	J026368
	A0088T	J026307
	A014TT	J026310
	A0140T	J026359
	A0142T	J026326
	A0144T	J026357
	A0146T	J026303
	A0148T	J026356
	A0200T	J026417
	A0202T	J026415
	A2204T	J026405
	A0206T	J026408
	A0208T	J026377
	A0260T	J026418
	A0264T	J026395
	A0268T	J026393
	A0324T	J026391
	A0384T	J026394
	A0TU	
Pressure	A0084P	Roctest 9934
	A0084W	Roctest 9932
	A0144P	Geokon Unit 8
	A0144W	Geokon Unit 9
	A0204P	Roctest 9917
Moisture	A0084M	4.0m 3040001
	A0142M	3.5m 3040002
	A0147M	3.5m 3040003
	A0204M	3.0m 3040004
Various tubes	A0TUBE1	Saturation Tube 1 Block 05, 18, 32 4.8m
	A0TUBE2	Saturation Tube 2 Block 05, 18, 32 4.8m
	A0TUBE3	Saturation Tube 3 Block 05, 18, 32 4.8m
	A0TUBE4	Waterpressure bottom 4.8m
	A0TUBE5	Waterpressure upper sand 1.5m

Block no.	Manufacturing no.
A0 01	59
A0 02	143
A0 03	81
A0 04	50
A0 05	60
A0 06	57
A0 07	106
A0 08	55
A0 09	65
A0 10	43
A0 11	58
A0 12	49
A0 13	73
A0 14	68
A0 15	46
A0 16	69
A0 17	71
A0 18	63
A0 19	54
A0 20	48
A0 21	56
A0 22	72
A0 23	104
A0 24	67
A0 25	64
A0 26	107
A0 27	76
A0 28	47
A0 29	51
A0 30	79
A0 31	75
A0 32	61
A0 33	74
A0 34	66
A0 35	78
A0 36	52
A0 37	89
A0 38	110

A0 02

Sensors:

A0020T
A0024T
A0028T

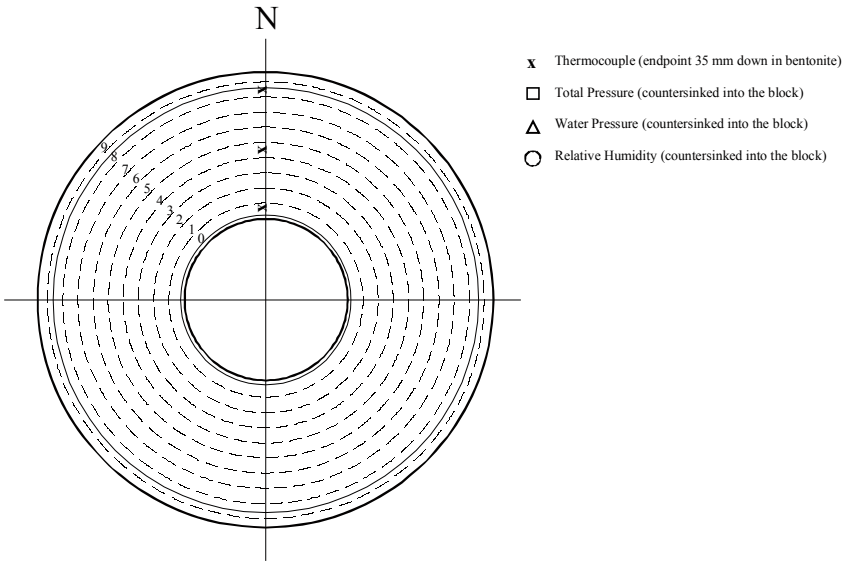

A0 05

Sensors:

Tracertest by filter and plugs

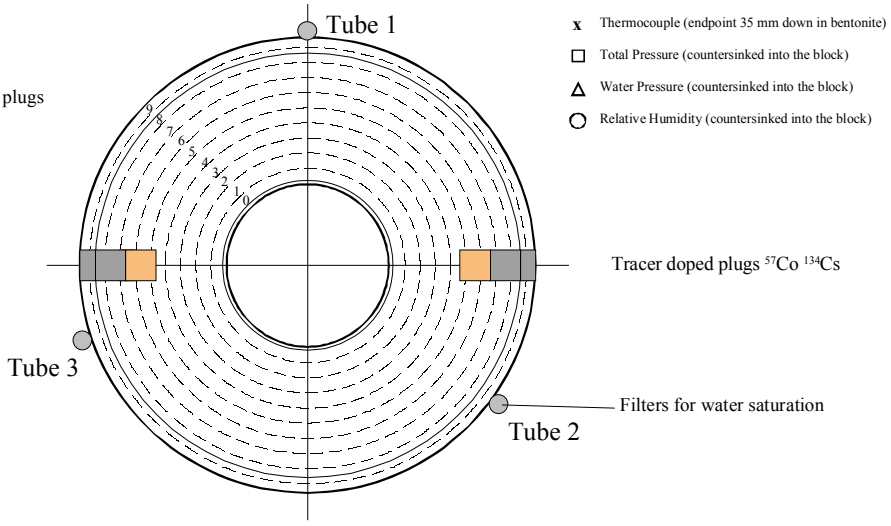

A0 08

Sensors:

A0080T
A0082T
A0084T
A0086T
A0088T

A0084P
A0084W
A0084M

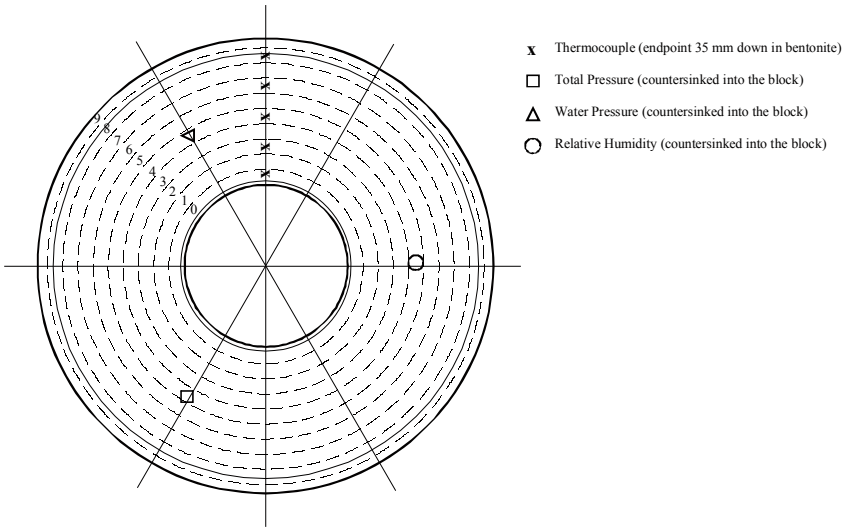

A0 10

Sensors:

Water sampling
10% CaCO3

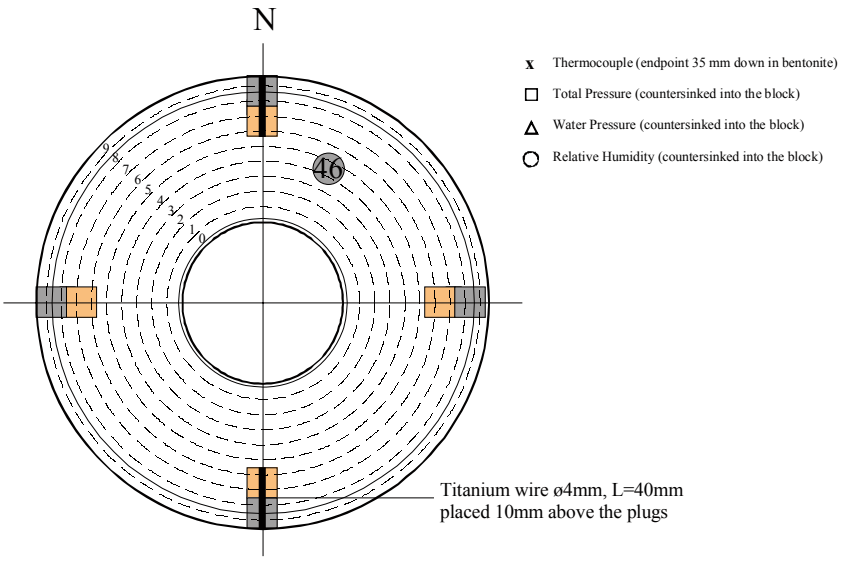

A0 12

Sensors:

Water sampling
10% CaSO4

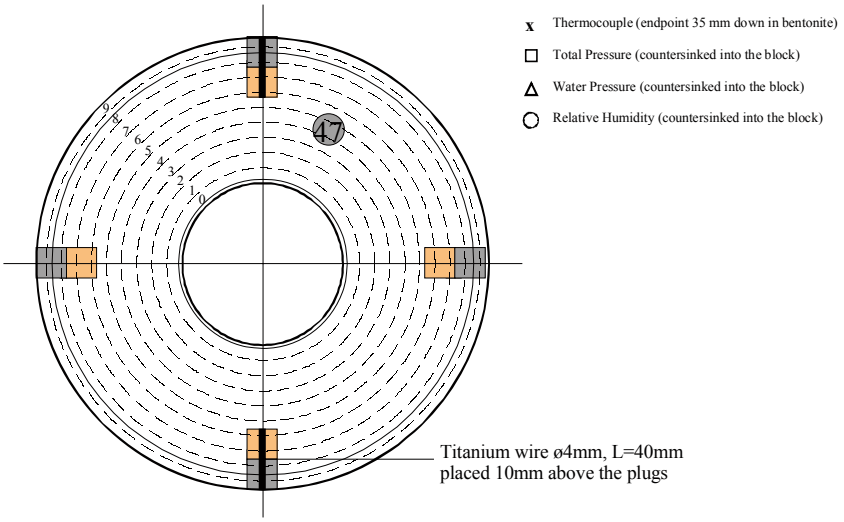

A0 14

Sensors:

A014TT
A0140T
A0142T
A0144T
A0146T
A0148T

A0144P
A0144W
A0142M
A0147M

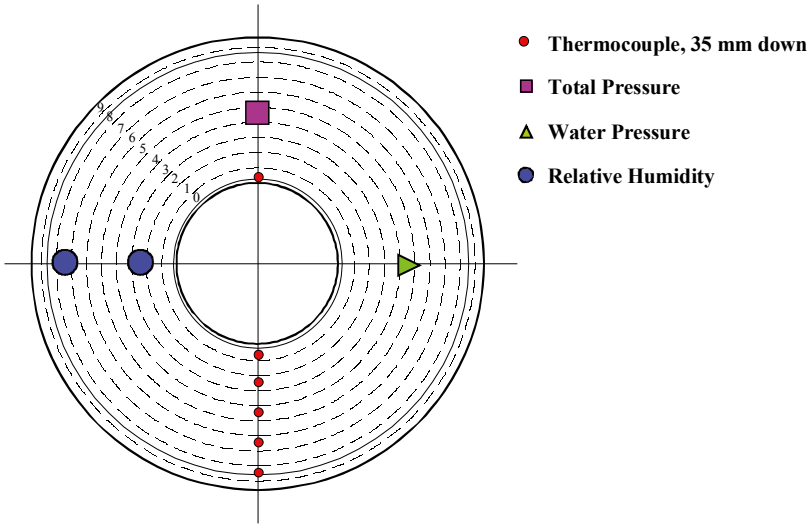

A0 16

Sensors:

Water sampling
50% K-feldspar

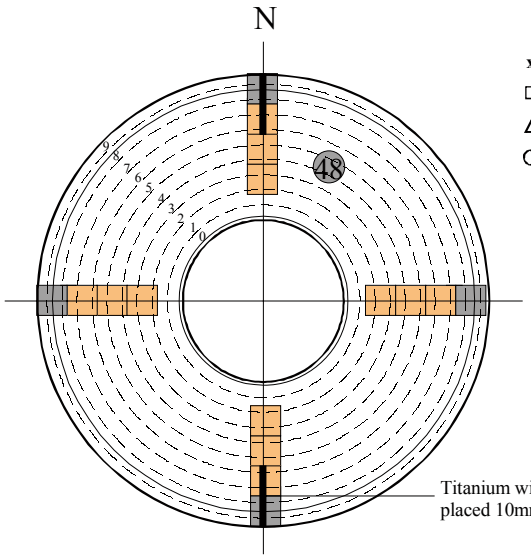

x Thermocouple (endpoint 35 mm down in bentonite)
□ Total Pressure (countersinked into the block)
△ Water Pressure (countersinked into the block)
○ Relative Humidity (countersinked into the block)

A0 18

Sensors:

Water sampling

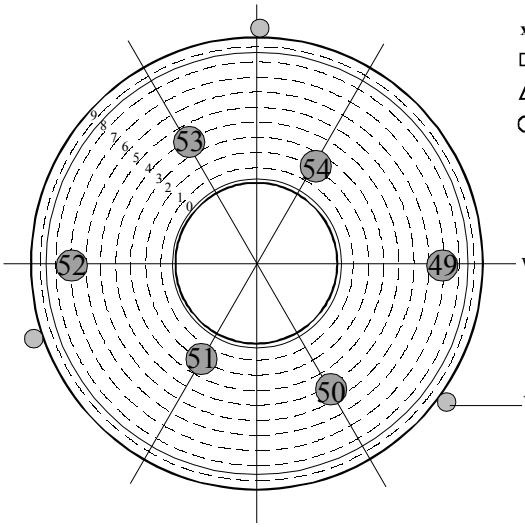

x Thermocouple (endpoint 35 mm down in bentonite)
□ Total Pressure (countersinked into the block)
△ Water Pressure (countersinked into the block)
○ Relative Humidity (countersinked into the block)

A0 20

Sensors:

A0200T
A0202T
A0204T
A0206T
A0208T

A0204P
A0204W
A0204M

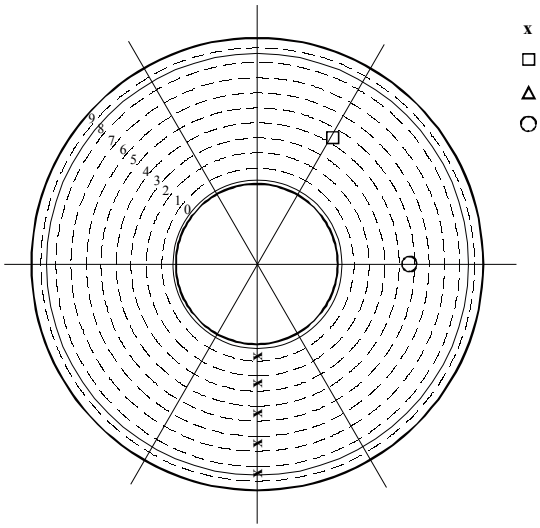

x Thermocouple (endpoint 35 mm down in bentonite)
□ Total Pressure (countersinked into the block)
△ Water Pressure (countersinked into the block)
○ Relative Humidity (countersinked into the block)

A0 22

Sensors:
Cu plate

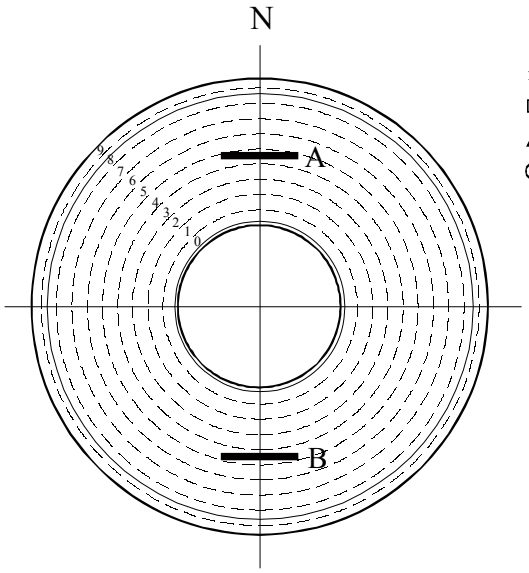

x Thermocouple (endpoint 35 mm down in bentonite)
□ Total Pressure (countersinked into the block)
△ Water Pressure (countersinked into the block)
○ Relative Humidity (countersinked into the block)

A0 24

Sensors:

Cement Aalborg AWP w/c=0.8

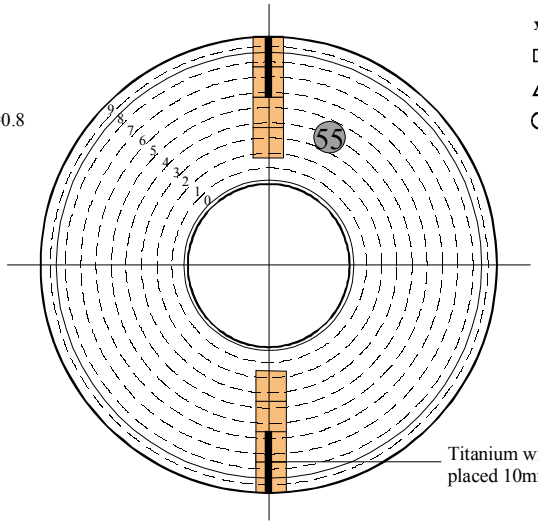

x Thermocouple (endpoint 35 mm down in bentonite)
□ Total Pressure (countersinked into the block)
△ Water Pressure (countersinked into the block)
○ Relative Humidity (countersinked into the block)

A0 26

Sensors:

A0260T
A0264T
A0268T

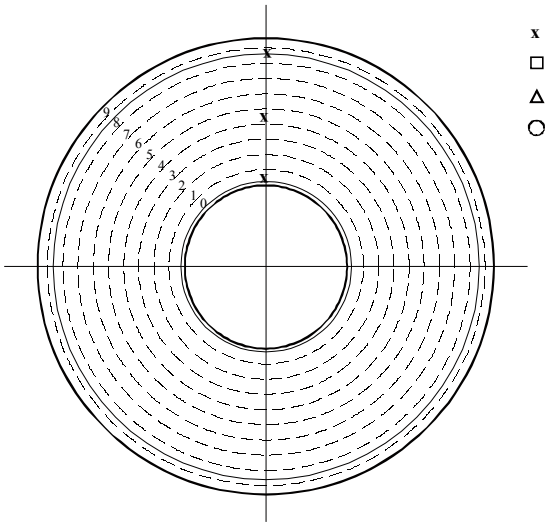

x Thermocouple (endpoint 35 mm down in bentonite)
□ Total Pressure (countersinked into the block)
△ Water Pressure (countersinked into the block)
○ Relative Humidity (countersinked into the block)

A0 30

Sensors:

Cu plate

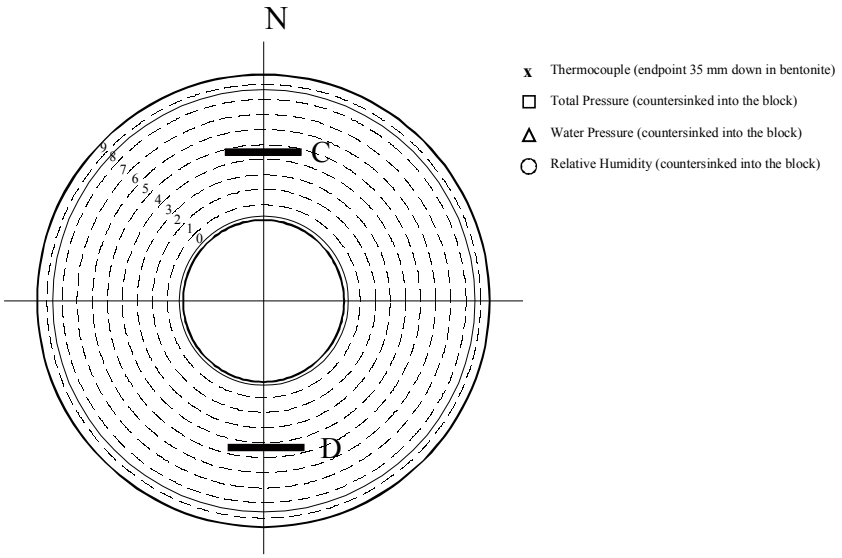

A0 32

Sensors:

A0324T
Water sampling

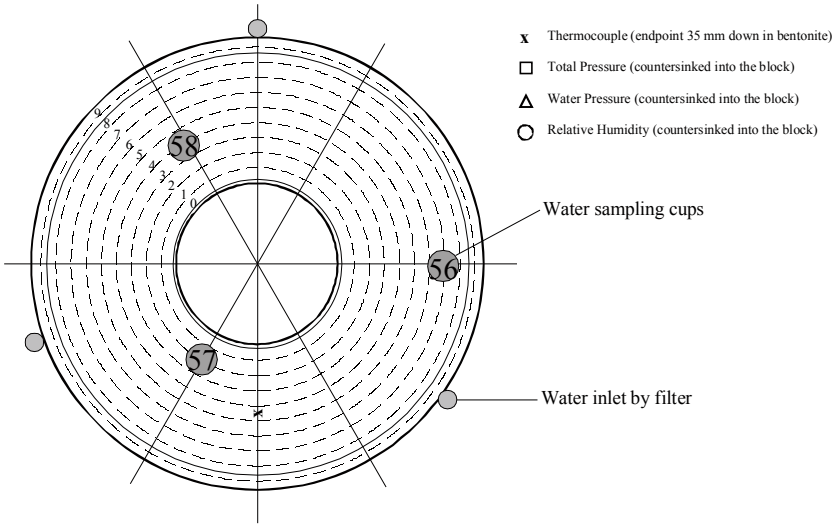

A0 34

Sensors:

Cement Aalborg AWP w/c=0.8

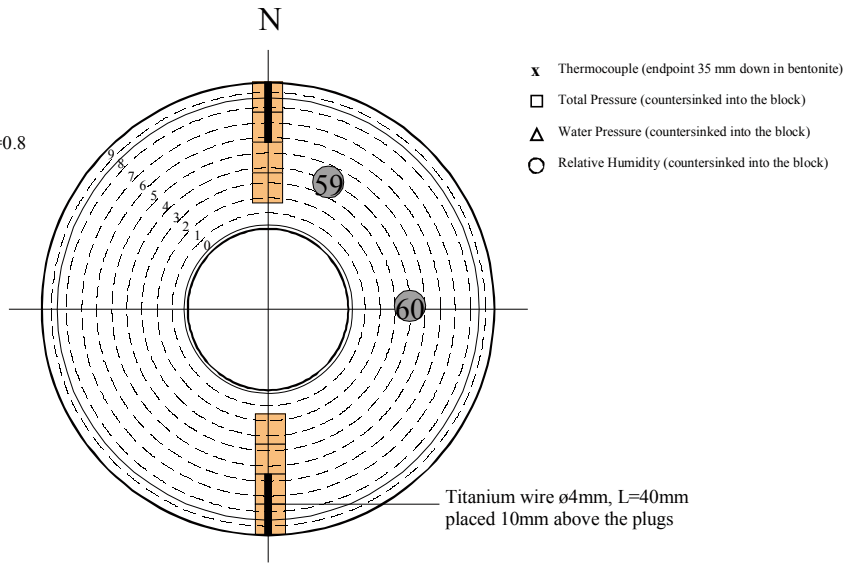

A0 38

Sensors:

A0384T

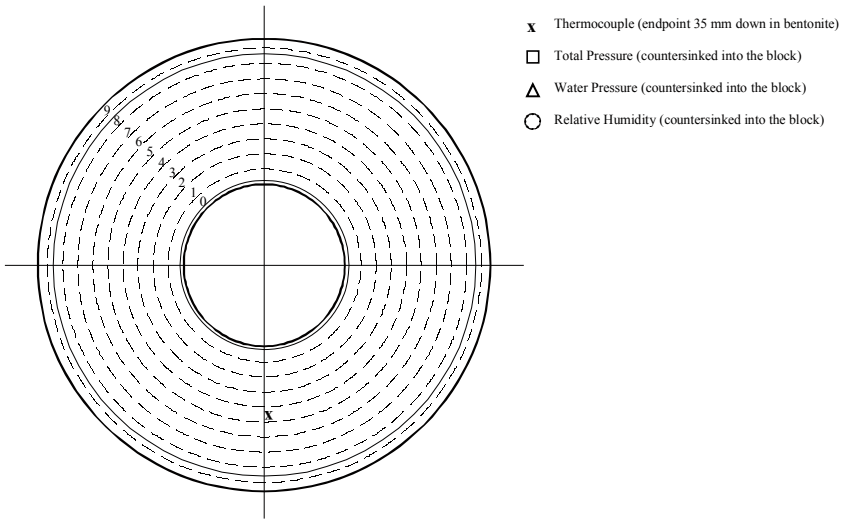

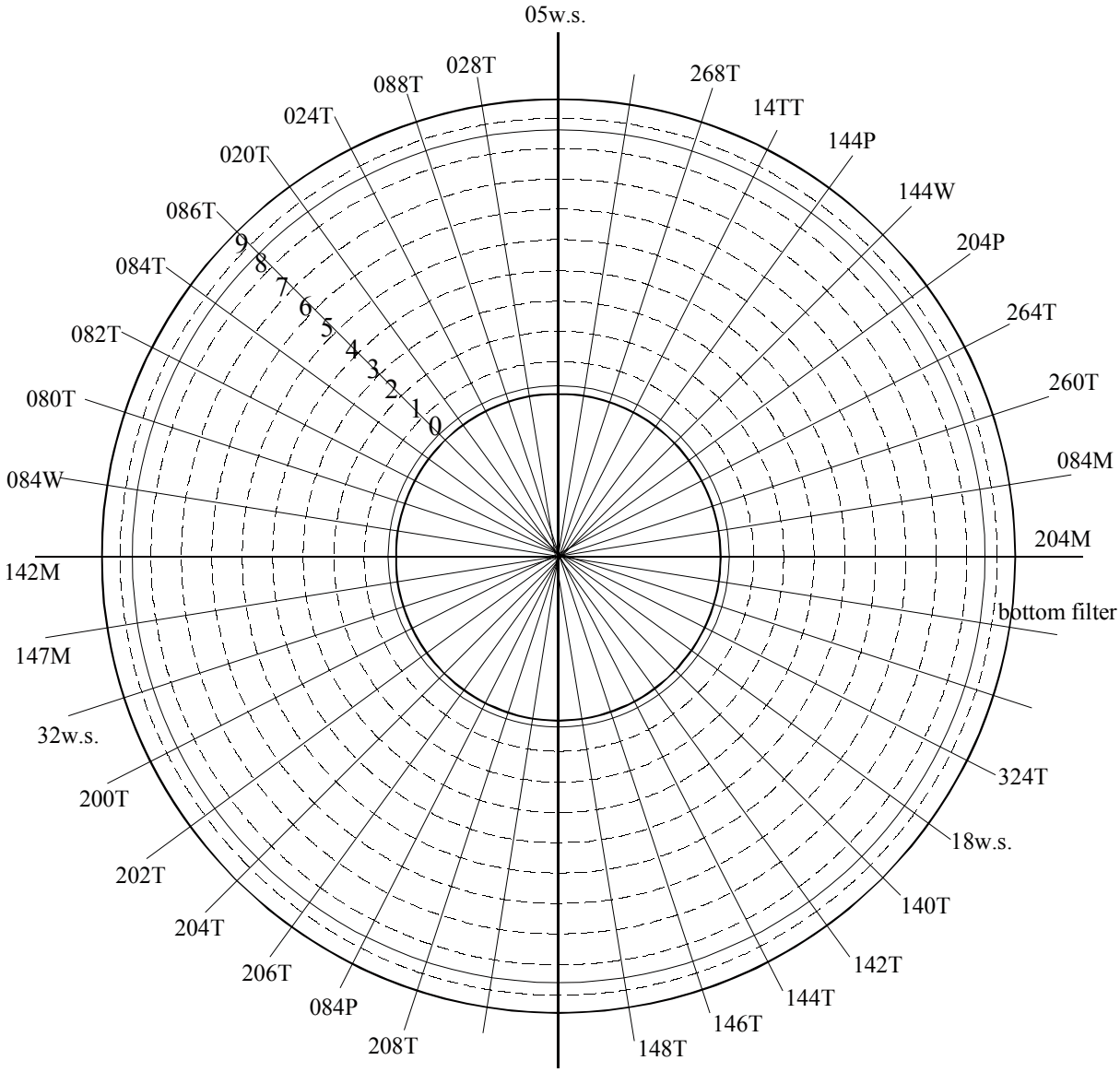
05w.s.
028T
088T
024T
020T
086T
084T
082T
080T
084W
142M
147M
32w.s.
200T
202T
204T
206T
084P
208T
148T
146T
144T
142T
140T
18w.s.
324T
bottom filter
204M
084M
260T
264T
204P
144W
144P
14TT
268T
9
8
7
6
5
4
3
2
1
0

Appendix D

Chemical conditions in the A0 parcel of the long-term test of buffer material in Äspö (LOT)

Arto Muurinen, VTT Processes

Abstract

The Long-Term Test of Buffer Material (LOT) is underway in the Äspö Hard Rock Laboratory in Sweden. The test parcels contain prefabricated bentonite blocks placed around a copper tube. The parcels are placed in vertical boreholes in a granitic rock structure. A heater is placed in the lower part of the copper tube. This report concerns the chemical studies performed on the parcel, which was excavated after about one and a half years of the experiment. Porewaters were squeezed out from the bentonite samples and their pH, Eh and S(–II), Fe^{2+}, Na^{+}, K^{+}, Ca^{2+}, Mg^{2+}, Cl^{-}, SO_4^{2-} and HCO_3^{-} concentrations were determined. The exchangeable cations and the water contents of the bentonite were also determined.

The water contents were somewhat higher at the upper, cool part of the parcel and close to the rock surface. The additives, (cement, K-feldspar, $CaSO_4$, $CaCO_3$) did not have any clear effect on the water content.

In the upper part of the parcel close to the rock surface, the TDS in the porewater was slightly below the TDS of the groundwater, but increased over that closer to the copper tube. In the lower, dryer parts, the TDS in the porewater was higher than the TDS of the groundwater at all distances from the copper tube. The general behaviour of the individual components mostly followed that of the TDS. The additives caused an increase in the TDS in some samples.

The pH values varied from 6.8 to 9.2. In the blocks without additives they varied from 7.6 to 8.5, with the high values being found close to the copper tube. The effects of the additives could be clearly seen in some samples. The added cement changed the pH of the porewater, but the effects were different in the cool and hot areas. In the cool area, the pH was higher without additives, while in the hot area the pH was lower. The added $CaSO_4$ clearly decreased the pH. The effects of the added K-feldspar were small. A low concentration of potassium could be found in the porewater, however. No special effects caused by the $CaCO_3$ additive were seen.

The concentration of the exchangeable calcium had increased in all the bentonite samples compared to the initial MX-80. This was in line with the low calcium concentrations in the porewater. The effects of the additives on the exchangeable cations were mostly within normal scattering.

Key words: nuclear waste, disposal, bentonite, buffer, porewater chemistry, rock laboratory.

Tiivistelmä

Äspön kalliolaboratoriossa Ruotsissa on menossa pitkäaikainen puskurimateriaalin testaus n.s. LOT-koe. Testisylinterit on tehty esivalmistetuista bentoniittipaloista, jotka on asetettu kupariputken ympärille. Bentoniittisylinterit on asetettu pystysuoriin porareikiin graniittikallioon. Kupariputken alaosaan on asetettu kuumennin. Tässä raportissa käsitellään kemiallisia tutkimuksia, joita tehtiin yhdelle sylinterille noin puolitoista vuotta kestäneen koejakson jälkeen. Bentoniittinäytteistä puristettiin huokosvesiä, joista määritettiin pH, Eh, S(–II), Fe^{2+}, Na^{+}, K^{+}, Ca^{2+}, Mg^{2+}, Cl^{-}, SO_4^{2-} ja HCO_3. Samoin määritettiin bentoniitin vaihtuvat kationit ja vesipitoisuus.

Vesipitoisuudet olivat jonkin verran suurempia sylinterin kylmemmässä yläosassa ja kallion läheisyydessä. Lisäaineilla (sementti, kalimaasälpä, $CaSO_4$, $CaCO_3$) ei ollut selvää vaikutusta vesipitoisuuteen.

Sylinterin yläosassa, kallion läheisyydessä, huokosveden liuennut kiintoaine oli hiukan pienempi kuin Äspön pohjaveden kiintoaine, mutta pitoisuus kasvoi sitä suuremmaksi lähellä kupariputkea. Alempana, kuivemmassa osassa, huokosveden liuenneen kiintoaineen pitoisuus oli suurempi kuin

pohjaveden kiintoaineen pitoisuus, kaikilla etäisyyksillä kupariputkesta. Sama käyttäytyminen oli havaittavissa huokosveden erillisillaä komponenteilla. Lisäaineet aiheuttivat kiintoainepitoisuuden kasvua eräissä näytteissä.

Huokosveden pH-arvot vaihtelivat 6,8:n ja 9,2:n välillä. Paloissa, joihin ei ollut pantu lisäaineita, pH vaihteli 7,6:sta 8,5:een, suurinpien arvojen esiintyessä lähellä kupariputkea. Lisäaineiden vaikutus pH-arvoon oli havaittavissa joissakin näytteissä. Sementti muutti huokosveden pH:ta, mutta vaikutukset olivat erilaisia kylmällä ja kuumalla alueella. Kylmällä alueella pH:t olivat korkeampia ja kuumalla alueella alempia kuin bentoniitissa ilman sementtiä. Lisätty $CaSO_4$ laski pH:ta selvästi. Kalimaasälvän vaikutukset olivat pieniä. Alhainen kalium konsentraatio oli havaittavissa kuitenkin huokosvedessä. $CaCO_3$:n lisäyksellä ei ollut erityistä vaikutusta.

Bentoniitin vaihtuvan kalsiumin pitoisuus oli kasvanut alkuperäiseen MX-80 bentoniittiin verrattuna. Tämä oli yhdenmukaista huokosvessä havaittujen alhaisten kalsiumpitoisuuksien kanssa. Lisäaineiden vaikutukset vaihtuviin kationeihin jäivät enimmäkseen normaalin hajonnan puittesiin.

Avainsanat: ydinjäte, loppusijoitus, bentoniitti, puskuri, huokosvesikemia, kalliolaboratorio.

Preface

The Long-Term Test of Buffer Material (LOT) is underway in the Äspö Hard Rock Laboratory in Sweden, which is organized by the Swedish Nuclear Fuel and Waste Management Co. (SKB). The project is coordinated by Clay Technology AB and many other partners are participating in the project. The Finnish nuclear waste company, Posiva Oy, is participating in the project through the work carried out by VTT Processes.

Contents

D1 Introduction

The Long-Term Test of Buffer Material (LOT) project is underway in the Äspö Hard Rock Laboratory in Sweden. The LOT test series may be described as a multi-task experiment in which test parcels are exposed to conditions similar to those in a KBS3-repository and to conditions that accelerate the alteration processes, respectively. The test parcels contain prefabricated bentonite blocks placed around a copper tube, which are placed in vertical boreholes in a granitic rock structure. The diameters of the holes are 300 mm and the depths around 4 m. In total, the test series includes 7 test parcels (Table D-1) of which three are exposed to standard KBS-3 conditions and 4 test parcels are exposed to adverse conditions. The two pilot tests (A1 and S1) have been already completed (Karnland et al. 2000). All five later test parcels (S2, S3, A0, A2 and A3) have in principle identical constructions, except for a number of different additives at specific locations in the bentonite blocks in the A-type parcel (Figure D-1). In addition, there are nine water inlet points in the A0 parcel instead of a single point in the others. Small titanium ampoules equipped with titanium filters, were placed at strategic positions in the bentonite in order to get representative water samples from the bentonite at test termination.

Temperature, total pressure, water pressure, and water contents, are measured during the heating period. At test termination, the parcels are extracted by overlapping core drilling around the original borehole, and the parcels are lifted and partitioned. Material from defined positions in the test parcels and reference material are thereafter examined by a general, well-defined set of tests and analyses in order to provide data for the different objectives. This report concerns studies performed by VTT on the A0 parcel, which was excavated after about one and half years' operation in October 2001. The aim of the work carried out by VTT in the LOT project is to obtain data about the chemical conditions to be developed in bentonite. Porewaters were squeezed out from the bentonite samples next to the ampoules and chemical additives placed in bentonite. Their chemical compositions and occupation of the exchangeable cations of the bentonite samples were determined.

Table D-1. Lay out of the planned Long-Term Test series (SKB 1999).

Type	No.	T (°C)	Controlled parameter	Time (years)	Remark
A	1	130	T, $[K^+]$, pH, am	1	Pilot test
A	0	120–150	T, $[K^+]$, pH, am	1	Main test
A	2	120–150	T, $[K^+]$, pH, am	5	Main test
A	3	120–150	T	5	Main test
S	1	90	T	1	Pilot test
S	2	90	T	5	Main test
S	3	90	T	>> 5	Main test

A= adverse conditions
T= temperature
pH= high pH from cement
S= standard conditions
$[K^+]$= potassium concentration
am= accessory minerals added

D2 Experiment with the A0 parcel

A detailed description of the parcels is given in the present main report. Figure D-1 presents the construction of the A0 parcel. Wyoming bentonite sold under the commercial name MX-80 was the source material for all bentonite components in the system. The bentonite material was compacted so that the intended water-saturated density was 2,000 kg/m^3.

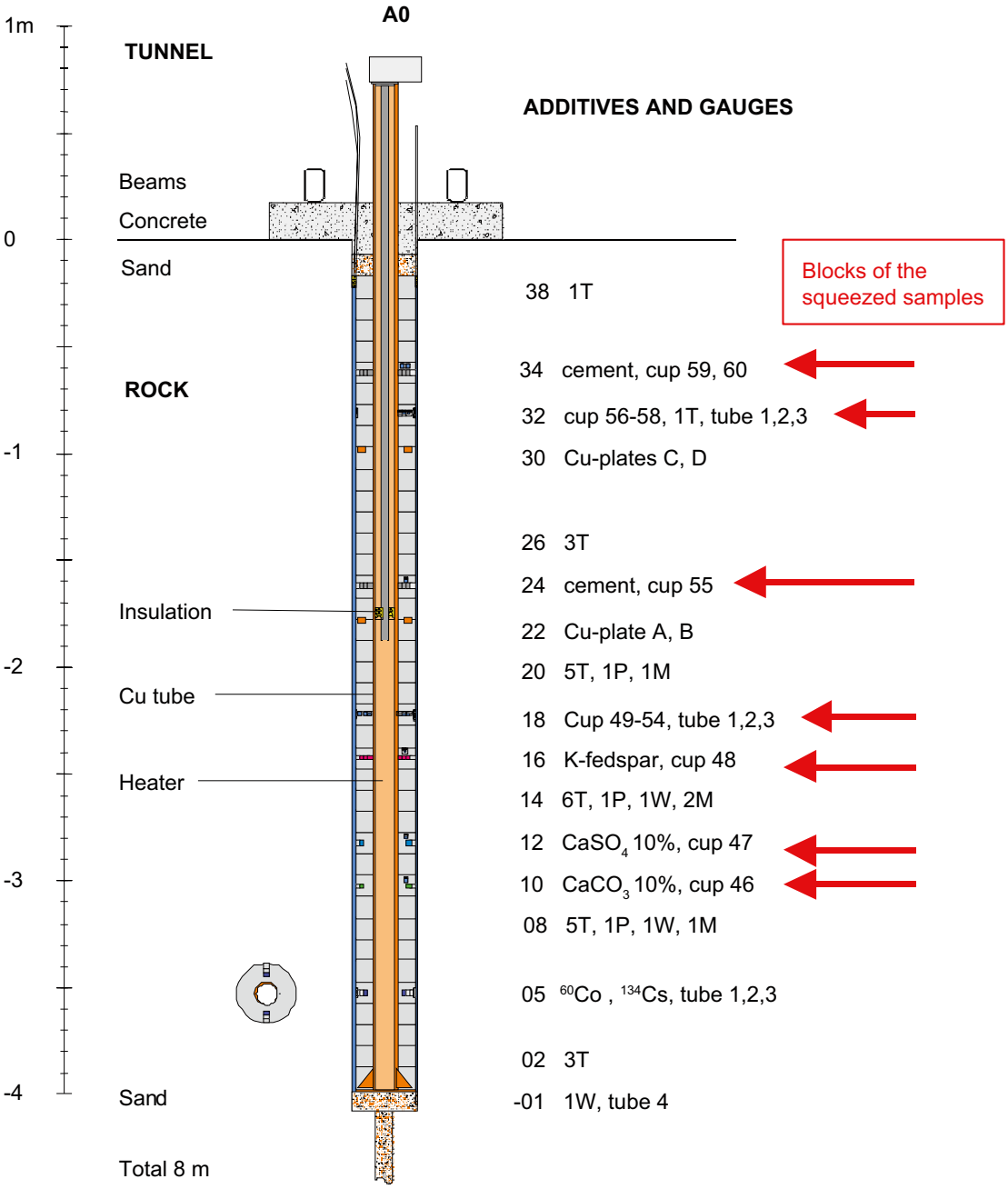

Figure D-1. *Principle layout of an A-type test parcel. "T" denotes temperature gauges, "W" water pressure gauges, "P" total pressure gauges, "M" moisture gauges, "cup" ampoules for water sample. The figure shows the block number (first) and number of gauges at each level. The places from where the bentonite samples were taken for chemical studies have been marked with arrows in the figure.*

In order to study the chemical changes, a higher content of accessory minerals (calcite, gypsum, K-feldspar) and Portland cement were placed in the bentonite. All bentonite-containing plugs with additives had a cylindrical form with a length and diameter of 20 mm. The plugs were compacted to a density corresponding to the standard density of 2,000 kg/cm^3 after full water saturation regardless of the additives. The plugs were placed in cylindrical holes, which were drilled from the mantle surface into the specified blocks. The calcite plugs had 10% (by weight) content of calcite ($CaCO_3$), the gypsum plugs had 10% content of gypsum and the K-feldspar plugs had 50% feldspar.

The A0 parcel was installed in the test hole on December 16, 1999. Power to the heater was first turned on February 2, 2000, and regulated to give a constant maximum temperature of 50°C. The maximum temperature target was thereafter increased in steps of 10°C. On April 19, 2000, the regulation of power to meet a fixed temperature was changed to a fixed power of 480 W. The power was thereafter increased in steps to the final power of 850 W. The slot between the clay column and the rock was water filled from the outward filters starting February 2, 2000. The system sealed quickly and groundwater pressure was therefore applied in the outer filters in block 05, 18, and 32.

The A0 parcel was over-cored from the rock in October 2001, the final uplift occurred October 27, 2001. The rock around the bentonite was removed and the bentonite cylinder was cut into 0.5 metre-long pieces. The pieces were closed in plastic and transported to Lund, where the bentonite samples were further cut so that their heights corresponded to the original heights of the blocks. From these blocks, sub-samples were cut for VTT. The blocks and places of the samples taken for VTT are presented in Figure D-1 and Appendix AD3. The samples were closed in metal vessels and flushed with nitrogen in order to prepare low-oxygen conditions in the transportation vessels.

D3 Studies on bentonite samples

D3.1 Splitting of bentonite

The samples were sent by Clay Technology AB to VTT in metallic transportation vessels flushed with nitrogen for oxidation shielding. The vessels were stored in the laboratory and one by one the samples were taken for splitting. First, the transportation vessel was moved into an anaerobic glove-box (Mecaplex, O_2 1–3 ppm) where it was opened. The bentonite was then closed into a gas-tight plastic bag and moved into another nitrogen glove-box (N-box, O_2 about 500 ppm) for splitting. Sample bottles of 60 and 125 ml, which had been in nitrogen atmosphere for removing the oxygen from their surfaces, were moved into the N-box before starting the splitting.

The bentonite sample was cut in the N-box with a band saw, as seen in Figure D-2. First the upper and lower layers (A, C) were removed. The middle layer (B) was used for sampling in which it was cut into 3 to 4 sectors depending on the size of the sample. The sectors were marked with the numbers 1, 2, 3 and 4 when turning to the direction from North to East. Each sector piece was cut into 3 pieces on the basis of the radial distance from the surface of the copper tube. The radial distances were marked with a, b, and c representing the distances 0–33, 33–66 and 66–100 mm, respectively. The sub-samples were closed in plastic bottles. A metal detector was used to identify the pieces where the sinter cups were closed, if not found otherwise.

The sample bottles were moved to the Mecaplex and opened for a while in order to change the gas in the bottle for one of a lower O_2 concentration. The bottles were then stored in the Mecaplex until used in the studies. Appendix AD3 presents in detail the places where the sub-samples were obtained from the splitting.

D3.2 Titanium cups

The titanium cups were removed from the bentonite sub-samples as soon as practically possible in order to avoid the suction of water to the bentonite. A hole was bored into the sinter of the cup, and through this hole a pipette was used to attempt to remove the water. However, it appeared that all the sinter cups were empty.

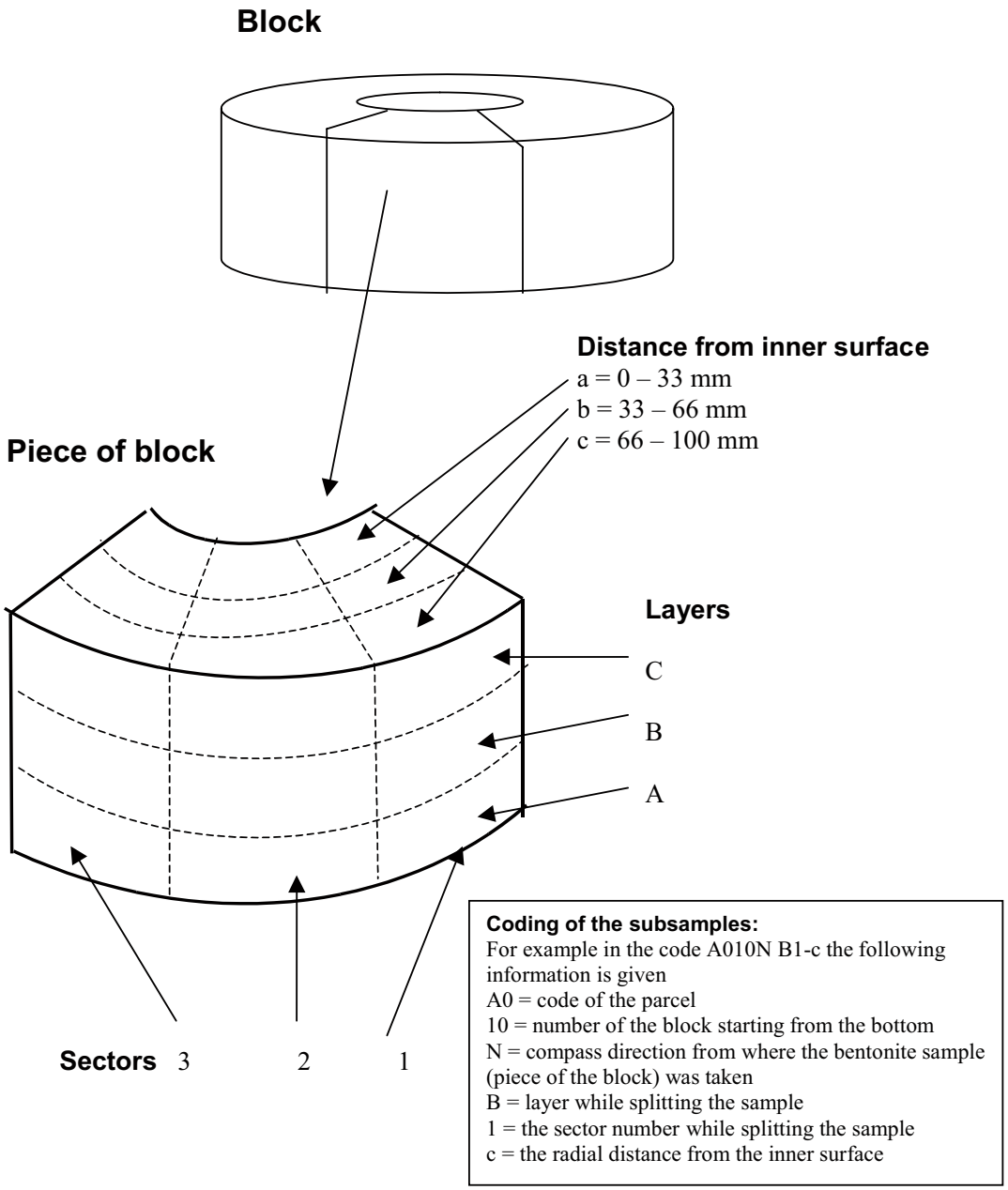

Figure D-2. *Splitting and coding of the bentonite sub-samples taken from the A0 parcel.*

D3.3 Analysis methods used for bentonite

Squeezing of the porewaters was carried out in the nitrogen glove-box (Mecaplex) in titanium cells, as shown in Figure D-3. The pressure was increased stepwise to about 100 MPa and the porewater was collected in a syringe. Altogether 34 squeezings were performed.

The porewater analyses were carried out by the method described in Figure D-4. More details of the methods are given in Muurinen (2001). The porewater sample squeezed into the syringe is first moved into a centrifugal tube and the sample is centrifuged 20 minutes at 10,000 rpm in order to remove possible particular material.

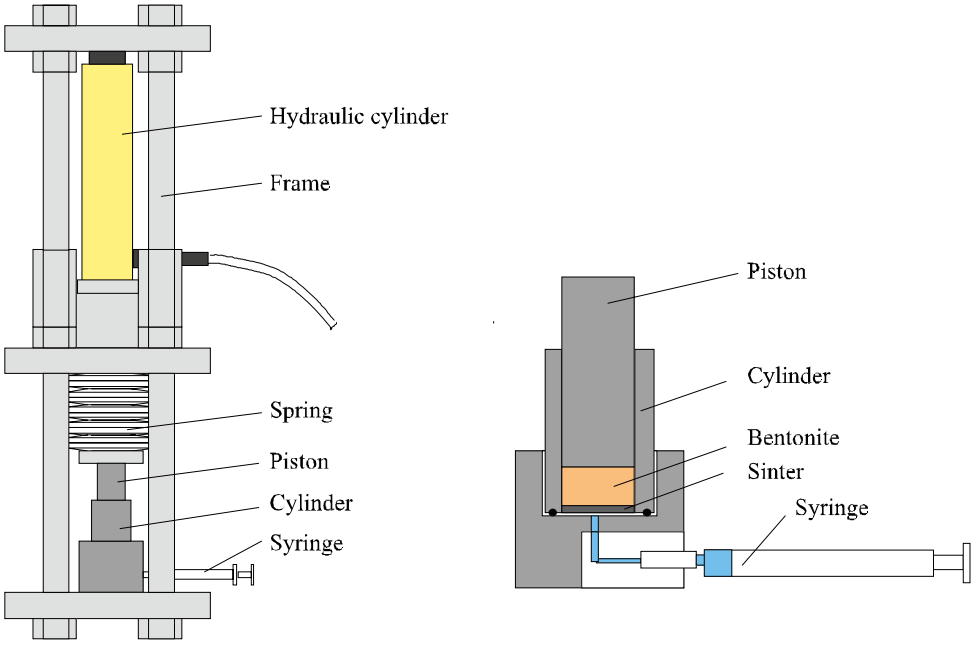

Figure D-3 . *Device used for squeezing of the porewater.*

For pH and Eh measurement, a sample of 0.3 ml was taken from the centrifugal tube to the pH/Eh measurement cell that had a magnetic ball on the bottom. The pH was measured with a micro-glass combination electrode (Orion Model 98-03) calibrated beforehand. To avoid changing of the sample, the measurement was carried out within a few minutes. Eh was measured with the sample used for pH measurement. The pH electrode was replaced by an Eh electrode (Microelectrodes Inc., Model MI-800-710). The cell was carefully closed and the Eh readings recorded until the electrode was stabilized. Normally, this took from a few hours to one day.

For ultrafiltering, the rest of the sample in the centrifugal tube was moved into a centrifuge filter tube (Whatmann, Vectra Spin^{TM} Micro, MWCO 12 k). The ultrafiltered sample was used in the analyses below.

For ICP-AES (Na^+, K^+, Ca^{2+}, Mg^{2+}) and IC (Cl^-, SO_4^{2-}) analyses a sample of 0.3 ml was diluted to 10 ml. Further dilutions are made according to the needs of the analysis method.

For titration of HCO_3^- a sample of 0.3 ml was diluted with CO_2-free water to 5 ml and titrated with dilute HCl to pH 4.5. HCO_3^- was determined on the basis of the Gran curve.

For determination of S(–II) a sample of 0.2 ml was diluted to 3 ml with oxygen-free water. The reagents were added into the sample according the standard method (SFS 3038). The sample was taken from of the glove-box and measured with a spectrophotometer.

For determination of Fe(II) a sample of 0.2 ml was taken from the centrifugal tube and diluted to 3 ml with oxygen-free water. The ferrozine reagent was added into the sample, according to the method by (Dimmock et al. 1979), and (Ruotsalainen et al. 1994). The sample was taken out of the glove-box and measured with a spectrophotometer.

The water content of the bentonite was determined by drying the sample at 105°C.

Determination of the exchangeable cations was performed with the dried bentonite samples obtained from the water content measurement. The determination was carried out by the method given by (Müller-Vonmoos and Kahr 1983), where the cations are released with NH_4SCN in ethanol.

D3.4 Groundwater samples

Samples from the groundwater used to saturate the bentonite parcel were taken in plastic bottles in December 2001. Principally similar analysis methods were used for the groundwater as for the porewater samples.

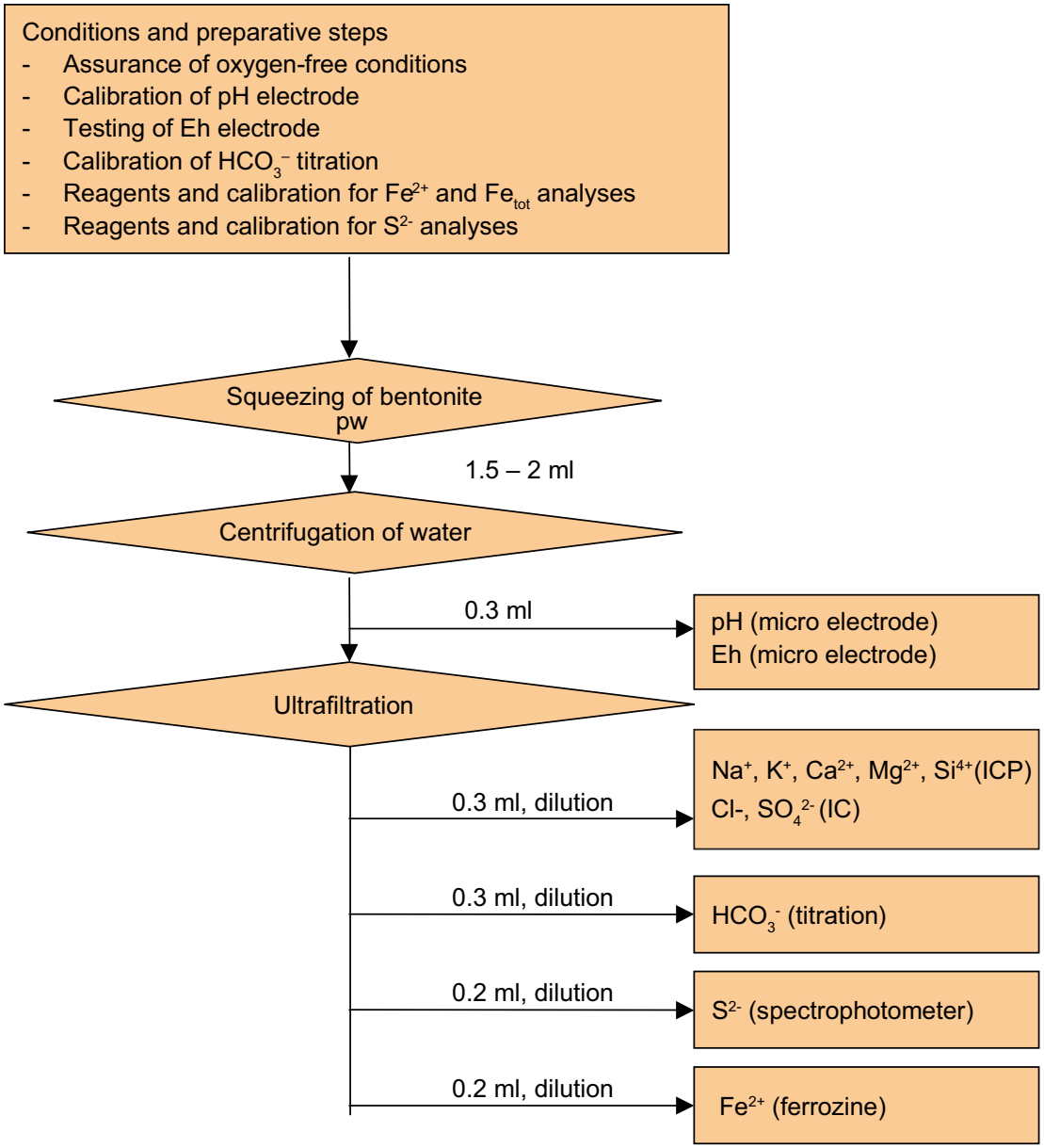

Figure D-4. *Analysis method used for the squeezed porewaters.*

D4 Results and discussion

D4.1 Groundwater samples

The analysis results of the Äspö groundwater used to saturate the bentonite A0 parcel are presented in Table D-2. No determination of Eh or concentrations of redox-sensitive components were made, because it could not be guaranteed that the samples were taken without oxidation.

Table D-2. Concentrations of different components in Äspö groundwater used to saturate the A0 sample. The accuracy of the analyses is ±10%.

	pH	Na^+	K^+	Ca^{++}	Mg^{++}	Cl^-	$SO_4^=$	HCO_3^-
Äspö gw.	6.9±0.1	2,300 mg/l	11 mg/l	1,900 mg/l	58 mg/l	6,300 mg/l	440 mg/l	27 mg/l
Äspö gw.	6.9±0.1	100 meq/l	0.28 meq/l	94.6 meq/l	4.8 meq/l	178 meq/l	9.2 meq/l	0.44 meq/l

D4.2 Titanium cups

All the titanium cups appeared to be empty.

D4.3 Studies on bentonite

Places of the studied samples

Figure D-1 shows the blocks from which the samples were taken for chemical studies and Appendix 3 clarifies the places in each block from where bentonite sub-samples were taken. The codes of the studied samples marked in Appendix AD3 correspond to those in Appendices AD1 and AD2, where the analysis data are presented. Some of the samples taken from the parcel were not perfect in shape. In the samples A0 10N and A0 12N, the inner part was missing and in the sample A0 16N only the inner part could be identified. The studied samples represent nevertheless the different distances from the bottom (blocks), different distances from the heater and the effects of the additives.

Water content in bentonite

The columns 2 and 3 of Appendix AD1 present the water contents in each studied bentonite sample, as gram of water per gram of dry bentonite. Figure D-5 gives an overview of the vertical behaviour of the water contents in the studied samples. The figure also presents the water contents after squeezing of the porewaters. The additives placed in some blocks are also marked in the figure. Figure D-6 presents the water content at different distances from the copper tube, with the distances from the bottom given in the legend.

The general trend is that the water content is somewhat higher in upper parts of the parcel, in the cool area. The additives do not have any clear effect on the water content. Although there is some scattering in the results of Figure D-6, it is evident that the water content decreases close to the copper tube. The planned saturated density, 2,000 kg/m^3, would mean theoretically a water content of about 0.28 g/g. It is clearly exceeded in part of the samples, which means that the density has been lower than the theoretical value. The average water content after squeezing was 0.19 g/g.

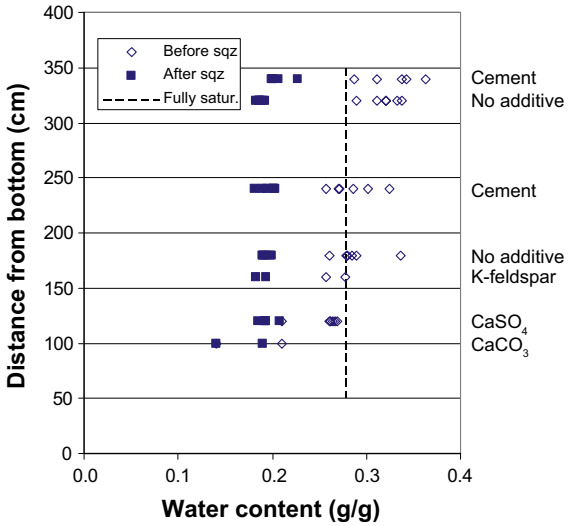

Figure D-5. *Water contents in the samples at different distances from the bottom before and after squeezing. The value for the saturated density of 2,000 kg/m³ is represented with a dotted line.*

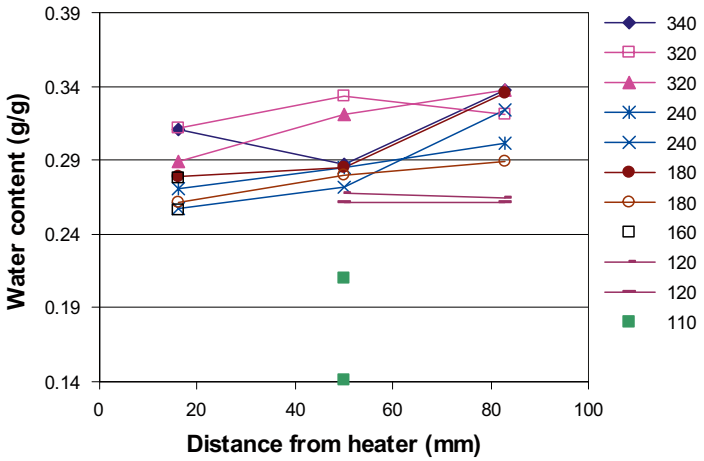

Figure D-6. *Water content at different distances from the copper tube. The distances in centimetres from the bottom are given in the legend.*

Porewater compositions and cation occupations

The results of the squeezed porewater samples are presented in Appendix AD1. The water contents before squeezing varied considerably, while after squeezing they were quite equal. This means that very different porewater volumes could be squeezed out from different samples, as seen in column 4 of Appendix AD1.

Sodium, calcium, magnesium, chloride, sulphate, bicarbonate concentrations and pH and Eh could be determined in most of the porewater samples. Sulphide and iron concentrations were analyzed only in special samples of blocks 18 and 32. The squeezed porewater volumes of those samples were larger than in the other samples in order to avoid dilution during the analyses. The S(–II) and Fe^{2+} concentrations were below the determination level (0.02 mg/l), however. The Eh values varied from about 190 mV to –110 mV. The potassium concentrations were below the determination level in most of the samples.

The results of the exchangeable cations are presented in Appendix AD2 together with the values of the initial MX-80 (reference samples).

The results about the porewater chemistry and occupation of the exchangeable cations in the samples of each block are presented in the figures of Appendix AD3. The cross-sections of the blocks show the places from where the samples were taken for studies. The concentrations of the components in the squeezed porewaters and the occupations of the cations are presented as a function of the distance from the copper surface. Potassium has been omitted from the figures because its concentrations were very low in the bentonite, and in most cases under the determination level in the porewater.

Figure D-7 presents total dissolved solids (TDS) in the squeezed porewater samples at different distances from the bottom, together with the TDS of the Äspö groundwater, and Figure D-8 show the TDS as a function of the distance from the copper tube. TDS increases while going down towards the bottom of the hole. The TDS of the upper blocks are slightly below the TDS of the groundwater near the outer surface but increase above that closer to the copper tube. In the lower, dry blocks the TDS in the porewater is higher than the TDS of the groundwater at all distances from the copper tube. The additives cause an increase of the TDS in some samples, which is seen as a horizontal spreading of the values in Figure D-7.

Figure D-9 presents pH in the squeezed porewater samples at different distances from the bottom. The pH values vary from 6.8 to 9.2. The values in the blocks without additives (Blocks 32 and 18) are rather equal, however. The effects of the additives can be seen clearly in the figure.

An overview of the concentrations of anions and cations in the squeezed porewater samples is presented in Figures D-10 and D-11 together with the corresponding values in the Äspö groundwater. The general behaviour of the individual components mostly follows that of the TDS. The concentrations increase while going down and close to the copper tube.

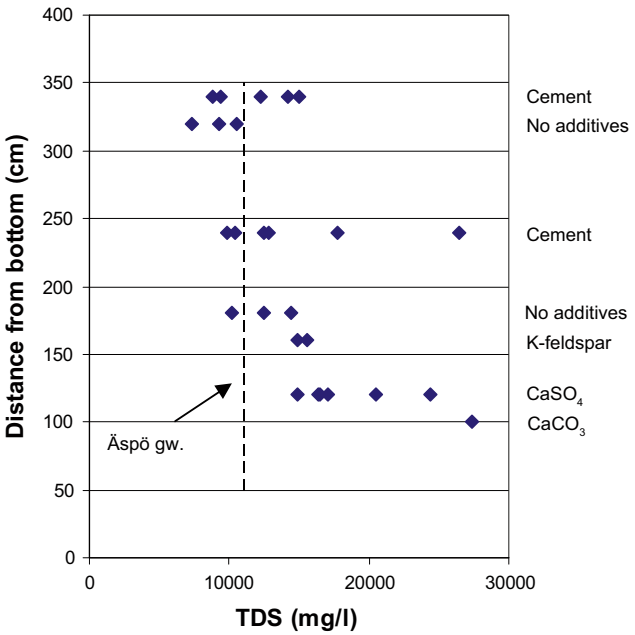

Figure D-7. *Total dissolved solids (TDS) in the squeezed porewater samples at different distances from the bottom. TDS in the Äspö groundwater is also marked in the figure.*

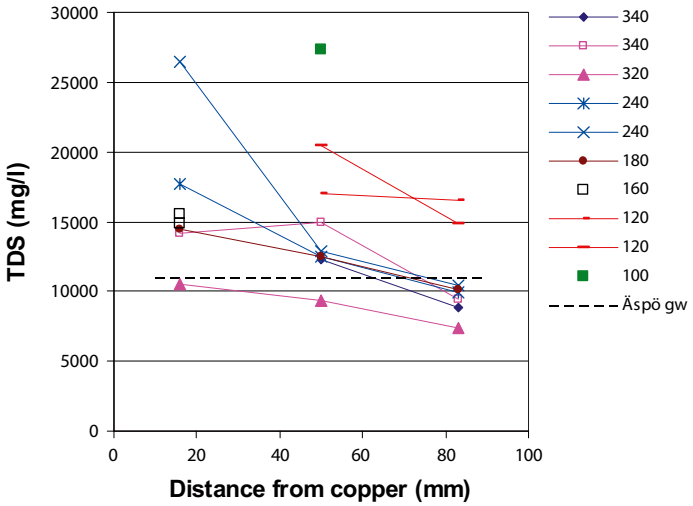

Figure D-8. *TDS at different distances from the copper tube. The distances in centimetres from the bottom are given in the legend. The TDS in the Äspö groundwater is also marked in the figure.*

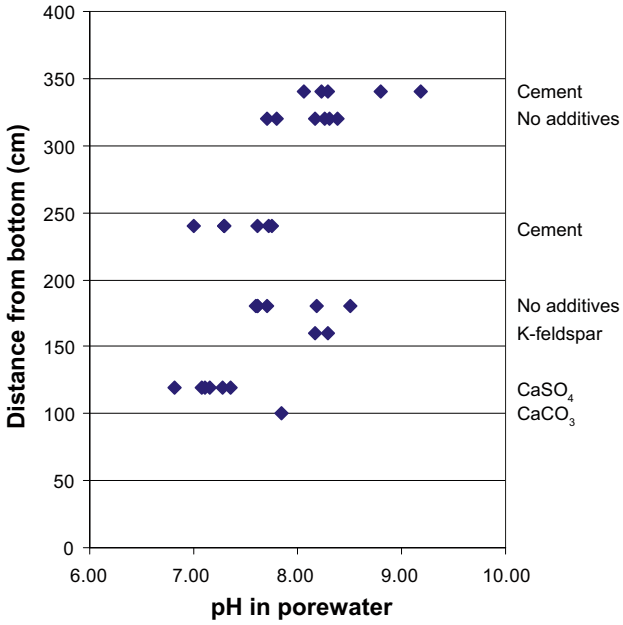

Figure D-9. *Measured pH values in the squeezed porewater samples at different distances from the bottom.*

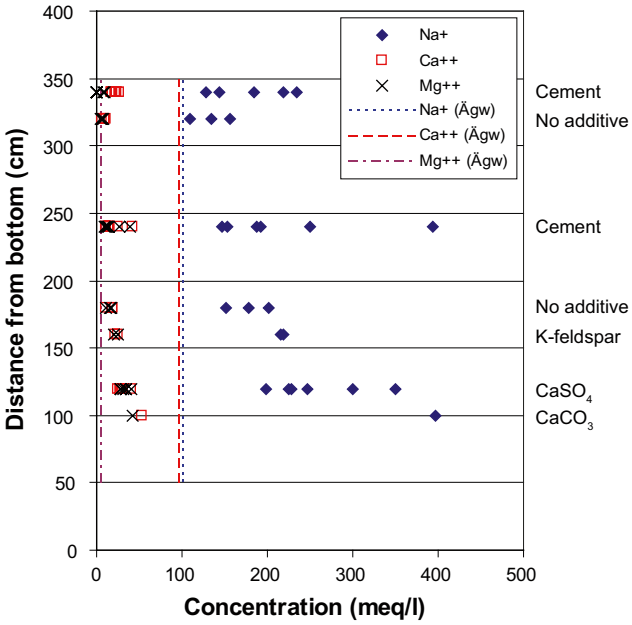

Figure D-10. *The concentrations of major cations in the squeezed porewater samples at different distanced from the bottom. The concentrations in the Äspö groundwater are represented with vertical lines.*

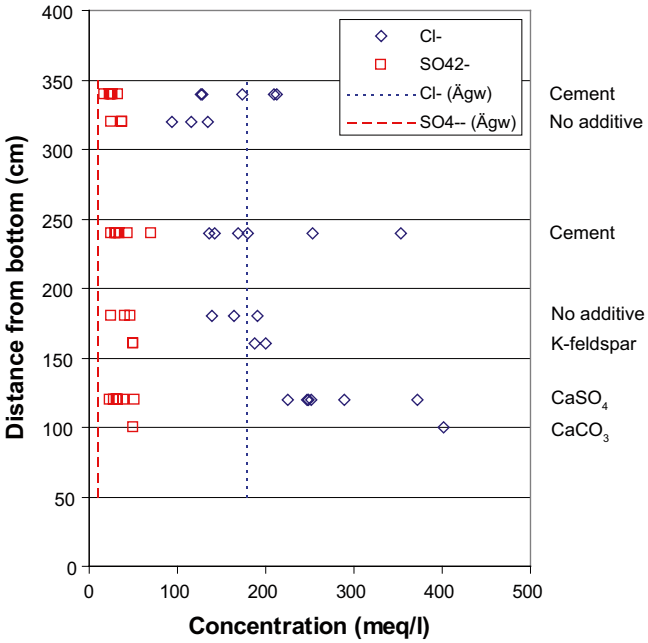

Figure D-11. *Concentrations of the major anions in the squeezed porewaters at different distances from the bottom. The concentrations in the Äspö groundwater (Ägw) are represented with vertical lines.*

The components in the porewater are expected to come from the dissolving components in the clay, the ions coming with the saturating water and cation exchange between the exchangeable cations of montmorillonite and those in the porewater. Assuming in bentonite a sulphate content of 4 mg/g and a chloride content of 0.1 mg/g (Muurinen and Lehikoinen 1999) and a porewater content of 0.3 g/g, we can evaluate the magnitude that those components would cause in the porewater if they were to dissolve totally. Dissolving chloride would cause a concentration of about 10 meq/l. The chloride concentration in the squeezed porewater vary from about 100 meq/l to 400 meq/l and cannot be caused only by the dissolving chloride in bentonite, which means that it comes mostly with the saturating water. The sulphate content of the clay would cause in the porewater about 300 meq/l, while its concentration in the groundwater is only 9 meq/l. The sulphate concentrations in the porewater samples vary between 8 and 25 meq/l. The sulphate in the porewater is thus caused partly by the saturating water and partly by the dissolving accessory minerals, but it is probably solubility limited.

The sodium concentration in the porewater is clearly higher, and that of calcium clearly lower than the concentrations in the groundwater. It is obvious that calcium coming with the groundwater is changed with the sodium in the bentonite so that sodium is released into the porewater.

The magnesium and calcium concentrations follow each other in most samples. The only exception is the block 34 where cement was used an additive. There the magnesium concentrations are clerly decreased.

There is a general trend of increase in all the concentrations while going downwards. The additives seem to increase also chloride concentrations in the inner parts of those blocks where additives were placed. Because no chloride was in the additives there must be some more complex mechanism which causes the increase.

Figure D-12 presents the concentrations of the exchangeable cations of bentonite at different distances from the bottom. The average values of the initial MX-80 samples have also been presented in the figure with vertical lines. Calcium concentration has increased in all the blocks. This is in line with its low concentrations in the porewater. Increase of calcium concentration as the exchangeable cation should mean decreased sodium concentration. This cannot be seen in the sodium values but the total concentration of the exchangeable cations seems to increase from the initial value. This most probably means that at least part of the released sodium has dissolved while doing the cation exchange. The values for sodium are probably about 10% too high. The effects of the additives are generally rather small. Only in block 34, where cement plugs were placed, is the calcium concentration clearly higher than in the other blocks. The effect is also seen as increasing CEC.

The detailed behaviour of different components in porewater and bentonite in each block can be seen in Appendix AD3.

Blocks A0 32 and A0 18

The blocks A0 32 and A0 18 without any additives form the basic case. Porewaters for the analyses of the major components were squeezed from the samples A0 32 B1-x and A0 18 B2-x. The samples A0 32 B2-x* and A0 18 B3-x* were used for the analyses of the redox components (Fe^{2+}, S(–II)) only, and no other porewater data about them is available. The exchangeable cations were analyzed from all samples, however.

The concentrations of all the ions are somewhat lower in the samples of block 32 where the temperature is lower and the water content is higher. The concentrations increase systematically while going from the rock surface closer to the copper tube. This increase is very similar in the cool and hot areas. The pH values are below 8 in the outer parts of the clay, but increase over 8 closer to the copper.

The cation occupations are quite similar in all the samples. No dependence on the distance from the copper can be seen.

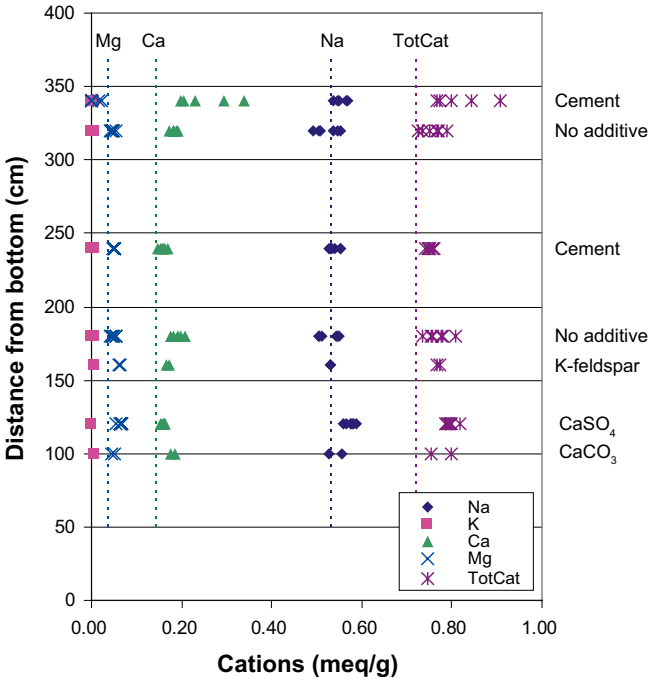

Figure D-12. *Concentrations of the exchangeable cations in bentonite at different distances from the bottom. The values for MX-80 (Muurinen 1999) are represented with vertical lines.*

Blocks A0 34 and A0 24

Cement was placed as the additive in the blocks A0 34 and A0 24. The concentrations of all the ions are somewhat lower in the samples of block 34 where the temperature is lower and water content is higher. The concentrations increase systematically while going from the rock surface closer to the copper tube. This increase is very similar in

the cool and hot areas. The chloride and sodium concentrations are higher in blocks 34 and 24 than in the blocks without additives. Sodium could be explained by the cation exchange with calcium coming from the cement, but the higher chloride concentration is more difficult to explain, when its only possible source is groundwater. The pH values are different in the cool and hot area. In the cool area pH vary from 8.1 to 9.2, while in the hot area the variation is from 7 to 7.8.

The concentration of the exchangeable calcium is increased in the outer parts of the sample 34N B2. The effect is also seen as an increase of CEC.

Block A0 16

K-feldspar was placed as the additive in this block. Only the sample close to the heater could be identified. The concentrations are quite similar as in the samples of the block 18. A low concentration of potassium could be found in the porewater, however. No clear effect was seen in the concentration of the exchangeable cations of the bentonite.

Block A0 12

$CaSO_4$ was placed as the additive in this block. Samples were obtained only from the middle and outer diameters.

The concentrations increase or stay constant while going from the rock surface closer to the copper tube. The high TDS, seen in Figures 7 and 8, are also in this case caused by sodium and chloride and not by calcium and sulphate. The pH varies from 6.8 to 7.4, which is lower than in any other block. The cation occupations are quite similar in all the samples. No dependence on the distance from the copper can be seen.

Block A0 10

$CaCO_3$ was placed as the additive in this block. Two samples from the middle radius were analyzed from this block. One of them was too dry for porewater squeezing, however. No special effects caused by the additive can be seen.

D4.4 Discussion

The A0 parcel is not yet fully saturated after over one and half years' operation. Especially the lower parts of the parcel close to the copper tube are still rather dry. Quite complex transportation processes are taking place, which concern both water and dissolved components therein. It is typical that the concentrations in the porewater of the dry samples are higher than those of the well saturated samples. There are at least two possible explanations for this. One possibility is that water evaporates close to the hot copper tube and causes an increase in the concentrations in the porewater. The fact that the phenomenon is seen also in blocks 32 and 34, which are rather cool, speaks against this theory. Another possible explanation is that part of the saturating groundwater goes into the interlamellar spaces, where at least part of the dissolved components cannot enter. They then stay in larger pores, where the concentrations increase from the initial ones. In some samples near the rock, it can be seen that the TDS is below the TDS of the groundwater. Equilibration with the groundwater has decreased the concentrations and exclusion can already be seen. The studies of the later parcels will possibly give answers to the open questions.

D5 Summary

The Long-Term Test of Buffer Material (LOT) is underway in the Äspö Hard Rock Laboratory in Sweden. This report concerns studies performed by VTT on the A0 parcel, which was excavated after about one and half years of the experiment. The aim of the work was to obtain data about the chemical conditions developed in the bentonite.

Porewaters were squeezed out from the bentonite samples and their chemical compositions were determined. The porewater analyses comprised pH, Eh, S(–II), Fe^{2+}, Na^{+}, K^{+}, Ca^{2+}, Mg^{2+}, Cl^{-}, SO_4^{2-} and HCO_3^{-}. The exchangeable cations and the water contents of the bentonite were also determined.

The water contents were somewhat higher in upper parts of the parcel, in the cool area. It was also evident that the water content decreased while going closer to the copper tube. The additives did not have any clear effect on the water content.

Sodium, calcium, magnesium, chloride, sulphate, bicarbonate concentrations and pH and Eh could be determined in most of the porewater samples. The S(–II) and Fe^{2+} concentrations were below the determination level (0.02 mg/l), however. The Eh values varied from about 190 mV to –110 mV. The potassium concentrations were below the determination level in most of the porewater samples.

In the upper part of the parcel close to the rock surface, the TDS in the porewater was slightly below the TDS of the groundwater, but increased over that closer to the copper tube. In the lower, dryer parts of the parcel, the TDS in the porewater was higher than the TDS of the groundwater at all distances from the copper tube. The general behaviour of the individual components mostly followed that of the TDS. The additives caused an increase in the TDS in some samples.

The pH values varied from 6.8 to 9.2. In the blocks without additives, they varied from 7.6 to 8.5, the high values being found close to the copper tube. The effects of the additives could be seen clearly in some samples.

The chloride concentrations in the squeezed porewater varied from about 100 meq/l to 400 meq/l. Chloride comes mostly with the saturating water. The sulphate concentrations in the porewater samples varied between 8 and 25 meq/l, being caused partly by the saturating water and partly by the dissolving accessory minerals. Sulphate was clearly solubility limited. Bicarbonate concentrations varied from 0.5 to 3.4 meq/l.

Calcium concentrations varied from 3 to 26 meq/l. Calcium coming with the groundwater is changed with the sodium in the bentonite such that sodium is released into the porewater. Sodium concentrations were typically a little higher than chloride concentrations. Magnesium concentrations varied from 0 to 21 meq/l.

The concentration of the exchangeable calcium had increased in all bentonite samples, compared to the initial MX-80. This is in line with its low concentrations in the porewater. Increase of calcium concentration as the exchangeable cation should mean decreased sodium concentration. This cannot be seen in the sodium values but the total concentration of the exchangeable cations seems to increase from the initial value. This most probably means that at least part of the released sodium has dissolved while doing the cation exchange. The effects of the additives in the exchangeable cations were mostly within normal scattering.

There was a general trend of increase in all the concentrations while going downwards. The additives seem to increase also chloride concentrations in the inner parts of those blocks, where the additives were placed. The added cement changed the pH of the porewater, but the effects were different in the cool and hot area. In the cool area pH was higher than without cement, while in the hot area pH was lower. The effects of the added K-feldspar were small. A low concentration of potassium could be found in the porewater, however. The added $CaSO_4$ decreased the pH of the porewater. No special effects caused by the $CaCO_3$ additive were seen.

Appendix AD1

Properties of squeezed porewaters

Place	Water in bent. before sqz (g/g)	Water in bent. after sqz (g/g)	Squeezed Porewater (ml)	pH	Eh (mV)	S(–II) (mg/l)	Fe++ (mg/l)	Na+ (mmol/l)	K+ (mmol/l)	Ca++ (mmol/l)	Mg++ (mmol/l)	Cl– (mmol/l)	SO4— (mmol/l)	HCO3 (mmol/l)
A034N B1-b	0.363	0.207	2.3	8.3	189			184	0.46	11.8	4.1	174	12.5	0.83
A034N B1-c	0.342	0.201	2.0	8.2	90			128	0.18	9.2	4.4	128	8.3	1.04
A034N B2-a	0.311	0.200	1.9	8.1	9			219		13.5	0.1	209	11.6	1.08
A034N B2-b	0.288	0.227	2.1	9.2	–22			234		11.1	0.0	212	16.8	0.66
A034N B21-c	0.338	0.199	1.1	8.8	–33			143		8.3	0.1	127	13.1	0.25
A032E B1-a	0.312	0.188	1.7	8.3	–60			156		5.3	3.7	134	18.5	1.54
A032E B1-b	0.333	0.190	1.8	7.7	–110			134		4.4	3.0	116	18.6	1.51
A032E B1-c	0.321	0.183	1.7	7.8	80			110		3.4	2.5	94	12.7	1.55
A032E B2-a*	0.289	0.191	3.8	8.3	70	0	0							
A032E B2-b*	0.321	0.191	3.7	8.2	80	0	0							
A032E B2-c*	0.337	0.191	4.2	8.4	130	0	0							
A024N B1-a	0.271	0.195	1.2	7.3	70			251		12.3	13.2	253	22.0	0.90
A024N B1-b	0.285	0.202	1.8	7.0	10			188		7.2	6.4	169	17.2	0.54
A024N B1-c	0.301	0.200	2.0	7.3	–20			147		5.5	5.9	136	12.7	1.80
A024N B2-a	0.257	0.182	1.0	7.6	59			394		20.9	19.5	354	35.5	2.46
A024N B2-b	0.272	0.190	1.8	7.7	51			193		7.7	7.0	180	15.4	1.95
A024N B2-c	0.324	0.203	1.9	7.8	–17			153		5.4	5.0	142	15.0	1.84
A018W B2-a	0.279	0.198	1.5	8.5	0			202		9.4	8.4	191	23.5	2.89
A018W B2-b	0.285	0.190	1.7	7.7	60			178		9.4	7.9	164	20.2	1.05
A018W B2-c	0.336	0.190	1.8	7.6	120			152		5.7	5.3	140	12.7	2.52
A018W B3-a*	0.261	0.198	2.3	8.2	–13	0	0							
A018W B3-b*	0.279	0.196	2.5	7.6	189	0	0							
A018W B3-c*	0.290	0.195	3.5	7.6	152	0	0							
A016N B1-a	0.278	0.182	1.1	8.2	17			215	0.69	10.6	10.5	188	24.9	2.54
A016N B2-a	0.257	0.194	1.5	8.3	104			219	0.59	12.1	12.1	201	25.3	3.43
A012N B1-b	0.267	0.193	1.6	6.8				228		14.6	17.2	246	15.4	1.47
A012N B11-c	0.269	0.192	1.6	7.2				225		14.2	15.3	248	14.0	2.43
A012N B12-c	0.264	0.193	1.6	7.3				198		15.4	17.1	225	11.8	2.84
A012N B2-b	0.261	0.207	1.2	7.1				247		12.7	14.0	251	16.7	< det.lev.
A012N B21-c	0.262	0.185	1.1	7.4				300		13.9	13.7	288	25.5	< det.lev.
A012N B3-b	0.210	0.193	0.6	7.1				350		20.1	20.5	372	19.8	< det.lev.
A010N B1-b	0.141	0.140	0.0											
A010N B2-b	0.210	0.190	0.5	7.9				397	0.66	26.2	20.9	401	25.4	not anal

Appendix AD2

Exchangable cations in bentonite

Sample code	Na (meq/g)	K (meq/g)	Ca (meq/g)	Mg (meq/g)	CEC (meq/g)
A034N B1-b	0.54	0.01	0.20	0.02	0.77
A034N B1-c	0.55	0.01	0.20	0.02	0.77
A034N B2-a	0.57	0.00	0.23	0.00	0.80
A034N B2-b	0.57	0.00	0.34	0.00	0.91
A034N B21-c	0.55	0.00	0.29	0.00	0.84
A032E B1-a	0.49	0.01	0.18	0.05	0.73
A032E B1-b	0.50	0.01	0.18	0.04	0.74
A032E B1-c	0.51	0.01	0.19	0.04	0.75
A032E B2-a	0.54	0.00	0.17	0.06	0.77
A032E B2-b	0.55	0.00	0.19	0.05	0.79
A032E B2-c	0.55	0.00	0.18	0.04	0.77
A024N B1-a	0.53	0.01	0.16	0.05	0.75
A024N B1-b	0.53	0.01	0.17	0.05	0.76
A024N B1-c	0.53	0.01	0.16	0.05	0.75
A024N B2-a	0.55	0.00	0.15	0.05	0.75
A024N B2-b	0.54	0.00	0.15	0.05	0.74
A024N B2-c	0.55	0.00	0.16	0.05	0.76
A018W B2-a	0.50	0.01	0.20	0.04	0.75
A018W B2-b	0.51	0.01	0.19	0.05	0.76
A018W B2-c	0.50	0.01	0.18	0.04	0.73
A018W B3-a	0.55	0.00	0.21	0.05	0.81
A018W B3-b	0.54	0.00	0.19	0.05	0.78
A018W B3-c	0.55	0.00	0.18	0.05	0.78
A016N B1-a	0.53	0.01	0.17	0.06	0.77
A016N B2-a	0.53	0.01	0.17	0.06	0.77
A012N B1-b	0.57	0.00	0.16	0.06	0.79
A012N B11-c	0.58	0.00	0.16	0.06	0.80
A012N B12-c	0.59	0.00	0.16	0.07	0.82
A012N B2-b	0.58	0.00	0.16	0.05	0.79
A012N B21-c	0.58	0.00	0.15	0.06	0.80
A012N B3-b	0.56	0.00	0.16	0.07	0.79
A010N B1-b	0.53	0.01	0.18	0.05	0.76
A010N B2-b	0.55	0.01	0.18	0.05	0.80
11R	0.52	0.016	0.14	0.035	0.71
15R	0.55	0.015	0.14	0.036	0.74
33R	0.52	0.015	0.14	0.035	0.71

The samples R11, R15 and R33 are reference samples.

Porewater composition and exchangeable cations in bentonite blocks

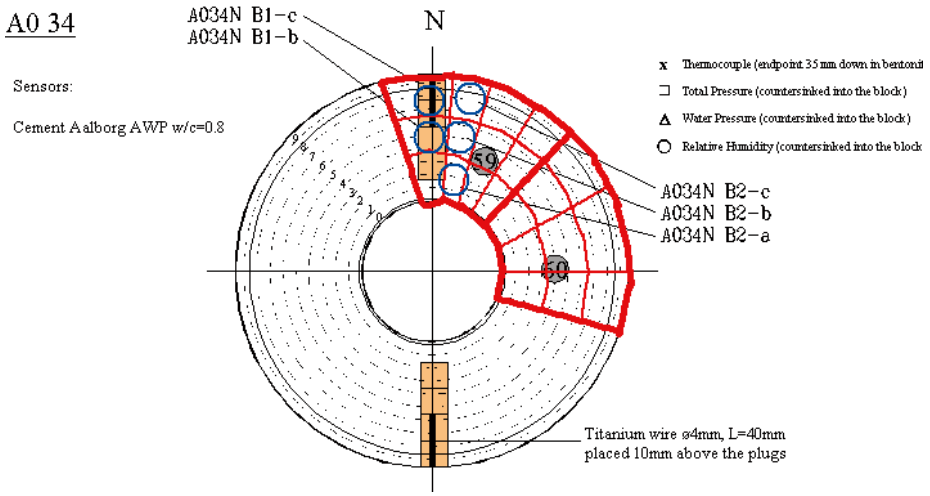

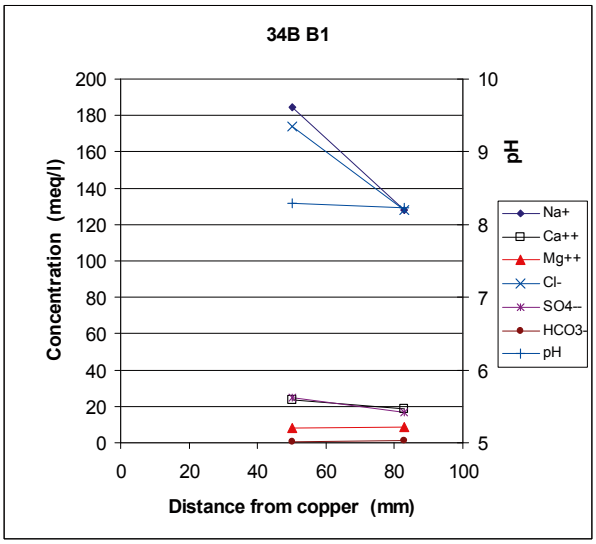

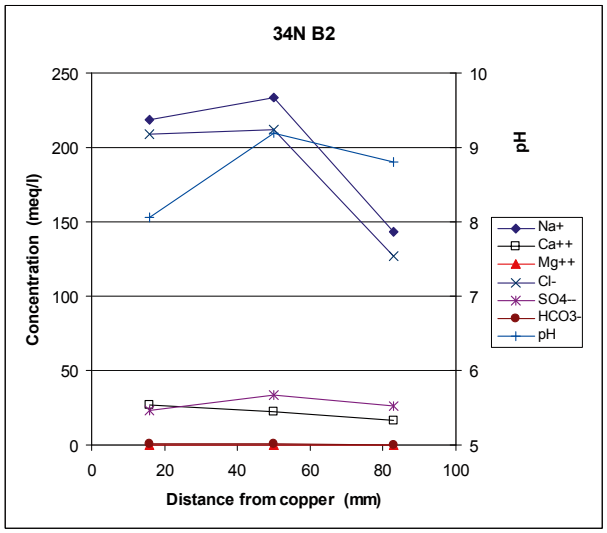

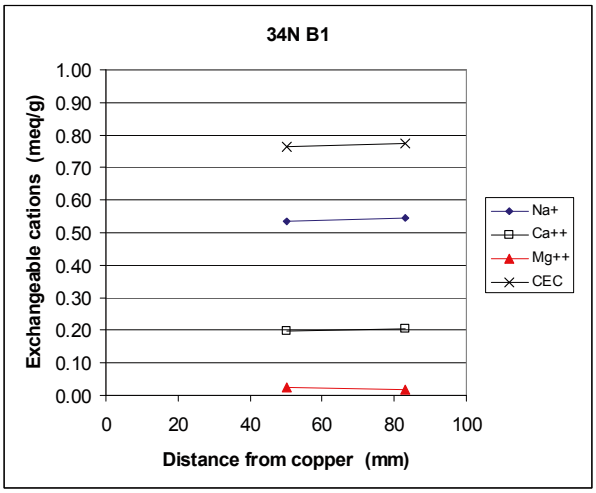

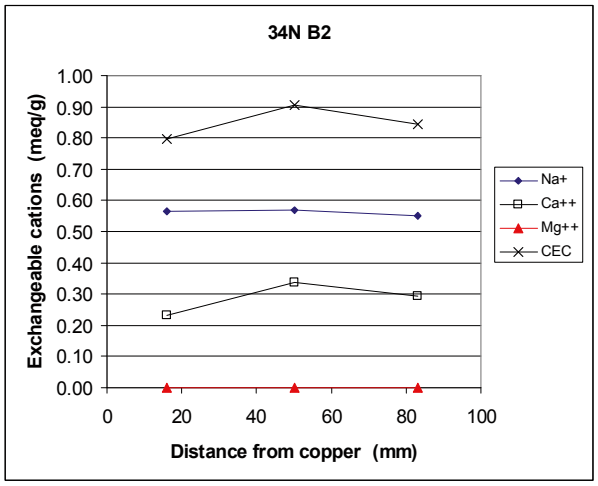

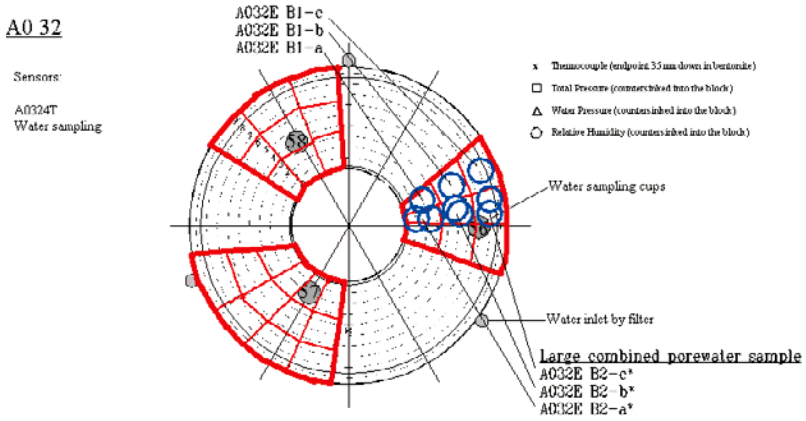

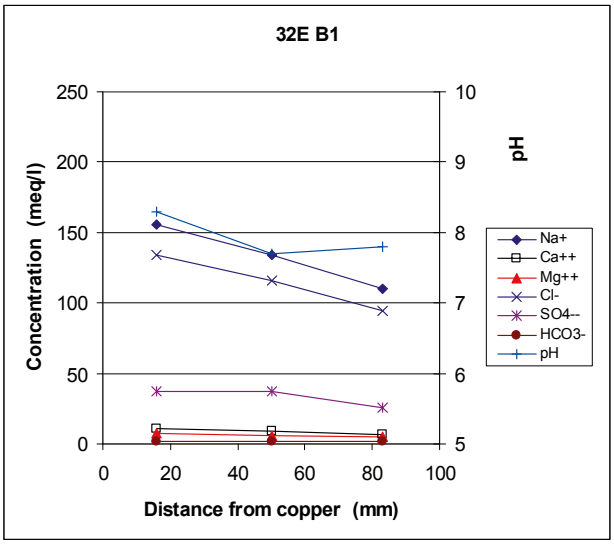

32E B2

No porewater data

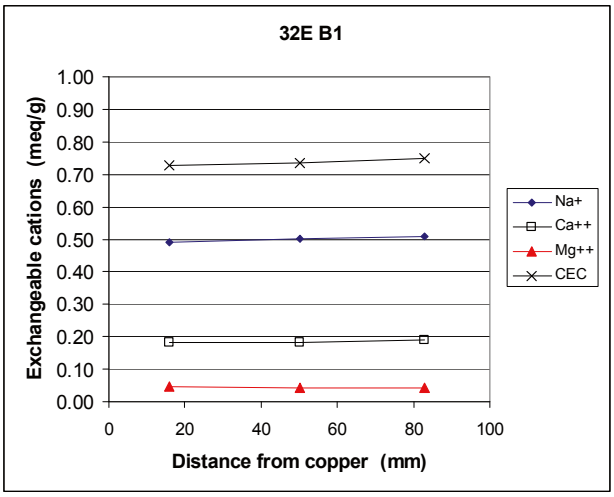

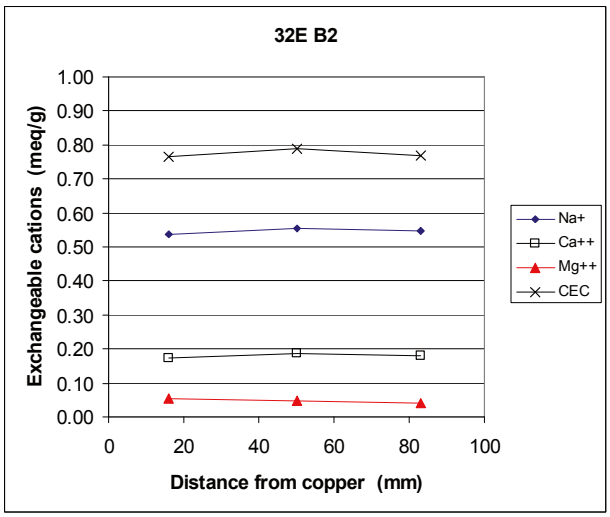

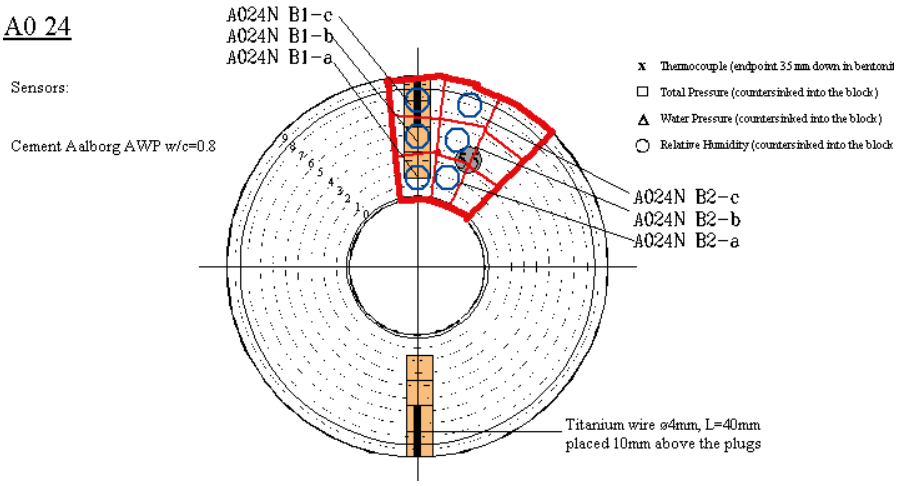
A0 24
Sensors:
Cement Aalborg AWP w/c=0.8
A024N B1-c
A024N B1-b
A024N B1-a
A024N B2-c
A024N B2-b
A024N B2-a
Thermocouple (endpoint 35 mm down in bentonit
Total Pressure (countersinked into the block)
Water Pressure (countersinked into the block)
Relative Humidity (countersinked into the block
Titanium wire ø4mm, L=40mm
placed 10mm above the plugs

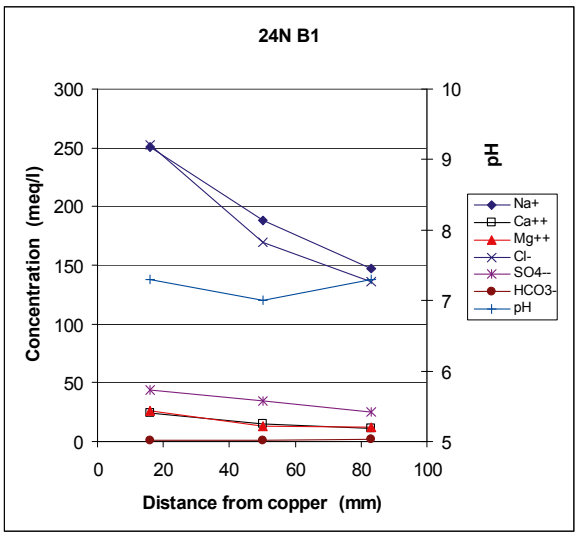
24N B1
Concentration (meq/l)
pH
Distance from copper (mm)
Na+
Ca++
Mg++
Cl-
SO4--
HCO3-
pH

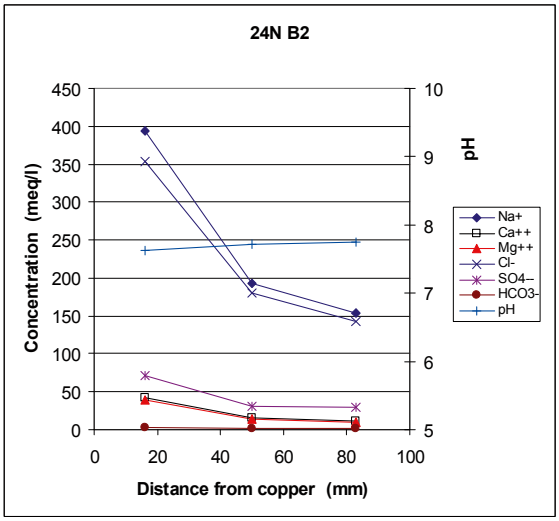
24N B2
Concentration (meq/l)
pH
Distance from copper (mm)
Na+
Ca++
Mg++
Cl-
SO4--
HCO3-
pH

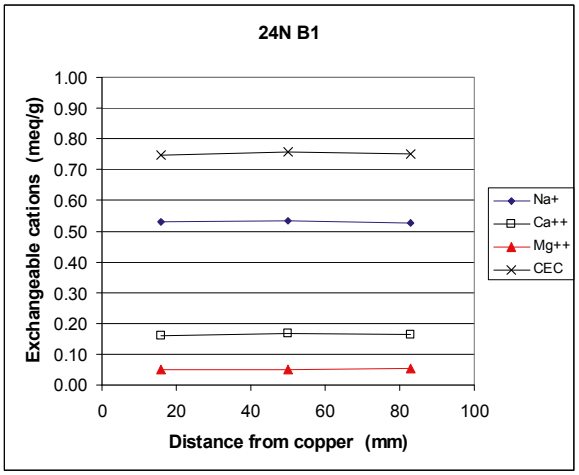
24N B1
Exchangeable cations (meq/g)
Distance from copper (mm)
Na+
Ca++
Mg++
CEC

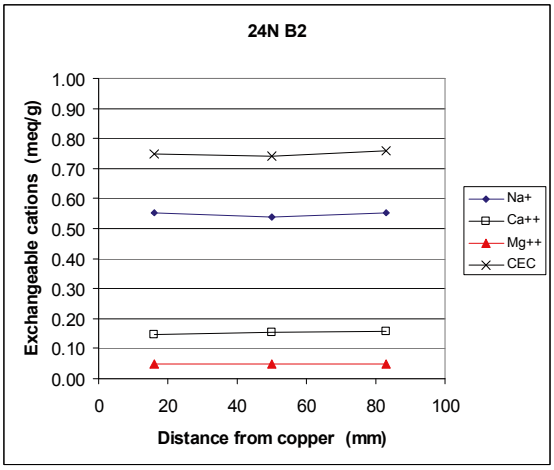
24N B2
Exchangeable cations (meq/g)
Distance from copper (mm)
Na+
Ca++
Mg++
CEC

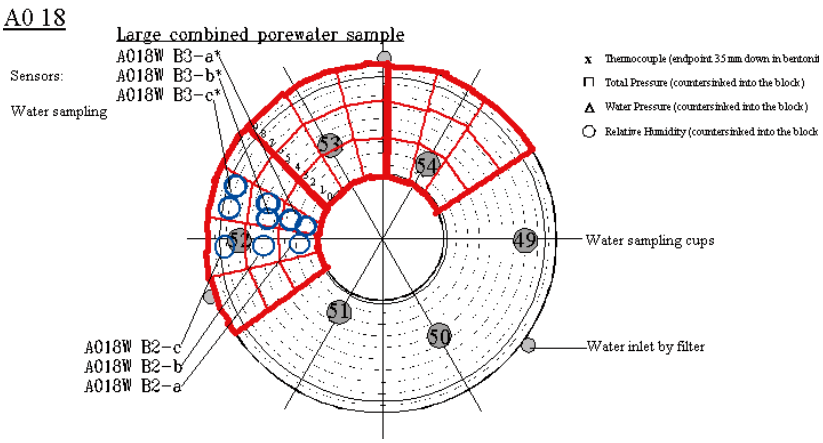

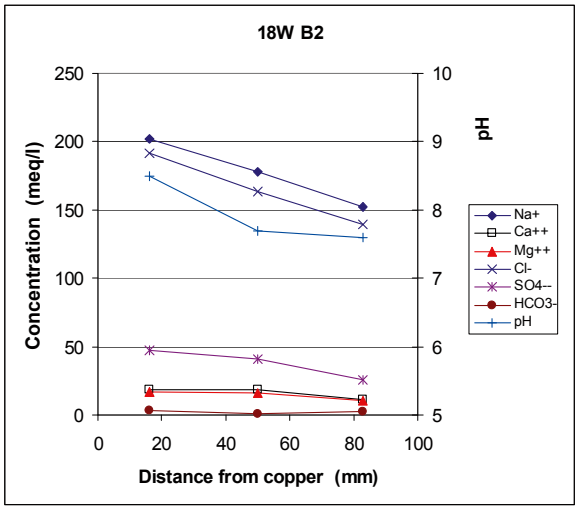

18W B3

No porewaterdata

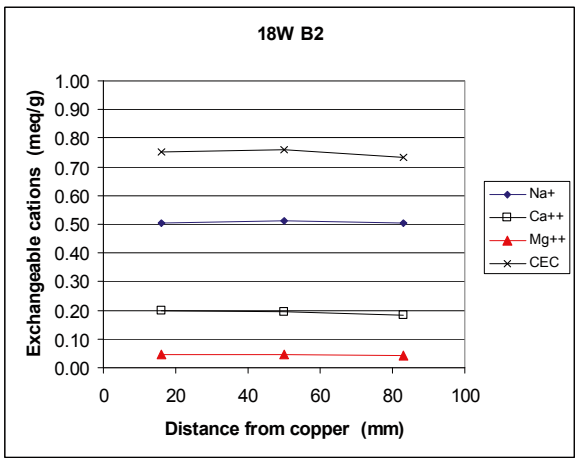

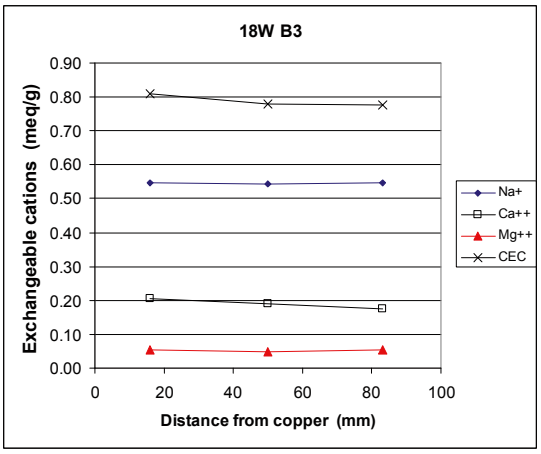

A0 16

Sensors:

Water sampling
50% K-feldspar

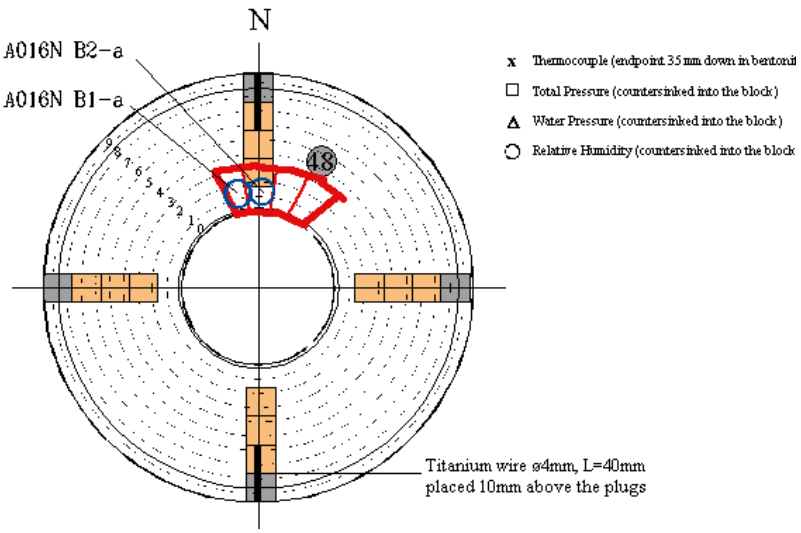

Porewater composition

Sample	pH	Na+ (mmol/l)	K+ (mmol/l)	Ca++ (mmol/l)	Mg++ (mmol/l)	Cl– (mmol/l)	SO4– (mmol/l)	HCO3– (mmol/l)
16N B1-a	8.17	215	0.69	10.6	10.5	188	24.9	2.54
16N B2-a	8.30	219	0.59	12.1	12.1	201	25.3	3.43

Exchangeable cations in bentonite

Sample	Height posit. (cm)	Dist. from copper (mm)	Na (meq/g)	K (meq/g)	Ca (meq/g)	Mg (meq/g)	CEC (meq/g)
16N B1-a	160	16	0.53	0.01	0.17	0.06	0.77
16N B2-a	160	16	0.53	0.01	0.17	0.06	0.77

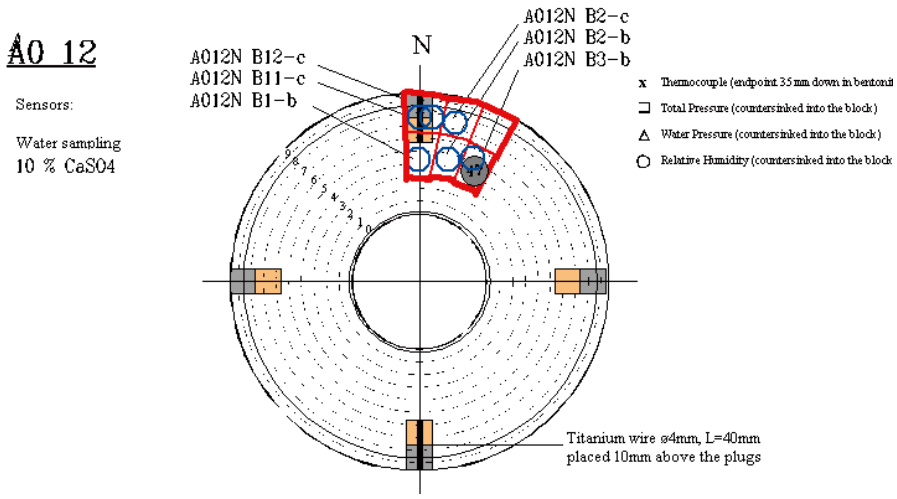
A0 12
Sensors:
Water sampling
10 % CaSO4
A012N B12-c
A012N B11-c
A012N B1-b
N
A012N B2-c
A012N B2-b
A012N B3-b
x Thermocouple (endpoint 35 mm down in bentonit
Total Pressure (countersinked into the block)
Water Pressure (countersinked into the block)
Relative Humidity (countersinked into the block
Titanium wire ø4mm, L=40mm
placed 10mm above the plugs

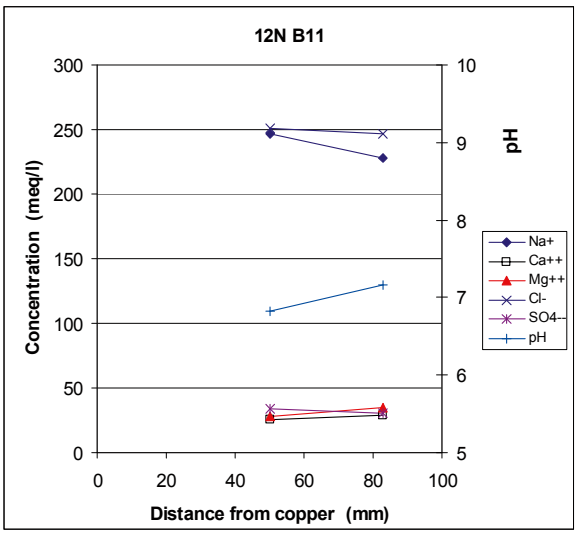
12N B11
Concentration (meq/l)
pH
Distance from copper (mm)
Na+
Ca++
Mg++
Cl-
SO4--
pH

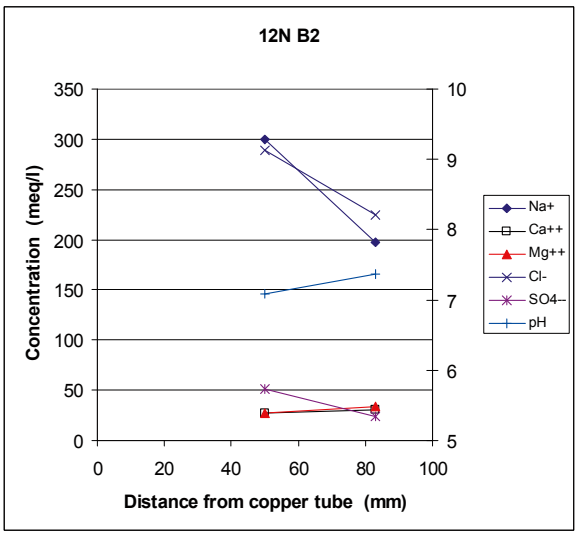
12N B2
Concentration (meq/l)
Distance from copper tube (mm)
Na+
Ca++
Mg++
Cl-
SO4--
pH

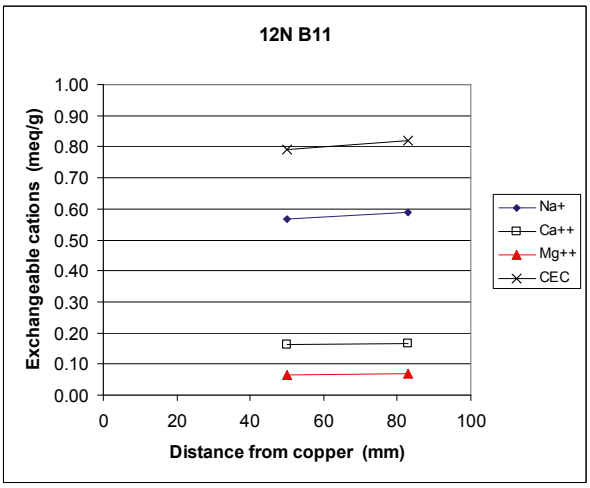
12N B11
Exchangeable cations (meq/g)
Distance from copper (mm)
Na+
Ca++
Mg++
CEC

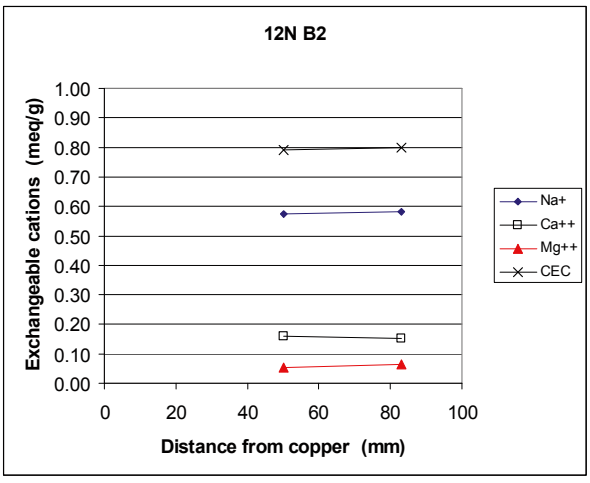
12N B2
Exchangeable cations (meq/g)
Distance from copper (mm)
Na+
Ca++
Mg++
CEC

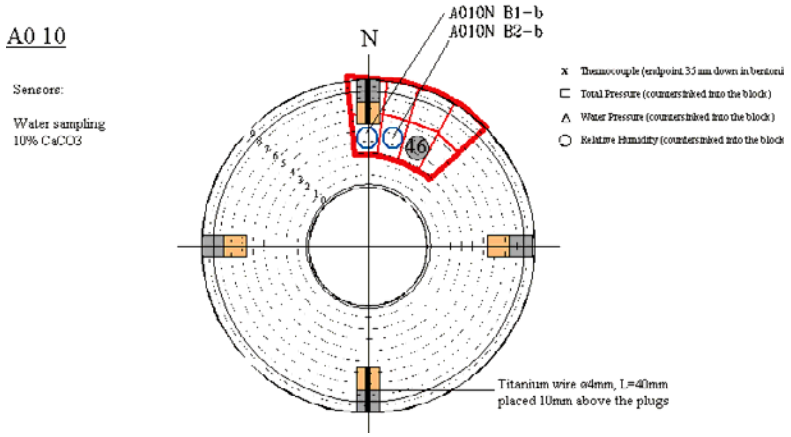

Porewater composition

Sample	pH	Na+ (mmol/l)	K+ (mmol/l)	Ca++ (mmol/l)	Mg++ (mmol/l)	Cl– (mmol/l)	SO4– (mmol/l)	HCO3 (mmol/l)
10N B1-b								
10N B2-b	7.9	397	0.66	26.2	20.9	401	25.4	not anal

Exchangeable cations in bentonite

Sample	Height posit. (cm)	Dist from heater (mm)	Na (meq/g)	K (meq/g)	Ca (meq/g)	Mg (meq/g)	CEC (meq/g)
10N B1-b	100	50	0.53	0.01	0.18	0.05	0.76
10N B2-b	100	50	0.55	0.01	0.18	0.05	0.80